2015

Design and Development of pH-Sensitive Peptides for Cancer Diagnostics

Ramona Cosmina Adochite
University of Rhode Island, ramona.vladea@gmail.com

DESIGN AND DEVELOPMENT OF pH-SENSITIVE PEPTIDES FOR CANCER DIAGNOSTICS

BY

RAMONA-COSMINA ADOCHITE

A DISSERTATION SUBMITTED IN PARTIAL FULFILLMENT OF THE REQUIREMENTS FOR THE DEGREE OF

DOCTOR OF PHILOSOPHY

IN

ELECTRICAL ENGINEERING

UNIVERSITY OF RHODE ISLAND

2015

DOCTOR OF PHILOSOPHY DISSERTATION

OF

RAMONA-COSMINA ADOCHITE

APPROVED:

Thesis Committee:

Major Professor: Ying Sun

Oleg Andreev

Yana Reshetnyak

Walter G. Besio

Nasser H. Zawia

DEAN OF THE GRADUATE SCHOOL

UNIVERSITY OF RHODE ISLAND

2015

ABSTRACT

The design and development of pH-sensitive peptides for cancer diagnostics provides an opportunity to study and address fundamental questions of *in vivo* bio-distribution of pH-sensitive peptides, as well as developing new targeting imaging and therapeutic agents for acidic diseased tissue such as cancer, infections, ischemia, stroke and others.

The main goal of the work presented here is to investigate the following problems:

- Targeting of highly metastatic mammary tumors and spontaneous breast tumors in transgenic mice with fluorescently labeled pHLIPs® (pH (Low) Insertion Peptides) pHLIP variants;
- Direct imaging of pHLIP insertion and cargo translocation in vivo;
- Targeting of mammary tumors using cyclic pH-sensitive peptides;
- Biodistribution of different pHLIP variants conjugated with various fluorescent dyes with the main purpose to identify the best pHLIP-based constructs for clinical applications.

It has been shown that extracellular acidity is associated with tumor progression. Elevated glycolysis and acidosis promote the appearance of aggressive malignant cells with enhanced multidrug resistance. The most effective pH-sensitive tumor targeting agents should sense pH at the surface of cancer cells, where it is expected to be the lowest. Thus, targeting tumor acidity might represent a novel approach for the prediction of tumor aggressiveness and delivery of therapeutic agents to tumor cells with the greatest metastatic potential. pHLIP belongs to the class of pH-sensitive

agents capable of delivering imaging and/or therapeutic agents to cancer cells within tumors. Also, cyclic pH-sensitive peptides containing a number of Trp and Glu residues can be developed for imaging of acidity in tumors.

pHLIP insertion is associated with the protonation of Asp/Glu residues in the transmembrane sequence and its inserting end. Carboxyl group protonation leads to an increase in the hydrophobicity that further triggers transmembrane formation and insertion of the peptide across a lipid bilayer. pHLIP insertion is predominantly uni-directional. In contrast to cell-penetrating peptides, pHLIP remains in the cellular membrane after insertion, translocating one end across the bilayer and comes out in the cytoplasm, while leaving the other end in the extracellular space. Therefore, pHLIP possesses dual delivery capabilities: it can translocate cell-impermeable cargo molecules into the cell cytoplasm or it can tether cargo molecules to the cell surface. Also, the process of peptide folding into a membrane ensures a much higher co-operativity of the transition compared to the pH-diffusion across a membrane. A family of novel pHLIP variants were introduced and demonstrated that tumor targeting, blood clearance and biodistribution of this peptides can be modulated by tuning their sequence and, as a result, their physical and chemical properties and their interaction with the cell membrane.

For demonstrating direct imaging of pHLIP insertion and cargo translocation *in vivo*, the cell-inserting end of the pHLIP-FIRE peptide has a fluorophore-fluorophore or fluorophore-quencher pair. A pair member is released by disulfide cleavage after insertion into the reducing environment inside a cell, resulting in de-quenching of the

probe. Thus, the fluorescence of the pHLIP-FIRE probe is enhanced upon cell-insertion in the targeted tissues, but is suppressed elsewhere due to quenching.

The cyclic pH-sensitive peptides used in this work, contain: i) single cysteine (Cys, C) residue for conjugation purposes, ii) at least one tryptophan (Trp, W) for ability to record fluorescence signal, iii) 3-5 protonatable glutamic acid (Glu) residues to trigger pH-dependent interaction with membrane. As in the case of pHLIP peptides, the presence of low pH leads to the protonation of carboxyl groups of Glu residues, which increases peptides hydrophobicity and promotes partition of peptides in bilayer.

Thus, there is an opportunity to develop new imaging and/or therapeutic agents, which are based on the use of pH-sensitive peptides. We have successfully established the bio-distribution of both pHLIP and cyclic pH-sensitive peptides attached to different fluorescent dyes and identified the best candidate for imaging and therapeutic applications.

ACKNOWLEDGMENTS

To think that the production of this dissertation was an individual effort would be a grave mistake. Countless people have contributed to this work in a variety of different ways and I am forever grateful to those folks for helping me through this great endeavor.

Several faculty members have served as mentors, helping me along the way. To them I am thankful. Particularly, I would like to thank my advisors, Dr Yana Reshetnyak and Dr Oleg Andreev, for their patience and guidance. I will always be grateful for their trust and loyal support during both happy times as well as the tough moments at URI. Their generosity has provided me with endless opportunities to grow as a scientist. I really treasure their contagious enthusiasm for science and their friendly advice at all times. Dr Anna Moshnikova for her scientific guidance and life advice. Her knowledge and unlimited zeal have been major driving forces through my graduate studies. Dr Ying Sun, for taking me on board and for helping me organize both the comprehensive exam and the defense. I am grateful to my graduate program committee members Dr Walter Besio, Dr Clinton Chichester and Dr John DiCecco for their time and effort.

This dissertation has been the result of a truly collaborative effort. I am thankful to Dr Sean Carlins from Memorial Sloan Kettering Cancer Center, as well to Dr Dragan Golijanin and Dr Ali Amin, both from Rhode Island Hospital, for their help and guidance on several projects.

I am endlessly thankful to Dr Felipe Vaz and Dr Luis Cunha from Minho University, Portugal for believing in me and being supportive when all I had was an

idea for a project and very little lab experience. Amazing people that inspired me to push and believe in myself.

I also want to acknowledge my friends spread across the globe, whose support kept me sane through this long journey. They made my life outside the lab colorful.

In the end, I would like to express my eternal gratitude towards my family. I dedicate this work to them. Each one of them had a hand in helping me achieve my goals. I owe everything to my parents because I would not be where I am today without the foundation they provided me with. I am thankful for their continuous love, support and encouragement. My siblings, for listening to me when the stresses of life became overwhelming, for their undying love and care. My beautiful nieces and nephews, Bianca, Silviu, Otilia, Luca, and Cami for being so pure and for brightening up my day when everything seemed too difficult. My parents and sisters in law for welcoming me in their family. My husband John, for his love, for never trying to hold me back, no matter how many things I attempt to drown myself with, being a strong endowment for me, and helping me remember what really matters.

You are all a large part of who I am.

PREFACE

This dissertation is written in the 'Manuscript Format' using the Thesis/Dissertation template of University of Rhode Island. There are four manuscripts, each organized into a chapter. Tables and figures of each manuscript are listed under the corresponding chapter in the list of tables and figures.

The results of our studies presented here were published and submitted for publishing in four papers:

1. **R. C. Adochite**, A. Moshnikova, S. D. Carlin, R. A. Guerrieri, O. A. Andreev, J. S. Lewis, Y. K. Reshetnyak, Targeting Breast Tumors with pH (Low) Insertion Peptides, Molecular Pharmaceutics, 11(8):2896-2905 (2014).
2. A.G. Karabadzhak, M. An, L. Yao, R. Langenbacher, A. Moshnikova, **R. C. Adochite**, O. A. Andreev, Y. K. Reshetnyak, D. Engelman, pHLIP-FIRE, a Cell Insertion-Triggered Fluorescent Probe for Imaging Tumors Demonstrates Targeted Cargo Delivery In Vivo, ACS Chemical Biology, 9(11):2545-53 (2014).
3. D. Weerakkody, A. Moshnikova, N. S. El-Sayed, **R. C. Adochite**, J. Golijanin, R. K. Tiwari, O. A. Andreev, K. Parang, Y. K. Reshetnyak, pH-Sensitive Cyclic Peptides for Tumor Targeting, Journal of Controlled Release, submitted in Angewandte Communications.
4. **R. C. Adochite**, A. Moshnikova, J. Golijanin, O. A. Andreev, Y. K. Reshetnyak, Comparative Sudy of Tumor Targeting and Biodistribution of pH (Low) Insertion Peptides conjugated with various fluorescent dyes, submitted in Journal of Molecular Biology.

Work was presented on the following Meetings/Conferences:

2015

Golijanin J, Brito J, Tran T, Adochite RC et al., Near infrared fluorescent (NIRF) imaging of the bladder tumors in fresh, ex vivo bladder specimens after pH low Insertion Peptide (pHLIP) - Indocyanine Green (ICG) compound (pHLIP-ICG) intravesical instillation, Abstract Submitted to **Annual Meeting of the New England Section of the AUA**, Bahamas.

R. C. Adochite, A. Moshnikova, O. A. Andreev, Y. K. Reshetnyak, pH (Low) Insertion Peptide Targets 4T1 Mammary Tumors, **Northeast Bioengineering Conference**, Troy, NY, USA.

2014

A.G. Karabadzhak, M. An, L. Yao, R. Langenbacher, A. Moshnikova, R. C. Adochite, O. A. Andreev, Y. K. Reshetnyak, D. Engelman, pHLIP-FIRE: A High-Contrast, Insertion-Triggered Fluorescent Probe for Targeting Tumors In Vivo, **Biophysical Society Annual Meeting**, San Francisco, USA.

2013

R. C. Adochite, R. A. Guerrieri, A. Moshnikova, O. A. Andreev, Y. K. Reshetnyak, Targeting of breast tumors by fluorescent pHLIP®s, **New England section of American Physical Society Meeting** at Bridgewater, USA.

R. A. Guerrieri, R. C. Adochite, J. Danniels, A. Moshnikova, D. Wijesinghe, O. A. Andreev, Y. K. Reshetnyak, pH-Low Insertion Peptide (pHLIP) Targets Breast Cancer Tumors in Transgenic Mice and Mediates Delivery of Gold Nanoparticles to A549 Cancer Cells, **SURF Conference**, Kingston, USA.

2012

R. C. Adochite, J. Danniels, L. Yao, A. Sigdel, A. Moshnikova, S. Sun, Y. K. Reshetnyak, O. A. Andreev, pHLIP®-mediated delivery of nanoparticles to cancer cells in vitro and in vivo, **Gordon Research Conference**, New Hampshire, USA.

TABLE OF CONTENTS

LIST OF TABLES

LIST OF FIGURES

CHAPTER 1 PAGE

CHAPTER 2

CHAPTER 3

CHAPTER 1

Published in Molecular Pharmaceutics on 27th of June, 2014

Targeting Breast Tumors with pH (Low) Insertion Peptides

Ramona-Cosmina Adochite[1], Anna Moshnikova[1], Sean D. Carlin[2,3], Renato Guerrieri[1], Oleg A. Andreev[1], Jason S. Lewis[2,3], Yana K. Reshetnyak[1]

[1]Physics Department, University of Rhode Island, 2 Lippitt Road, Kingston, RI 02881 USA;

[2]Program in Molecular Pharmacology and Chemistry, [3]Department of Radiology Memorial Sloan-Kettering Cancer Center, 1275 York Avenue, New York, NY 10065 USA.

KEYWORDS

Imaging, tumor acidity, glucose, lactate dehydrogenase, fluorescence, transgenic mice model

Abstract

Extracellular acidity is associated with tumor progression. Elevated glycolysis and acidosis promote appearance of aggressive malignant cells with enhanced multidrug resistance. Thus, targeting of tumor acidity can open new avenue in diagnostic and treatment of aggressive tumors and targeting metastatic cancers cells within a tumor. pH (Low) Insertion Peptides (pHLIPs) belong to the class of pH-sensitive agents capable of delivery of imaging and/or therapeutic agents to the cancer cells in tumors. Here, we investigated targeting of highly metastatic 4T1 mammary carcinoma and breast tumors in FVB/N-Tg (MMTV-PyMT)634Mul transgenic mice with three fluorescently-labeled pHLIP variants including well-characterized WT-pHLIP, and recently introduced, Var3- and Var7-pHLIPs. All pHLIPs demonstrated excellent targeting of breast tumors with signals increasing in tumors within 4 hours post-injection. Staining of non-cancerous tissue (breast muscle and fat) in transgenic mice was minimal. pHLIPs distribution in tumors showed co-localization with 2-deoxy-glucose and hypoxia marker, pimonidazole. The highest degree of co-localization of fluorescent pHLIPs was established with lactate dehydrogenase A, which is related to lactate production and acidification of tumors. pHLIP-based targeting imaging and therapeutic agents present an opportunity for the monitoring of metabolic changes, and as a means of tumor-selective delivery of therapeutic agents

Introduction

For a wide variety of cancers, extracellular pH is significantly more acidic than in normal tissues. An acidic pH shift within solid tumors can regulate multiple biological processes such as proliferation, angiogenesis, immunosuppression, invasion and chemoresistance [1-6]. Being a unique property of the majority of tumors, acidity may be heterogeneous within a single tumor [7, 8]. This heterogeneity does not correlate spatially with tumor oxygenation; both well- and poorly-oxygenated parts of tumors can be acidic. Exposure of cancer cells to low pH has previously been shown to promote selection of stable, more invasive phenotypes[6, 9, 10]. Therefore targeting of tumor acidity might represent novel approach in prediction of tumor aggressiveness and delivery of therapeutic agents to those tumor cells with the greatest metastatic potential.

Several pH-sensitive imaging and drug delivery systems have been introduced in which diagnostic or therapeutic agent release is specifically triggered by the acidic tumor microenvironment [11-15]. Among them are peptides of pHLIP (pH Low Insertion Peptides) family, which represent a unique class of water-soluble membrane polypeptides capable to undergo a pH-dependent membrane-associated folding [16, 17]. The energy of folding is used for targeting of imaging agents to acidic tumors, as well as translocation of polar cargo molecules across phospholipid bilayer of membrane. Transition of pHLIPs from the membrane-surface state at neutral pH to the membrane-inserted state at low pH is highly cooperative due to the accompanied coil-helix transformation within a lipid bilayer [18-20]. The well-characterized WT-pHLIP was employed for translocation of toxins and peptide nucleic acids into the cytoplasm of

cancer cells, delivery of various imaging agents and targeting of both liposomes and gold nanoparticles to tumors and other acidic diseased tissue [21-28]. Biophysical investigations allowed us to broaden the chemical space of pHLIP peptides and formulate design principles to set directions for different clinical uses. We introduced a family of rationally designed pHLIP variants and demonstrated that tuning of sequence and, as a result, physical and chemical properties of peptides interaction with membrane, can modulate tumor targeting, blood clearance and biodistribution [18]. Focus of our current research is in a comparative study of WT-, Var3- and Var7-pHLIPs targeting of breast tumors. The data presented here provides important information about pHLIPs distribution in tumors and co-localization with glucose, lactate dehydrogenase A (an enzyme involved in lactate production) and the hypoxia marker, pimonidazole.

Materials and Methods

Synthesis and Labeling of Peptides

pHLIP variants were prepared by solid-phase peptide synthesis using Fmoc (9-fluorenylmethyloxycarbonyl) chemistry and purified by reverse phase chromatography by Dr. James I. Elliott at the W.M. Keck Foundation Biotechnology Resources Laboratory at Yale University (New Haven, CT).

pHLIP variants were conjugated with Alexa488-, Alexa546-, Alexa647-maleimide (Life Technologies) and IR680-maleimide (LiCor Biosciences) in DMF (dimethylformamide) at a ratio of 1:1 and incubated at room temperature for about 8 hours and then at 4ºC until the conjugation was completed. The reaction progress was

monitored by reverse phase HPLC. The products were lyophilized and characterized by SELDI-TOF mass spectrometry.

The concentration of constructs was determined by absorbance using the following molar extinction coefficients: ε_{495}=71,000 $M^{-1}\cdot cm^{-1}$ (for Alexa488-pHLIPs), ε_{556}=104,000 $M^{-1}\cdot cm^{-1}$ (for Alexa546-pHLIPs), ε_{650}=239,000 $M^{-1}\cdot cm^{-1}$ (for Alexa647-pHLIPs) and ε_{672}=165,000 $M^{-1}\cdot cm^{-1}$ (for IR680-pHLIPs).

Cell line

The *4T1* mouse mammary tumor *cell line was obtained* from the American Type Culture Collection and cultured in RPMI medium supplemented with 10% fetal bovine serum, 10 μg/mL of ciprofloxacin in a humidified atmosphere of 5% CO_2 and 95% air at 37°C.

Tumor mouse models

Breast tumors were established by subcutaneous injection of 4T1 cells ($8x10^5$ cells/0.1 ml/flank) in the right flank of adult female BALB/c mice (about 19-22 g weight) obtained from Harlan Laboratories. FVB/N-Tg(MMTV-PyVT)634Mul/J transgenic female mice from Jackson Laboratory developed palpable mammary tumors at 12-15 weeks of age. All animal studies were conducted according to the animal protocol AN04-12-011 approved by the Institutional Animal Care and Use Committee at the University of Rhode Island, in compliance with the principles and procedures outlined by NIH for the Care and Use of Animals.

Fluorescence whole-body and organs imaging

When tumors were palpable in the MMTV-Py MT mice, single tail vein injections of a cocktail of 1 nmol of IR680-labeled pHLIPs and 10 nmoles of IR800-2DG per mouse were performed. Control mice received the same dose of fluorescent pHLIPs and glucose. In xenografted BALB/c mice, tumors were used when they reached approximately 6 mm in diameter. Single tail vein injections of 5 nmol of Alexa488-, Alexa546- and Alexa647-labeled pHLIPs (one pHLIP at the time or a cocktail of differently-labeled pHLIPs) were performed. Pimonidazole, a marker of hypoxia, (1.5 mg) and Hoechst 33342, a blood perfusion marker (1 mg) were administered 1 hour and 1.5 min before animal euthanization, respectively. Whole-body imaging followed by euthanization and necropsy was performed at 24 hours post-injection. The whole-body imaging of transgenic was performed while the animals were under ketamine/xylazine anesthesia and skin was removed from the breast area. Animals were euthanized at 2, 4, 24 and 48 hours post-injections followed by necropsy. Tumors and major organs of transgenic and BALB/c mice were imaged immediately after collection. The excised tumors were embedded in Tissue-Tek optimal cutting temperature (OCT) compound and stored at -80^{o}C until used for immunohistochemical analysis.

Imaging of Alexa-pHLIPs and IR-pHLIPs/IR-glucose were carried out using a FX Kodak in-vivo image station and an Odyssey IR scanner (Li-Cor Biosciences), respectively, using various magnifications and depth distances. Mean fluorescence intensity of tumor and organs was calculated using Kodak and Image J software. The contrast index (CI) was calculated according to the equation:

$$CI = \frac{F_{tumor} - F_{backg}}{F_{muscle} - F_{backg}}$$

where F_{tumor} , F_{muscle} and F_{backg} are the mean fluorescence intensities of tumor, muscle and background signal measured for control mice non-injected with fluorescent constructs.

Immunofluorescence staining and imaging of tumor sections

Frozen breast tumor tissues were sectioned at a thickness of 10 μm using a Vibratome UltraPro 5000 Cryostat. Sections were mounted on microscope slides, dried in air, and washed with deionized water. Tumor sections with pHLIPs-cocktail were analyzed without further processing, whist the remaining sections were fixed and stained. Slides were fixed in 4% paraformaldehyde (Sigma-Aldrich) for 12 minutes and washed with Dulbecco's Phosphate Buffered Saline (Life Technologies). The slides were dried in air and blocked using a mixture of 10% Goat serum (GeneTex), 1% bovine serum albumin (Life Technologies) and 0.3% Triton X-100 (Sigma-Aldrich) in phosphate buffered saline (Life Technologies) for 30 minutes. Then, immunofluorescence staining for lactate dehydrogenase A (LDHA) and pimonidazole was performed. For LDHA staining, rabbit polyclonal (NBP1-48336, Novus Biologicals) was used at 1:100 dilution, with goat anti-rabbit Alexa-568 (Life Technologies) at 1:100 for secondary detection. For pimonidazole staining, FITC-conjugated mouse monoclonal anti-pimonidazole antibody (Natural Pharmacia International Inc.) was used at 1:20 dilution. Following fluorescence imaging, the same sections were then stained with H&E.

Fluorescence and brightfield images were acquired at 4x magnification using an Olympus BX60 fluorescence microscope equipped with a motorized stage (Prior

Scientific Instruments Ltd.) and coolsnap EZ CCD (Photometrics) and CC12 RGB camera (Olympus Scientific). Whole-tumor montage images were obtained by acquiring multiple fields, followed by alignment using MicroSuite Biologic Suite (version 2.7; Olympus).

Results

The focus of our work was targeting of breast tumors by three pHLIP variants recently selected for pre-clinical development:

WT: ACEQNPIYWARYADWLFTTPLLLLDLALLVDADEGT

Var3: ACDDQNPWRAYLDLLFPTDTLLLDLLW

Var7: ACEEQNPWARYLEWLFPTETLLLEL

Each peptide has a single Cys residue at the N-terminus for conjugation with fluorescent Alexa or IR dyes. Labeled peptides were purified prior *in vivo* use. We selected two different breast tumor models for testing of pHLIPs tumor targeting: i) the highly tumorigenic and invasive 4T1 mammary carcinoma and ii) FVB/N-Tg (MMTV-PyMT)634Mul transgenic mouse model.

Targeting 4T1 mammary carcinoma

Small 4T1 tumors (tumor volume < 150 mm^3) generate significant level of lactate and serve as a good model of an aggressive, acidic tumor [29]. pHLIP variants labeled with Alexa546 showed significant targeting of tumors with minimal signal accumulation in liver, kidney and muscle (Figure 1a-d). The signal in tumors was increasing up to 4 hrs post-injection, and then declined within 48 hrs. The highest uptake in tumor was observed for Var3. At 48 hrs post-injection the signal in tumor was still higher than the background fluorescence, while fluorescence in muscle and liver was at the level

of autofluorescence. Var7 demonstrates fast clearance and steady decay of fluorescent signal from 2 to 24 hrs in all organs except tumor, where the maximum signal was reached at 4 hrs post-injection. For Var3, the renal fluorescence signal was maximal at 24 hrs, indicating a slower clearance profile of this pHLIP variant. The optimal tumor targeting was achieved with Var3, which showed a contrast index of 5 at 2-4 hrs and 19 at 24 hrs post-injection (Figure 2b). The contrast index for Var7 was increasing from 3, 5 and up to 19 for 2, 4 and 24 hrs post-injection, respectively. We did not calculate values of contrast index for time point of 48 hrs, since signal in muscle was at the level of background.

We compared the distribution of fluorescent-pHLIPs in both small and necrotic large, 4T1 tumors. The representative images of tumors cut into halves are shown on Figure 1e and f. In contrast to the smaller tumors, where the signal was homogeneously distributed within the entire tumor mass with maximal accumulation in the center of the tumor, the fluorescent signal in the necrotic core of the larger tumors was minimal. Previously, we proved pH-dependent tumor targeting by WT-pHLIP[27, 28, 30]. Novel pHLIP variants also show pH-dependent tumor staining, but different pharmacokinetics[18]. In this study, we compared cellular localization and distributions of different pHLIPs in tumors. Frozen sections were prepared from tumors collected at 4, 24 and 48 hrs after administration of a cocktail of pHLIPs labeled with different fluorescent dyes: Alexa488-Var7, Alexa546-Var3 and Alexa647-WT given as a single tail vein injection (Figure 3). We selected later time points to minimize the concentration of the peptides in blood. The distribution of all pHLIPs in tumors was identical. The intensity profiles for all pHLIPs obtained from the different areas of

tumor sections were very similar, with minor differences in general background. Thus, despite on the fact that pHLIP variants show different blood clearance profile, the cellular distributions were identical and all variants could be used as markers of tumor acidity.

Immunohistochemical analysis of breast tumor sections (small 4T1 tumors) revealed co-localization of fluorescent pHLIPs with hypoxia marker, pimonidazole, and excellent co-localization with lactate dehydrogenase A (LDHA) (Figure 4).

Targeting breast tumors in transgenic mice

It has been previously established that breast tumor progression from benign to metastatic correlates with age in FVB/N-Tg (MMTV-PyMT)634Mul transgenic mouse model [31-33], with invasive tumors developing in mice of age 12 weeks and older. We used mice with an age range from 12 to 15 weeks to investigate distribution of pHLIPs in spontaneous invasive breast tumors. Tumor and organs were analyzed at 24 hrs after iv administration of Alexa546- or IR680-pHLIPs given as a single injection, or in a mixture with the fluorescent non-metabolizible 2-deoxyglucose IR800-2DG. We observed pHLIP- targeting of breast tumors in transgenic mice with a minimal level of fluorescence from control mice, or detectable signal in muscle at 24 hrs post-injection (Figure 5a, b). Higher tumor uptake of Var3 was observed, along with higher signal in muscle at 24 hrs compared to the other pHLIPs. Fluorescent signal for WT and Var7 was comparable to the signal from fluorescent 2-deoxyglucose, which was given at concentrations 10 times higher than pHLIPs. Multiple tumors collected from the same mouse targeted by both IR680-Var3 and IR800-2DG are shown on Figure 5c. We observed heterogeneity in distribution of

IR800-2DG. Detailed analysis of 2-deoxygluoce and pHLIPs distribution in tumors indicates that accumulation of 2-deoxyglucose correlates with the accumulation of pHLIPs (Figure 5d and e). However pHLIPs also demonstrate targeting of adjacent spots.

Analysis of histological sections of breast tumors indicates that pHLIPs can clearly differentiate between regions of primarily tumor cells and non-malignant stromal tissues (Figure 6a, b, c). Regions consisting mainly of tumor cells stained strongly with all pHLIP variants. Uptake of pHLIPs was observed in poorly-perfused tumor regions (indicated by low Hoechst 33342 staining), which also accumulated the hypoxia marker pimidazole (Figures 6 and 7). However, we observed the highest degree of pHLIP co-localization with the lactate dehydrogenase A (LDHA) enzyme, confirming that uptake of pHLIP is closely related to the production of acidic glucose metabolites in this model system.

Discussion

Tumors of the same organ and cell type can have remarkably diverse appearances in different patients, which apply significant restriction for the use of targeting approaches based on over expression of particular protein biomarkers. Heterogeneity of the cancer cell population within a single tumor is assumed to lead to diminished treatment response. Cytotoxic therapies, whilst treating the majority of cancer cells, may spare multidrug resistant clones leading to tumor relapse and treatment failure [34, 35] . Moreover, this transient depopulation of sensitive tumor cells by chemotherapeutic agents may provide a growth advantages to the surviving cells, leading to outgrowth of resistant clones[35]. It is therefore important to develop targeted imaging agents,

which can reflect the underlying tumor microenvironment, and allow for the targeted therapy of otherwise resistant cell clones. pH-responsive imaging and therapeutic probes could be particularly well-suited to this role, as, decreased extracellular pH is a general property of tumor microenvironment reflective of tumor aggressiveness, and the most malignant cells within a tumor mass are glycolytic and acidic.

Previously we demonstrated that water soluble membrane peptide, WT-pHLIP, can deliver optical, PET and SPECT imaging agents to the primary tumors and metastatic lesions in a pH-dependent manner, and distinguish between aggressive and non-metastatic tumors[26-28, 30]. The main goal of this study was to establish pHLIP distribution in breast tumors and evaluate co-localization with other markers of stressed tumor microenvironment. In this case, we compared distribution of pHLIPs with a fluorescent glucose analog, 2-deoxyglucose, (indicating elevated glucose uptake), lactate dehydrogenase A (indicating glycolytic metabolism) and pimonidazole (a marker of tumor hypoxia). We selected two well-characterized breast cancer models: i) the murine 4T1 xenograft model, which closely mimic stage IV of human breast cancer [36-38], and ii) FVB/N-Tg (MMTV-PyMT)634Mul transgenic mouse model, which show different degree of disease progression, such as mammary hyperplasia, DCIS and invasive cancer at different ages of animals ranging from week 4 to 12, respectively [31-33].

Both 4T1 tumors and breast tumors in transgenic mice were targeted very well by fluorescently-labeled pHLIP variants, with minimal signal observed in other organs. We carried out our imaging studies on small, well-perfused 4T1 tumors (about 0.2 g in mass). Further growth of 4T1 tumors (up to mass of 0.5-0.6 g) leads to the appearance

of a necrotic core, which did not accumulate pHLIPs. This observation is consistent with previous studies showing that significant necrosis observed in enlarging 4T1 tumors is associated with lower levels of lactate production[29]. The fluorescent signal from pHLIPs in small 4T1 tumors reached maximum level at 4 hours post-injection. The highest signal was observed for Var3, which was over 2-fold greater than that observed with IR800-2DG (a fluorescent glucose analog).

The detailed analysis of the distribution in tumors of three pHLIP variants (WT, Var3 and Var7) labeled with different fluorescent dyes and given as a cocktail in a single iv injection showed a high degree of co-localization. Histological analysis of tumor sections from the transgenic mice clearly indicates a minimal level of non-tumor (stromal) staining and elevated staining of tumor-containing regions by the three pHLIPs. Var3 and Var7 were recently introduced as novel pHLIP variants, which show higher tumor targeting and fast blood clearance, respectively[18], and are able to target pancreatic tumors in various mouse models[39]. Despite on the difference in pharmacokinetics of pHLIP variants, Var3 and Var7 demonstrate distribution in tumors identical to the well-characterized WT-pHLIP. The pharmacokinetic properties of Var3 and Var7 could be suited well for imaging of tumor acidity by MRI/optical and PET/SPECT, respectively.

Using IR800-2DG we observed that the distribution of the glucose analog in tumors is heterogeneous, and correlates well with pHLIPs distribution. Regions of elevated pHLIPs uptake correlate with the hypoxia marker pimonidazole as well. At the same time, pHLIPs also target adjacent spots to 2-doxyglucose uptake and show accumulation in non-hypoxic tumor regions. The highest co-localization of pHLIPs

was seen with lactate dehydrogenase A in both transgenic and 4T1 small tumors. LDHA expression is partially regulated by the hypoxia-inducible HIF1 transcription factor, as is the glucose transporter GLUT-1. Our observation of a positive correlation between pHLIP uptake and markers of glucose transport and metabolism strongly implies that pHLIP is specifically accumulated in tumor regions displaying typical characteristics of a stressed microenvironment, such as hypoxia, elevated glucose uptake and glycolytic metabolism. Increased LDHA expression, with consequent increases higher lactate production and generation of hydrogen ions, would be expected to correlate most closely with pH-dependent uptake of pHLIP, as was observed in this study.

Despite an evident correlation between glucose uptake, lactate production and tumor acidification, it was shown that [^{18}F]2-deoxy-2-fluoro-D-glucose positron emission tomography ([^{18}F]FDG-PET) imaging was significantly less sensitive to differences in the metabolic phenotypes of tumors compare to the lactate-MRSI (magnetic resonance spectroscopic imaging)[29]. Although MRSI can provide additional information about metabolic activities in tumors, it is not yet widely implemented in a clinical setting. The potential exists for pHLIP to provide imaging data of a similar nature to lactate-MRSI, but with a clear path to rapid clinical translation . Use of any of three of pHLIP variants labeled with PET or SPECT agents (such as ^{18}F, ^{64}Cu, ^{99}Tc) could allow monitoring of metabolic changes in human tumors over time, or in response to therapeutic intervention. In addition, pHLIP peptides could be used for delivery of therapeutic cargoes to tumors, which might target the most aggressive cancer cell clones.

REFERENCES

1. Kallinowski, F.; Vaupel, P. pH distributions in spontaneous and isotransplanted rat tumours. Br J Cancer 1988, 58, (3), 314-21.

2. Lessi, E.; Marino, M. L.; Lozupone, F.; Fais, S.; De Milito, A. Tumor acidity and malignancy: novel aspects in the design of anti-tumor therapy. Cancer Therapy 2008, 6, 55-66.

3. Vaupel, P.; Kallinowski, F.; Okunieff, P. Blood flow, oxygen and nutrient supply, and metabolic microenvironment of human tumors: a review. Cancer Res 1989, 49, (23), 6449-65.

4. Gerweck, L. E.; Seetharaman, K. Cellular pH gradient in tumor versus normal tissue: potential exploitation for the treatment of cancer. Cancer Res 1996, 56, (6), 1194-8.

5. Bhujwalla, Z. M.; Artemov, D.; Ballesteros, P.; Cerdan, S.; Gillies, R. J.; Solaiyappan, M. Combined vascular and extracellular pH imaging of solid tumors. NMR Biomed 2002, 15, (2), 114-9.

6. Gatenby, R. A.; Gawlinski, E. T.; Gmitro, A. F.; Kaylor, B.; Gillies, R. J. Acid-mediated tumor invasion: a multidisciplinary study. Cancer Res 2006, 66, (10), 5216-23.

7. Garcia-Martin, M. L.; Martinez, G. V.; Raghunand, N.; Sherry, A. D.; Zhang, S.; Gillies, R. J. High resolution pH(e) imaging of rat glioma using pH-dependent relaxivity. Magn Reson Med 2006, 55, (2), 309-15.

8. Gillies, R. J.; Raghunand, N.; Garcia-Martin, M. L.; Gatenby, R. A. pH imaging. A review of pH measurement methods and applications in cancers. IEEE Eng Med Biol Mag 2004, 23, (5), 57-64.

9. Reichert, M.; Steinbach, J. P.; Supra, P.; Weller, M. Modulation of growth and radiochemosensitivity of human malignant glioma cells by acidosis. Cancer 2002, 95, (5), 1113-

10. Moellering, R. E.; Black, K. C.; Krishnamurty, C.; Baggett, B. K.; Stafford, P.; Rain, M.; Gatenby, R. A.; Gillies, R. J. Acid treatment of melanoma cells selects for invasive phenotypes. Clin Exp Metastasis 2008, 25, (4), 411-25.

11. He, X.; Li, J.; An, S.; Jiang, C. pH-sensitive drug-delivery systems for tumor targeting. Ther Deliv 2013, 4, (12), 1499-510.

12. Budker, V.; Gurevich, V.; Hagstrom, J. E.; Bortzov, F.; Wolff, J. A. pH-sensitive, cationic liposomes: a new synthetic virus-like vector. Nat Biotechnol 1996, 14, (6), 760-4.

13. Chen, D.; Jiang, X.; Liu, J.; Jin, X.; Zhang, C.; Ping, Q. In vivo evaluation of novel pH-sensitive mPEG-Hz-Chol conjugate in liposomes: pharmacokinetics, tissue distribution, efficacy assessment. Artif Cells Blood Substit Immobil Biotechnol 2010, 38, (3), 136-42.

14. Han, L.; Guo, Y.; Ma, H.; He, X.; Kuang, Y.; Zhang, N.; Lim, E.; Zhou, W.; Jiang, C. Acid Active Receptor-Specific Peptide Ligand for In Vivo Tumor-Targeted Delivery. Small 2013.

15. Zhang, S.; Wu, K.; Sherry, A. D. A Novel pH-Sensitive MRI Contrast Agent. Angew Chem Int Ed Engl 1999, 38, (21), 3192-3194.

16. Andreev, O. A.; Engelman, D. M.; Reshetnyak, Y. K. pH-sensitive membrane peptides (pHLIPs) as a novel class of delivery agents. Mol Membr Biol 2010, 27, (7), 341-52.

17. Andreev, O. A.; Engelman, D. M.; Reshetnyak, Y. K. Targeting diseased tissues by pHLIP insertion at low cell surface pH. Front Physiol 2014, 5, 97.

18. Weerakkody, D.; Moshnikova, A.; Thakur, M. S.; Moshnikova, V.; Daniels, J.; Engelman, D. M.; Andreev, O. A.; Reshetnyak, Y. K. Family of pH (low) insertion peptides for tumor targeting. Proc Natl Acad Sci U S A 2013, 110, (15), 5834-9.

19. Karabadzhak, A. G.; Weerakkody, D.; Wijesinghe, D.; Thakur, M. S.; Engelman, D. M.; Andreev, O. A.; Markin, V. S.; Reshetnyak, Y. K. Modulation of the pHLIP transmembrane helix insertion pathway. Biophys J 2012, 102, (8), 1846-55.

20. Andreev, O. A.; Karabadzhak, A. G.; Weerakkody, D.; Andreev, G. O.; Engelman, D. M.; Reshetnyak, Y. K. pH (low) insertion peptide (pHLIP) inserts across a lipid bilayer as a helix and exits by a different path. Proc Natl Acad Sci U S A 2010, 107, (9), 4081-6.

21. Yao, L.; Daniels, J.; Wijesinghe, D.; Andreev, O. A.; Reshetnyak, Y. K. pHLIP(R)-mediated delivery of PEGylated liposomes to cancer cells. J Control Release 2013, 167, (3), 228-237.

22. Yao, L.; Daniels, J.; Moshnikova, A.; Kuznetsov, S.; Ahmed, A.; Engelman, D. M.; Reshetnyak, Y. K.; Andreev, O. A. pHLIP peptide targets nanogold particles to tumors. Proc Natl Acad Sci U S A 2013, 110, (2), 465-70.

23. Wijesinghe, D.; Arachchige, M. C.; Lu, A.; Reshetnyak, Y. K.; Andreev, O. A. pH dependent transfer of nano-pores into membrane of cancer cells to induce apoptosis. Sci Rep 2013, 3, 3560.

24. Moshnikova, A.; Moshnikova, V.; Andreev, O. A.; Reshetnyak, Y. K. Antiproliferative effect of pHLIP-amanitin. Biochemistry 2013, 52, (7), 1171-8.

25. Daumar, P.; Wanger-Baumann, C. A.; Pillarsetty, N.; Fabrizio, L.; Carlin, S. D.; Andreev, O. A.; Reshetnyak, Y. K.; Lewis, J. S. Efficient (18)F-Labeling of Large 37-Amino-Acid pHLIP Peptide Analogues and Their Biological Evaluation. Bioconjug Chem 2012, 23, (8), 1557-66.

26. Reshetnyak, Y. K.; Yao, L.; Zheng, S.; Kuznetsov, S.; Engelman, D. M.; Andreev, O. A. Measuring tumor aggressiveness and targeting metastatic lesions with fluorescent pHLIP. Mol Imaging Biol 2011, 13, (6), 1146-56.

27. Vavere, A. L.; Biddlecombe, G. B.; Spees, W. M.; Garbow, J. R.; Wijesinghe, D.; Andreev, O. A.; Engelman, D. M.; Reshetnyak, Y. K.; Lewis, J. S. A novel technology for the imaging of acidic prostate tumors by positron emission tomography. Cancer Res 2009, 69, (10), 4510-6.

28. Macholl, S.; Morrison, M. S.; Iveson, P.; Arbo, B. E.; Andreev, O. A.; Reshetnyak, Y. K.; Engelman, D. M.; Johannesen, E. In vivo pH imaging with (99m)Tc-pHLIP. Mol Imaging Biol 2012, 14, (6), 725-34.

29. Serganova, I.; Rizwan, A.; Ni, X.; Thakur, S. B.; Vider, J.; Russell, J.; Blasberg, R.; Koutcher, J. A. Metabolic imaging: a link between lactate dehydrogenase A, lactate, and tumor phenotype. Clin Cancer Res 2011, 17, (19), 6250-61.

30. Andreev, O. A.; Dupuy, A. D.; Segala, M.; Sandugu, S.; Serra, D. A.; Chichester, C. O.; Engelman, D. M.; Reshetnyak, Y. K. Mechanism and uses of a membrane peptide that targets tumors and other acidic tissues in vivo. Proc Natl Acad Sci U S A 2007, 104, (19), 7893-8.

31. Hutchinson, J. N.; Muller, W. J. Transgenic mouse models of human breast cancer. Oncogene 2000, 19, (53), 6130-7.

32. Guy, C. T.; Cardiff, R. D.; Muller, W. J. Induction of mammary tumors by expression of polyomavirus middle T oncogene: a transgenic mouse model for metastatic disease. Mol Cell Biol 1992, 12, (3), 954-61.

33. Lin, E. Y.; Jones, J. G.; Li, P.; Zhu, L.; Whitney, K. D.; Muller, W. J.; Pollard, J. W. Progression to malignancy in the polyoma middle T oncoprotein mouse breast cancer model provides a reliable model for human diseases. Am J Pathol 2003, 163, (5), 2113-26.

34. Cheng, G. M.; To, K. K. Adverse Cell Culture Conditions Mimicking the Tumor Microenvironment Upregulate ABCG2 to Mediate Multidrug Resistance and a More Malignant Phenotype. ISRN Oncol 2012, 2012, 746025.

35. Gatenby, R. A.; Silva, A. S.; Gillies, R. J.; Frieden, B. R. Adaptive therapy. Cancer Res 2009, 69, (11), 4894-903.

36. Tao, K.; Fang, M.; Alroy, J.; Sahagian, G. G. Imagable 4T1 model for the study of late stage breast cancer. BMC Cancer 2008, 8, 228.

37. Yang, J.; Mani, S. A.; Donaher, J. L.; Ramaswamy, S.; Itzykson, R. A.; Come, C.; Savagner, P.; Gitelman, I.; Richardson, A.; Weinberg, R. A. Twist, a master

regulator of morphogenesis, plays an essential role in tumor metastasis. Cell 2004, 117, (7), 927-39.

38. Eckhardt, B. L.; Parker, B. S.; van Laar, R. K.; Restall, C. M.; Natoli, A. L.; Tavaria, M. D.; Stanley, K. L.; Sloan, E. K.; Moseley, J. M.; Anderson, R. L. Genomic analysis of a spontaneous model of breast cancer metastasis to bone reveals a role for the extracellular matrix. Mol Cancer Res 2005, 3, (1), 1-13.

39. Cruz-Monserrate, Z.; Roland, C. L.; Deng, D.; Arumugam, T.; Moshnikova, A.; Andreev, O. A.; Reshetnyak, Y. K.; Logsdon, C. D. Targeting pancreatic ductal adenocarcinoma acidic microenvironment. Sci Rep 2014, 4, 4410.

Figures

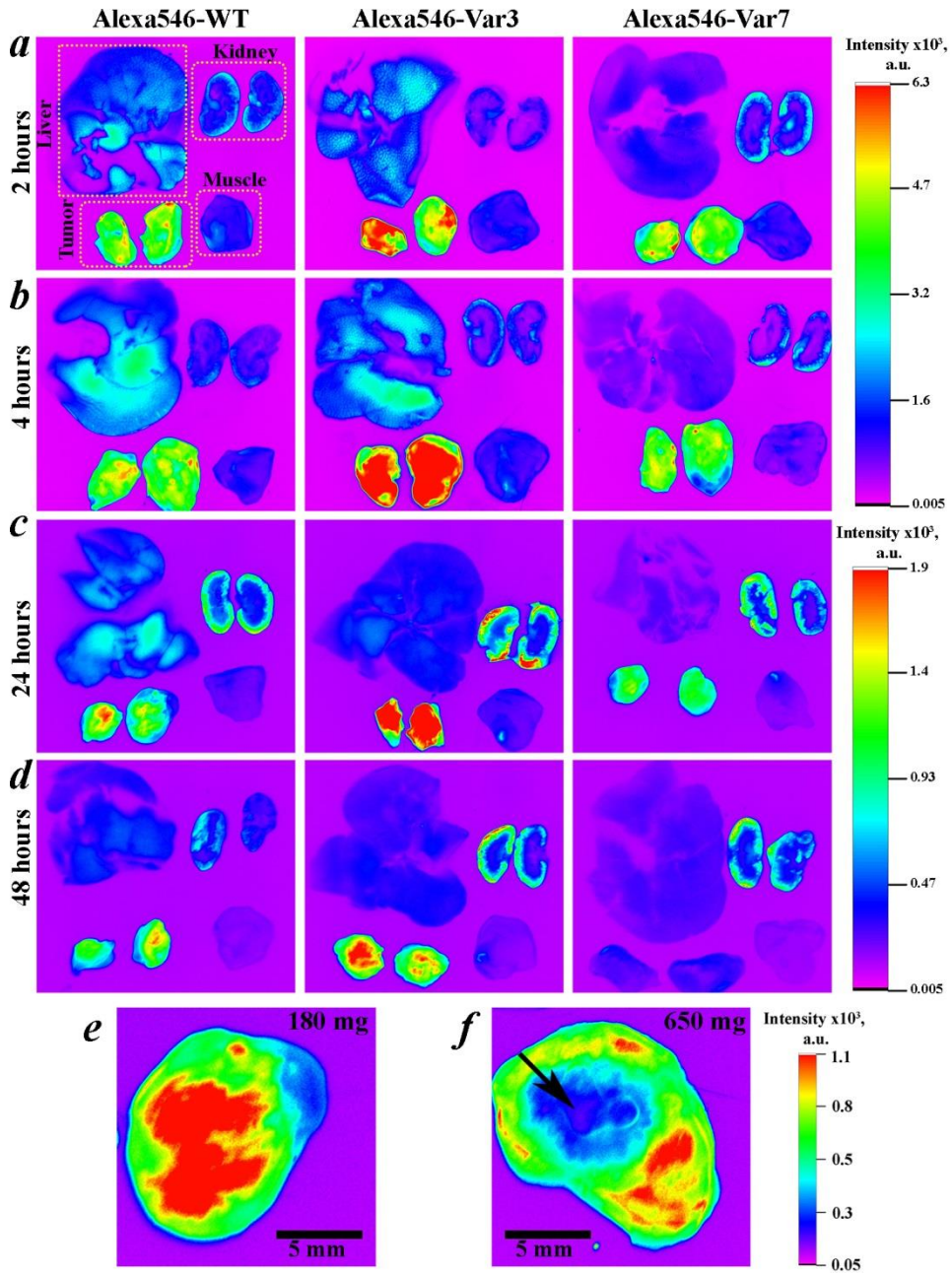

Figure 1. Distribution of pHLIPs in small breast 4T1 tumors, muscle, kidney and liver. Fluorescent images of organs obtained at 2 hrs (*a*), 4 hrs (*b*), 24 hrs (*c*) and 48 hrs (*d*) after i.v. administration of WT, Var3 and Var7 peptides conjugated with Alexa546 are shown. Distribution of pHLIPs is different in small (*e*) and big (*f*) 4T1

tumors (tumor mass is indicated in upper right corner). The necrotic region of the big breast 4T1 tumor is indicated by arrow.

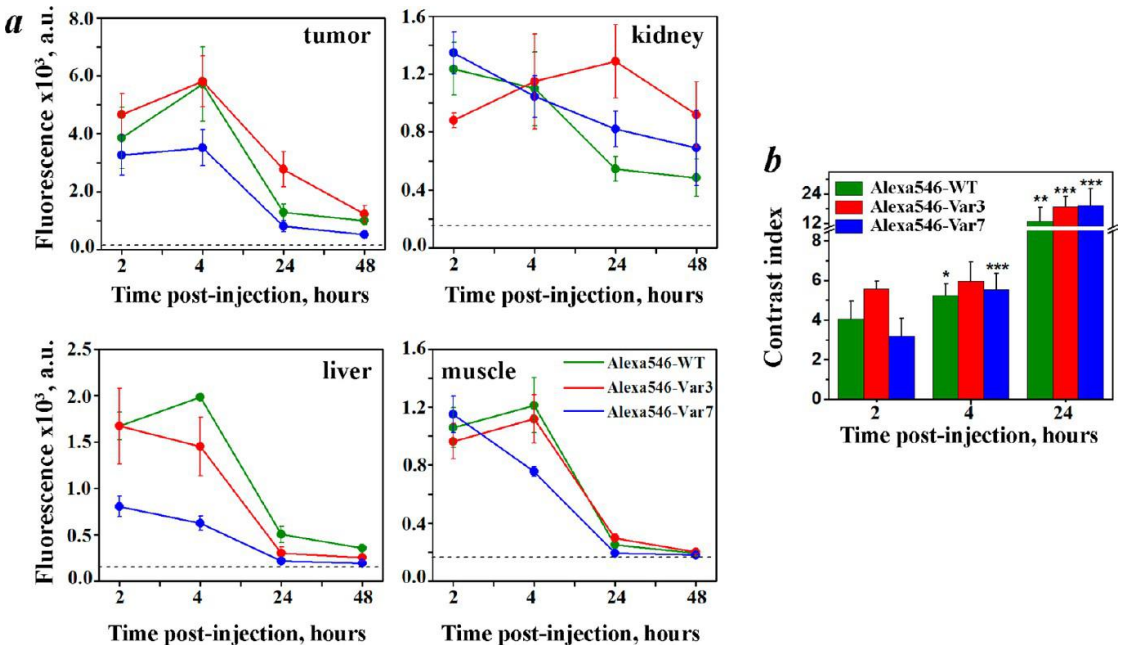

Figure 2. Time-dependent biodistribution of Alexa546-pHLIPs quantified by *ex-vivo* mean fluorescence in breast 4T1 tumors, muscle, kidney and liver (*a*). Contrast index was calculated for the breast 4T1 tumors (*b*). The values are given in Supplementary Tables 1 and 2.

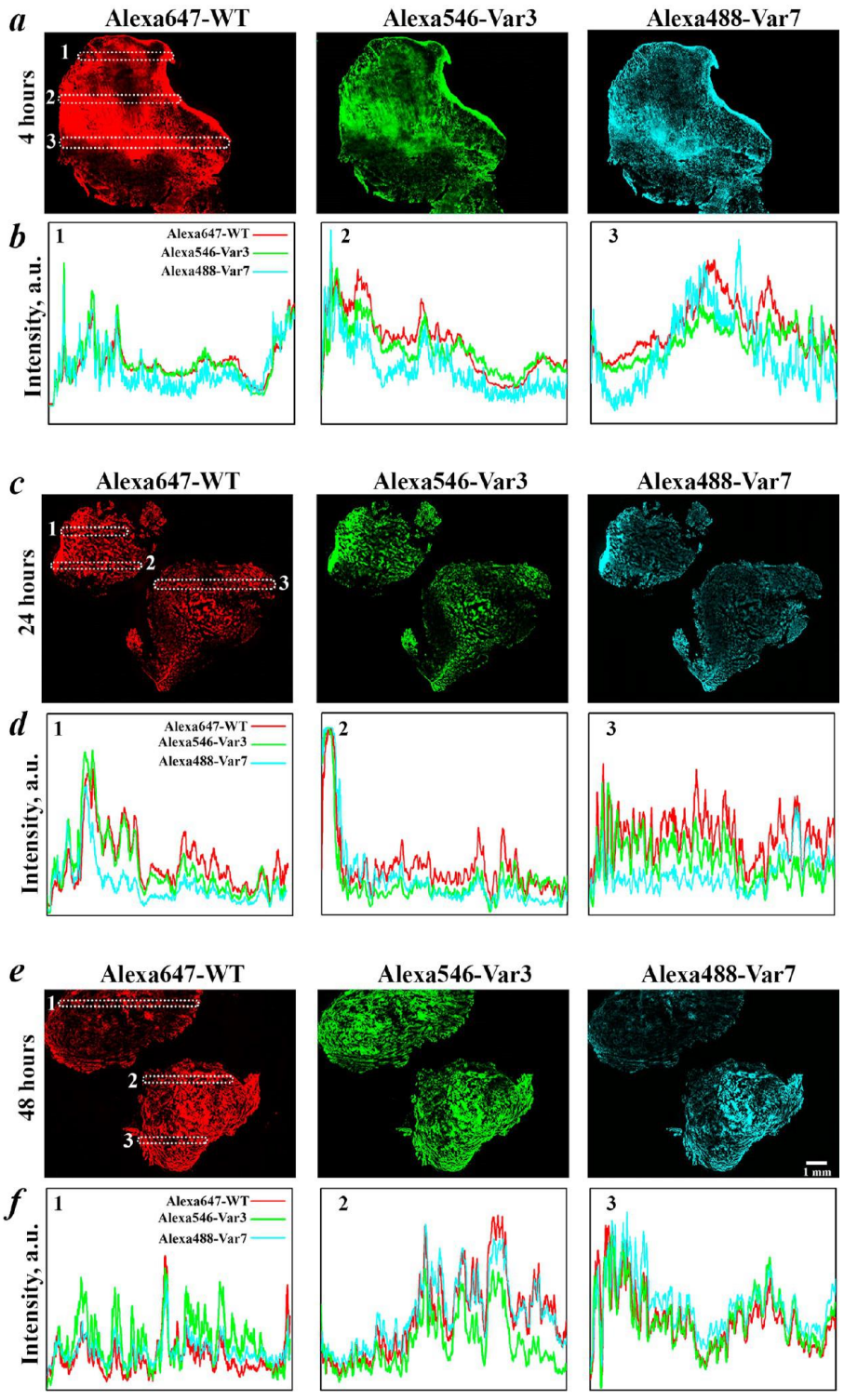

Figure 3. pHLIPs distribution in breast 4T1 tumors. Fluorescence images of tumor sections for 4 hrs (*a*), 24 hrs (*c*) and 48 hrs (*e*) post-injections of cocktail of Alexa647-

WT, Alexa546-Var3 and Alexa488-Var7 are shown. Intensity profiles of the fluorescent signal of various pHLIPs in the different lines are shown in *b, d, f.*

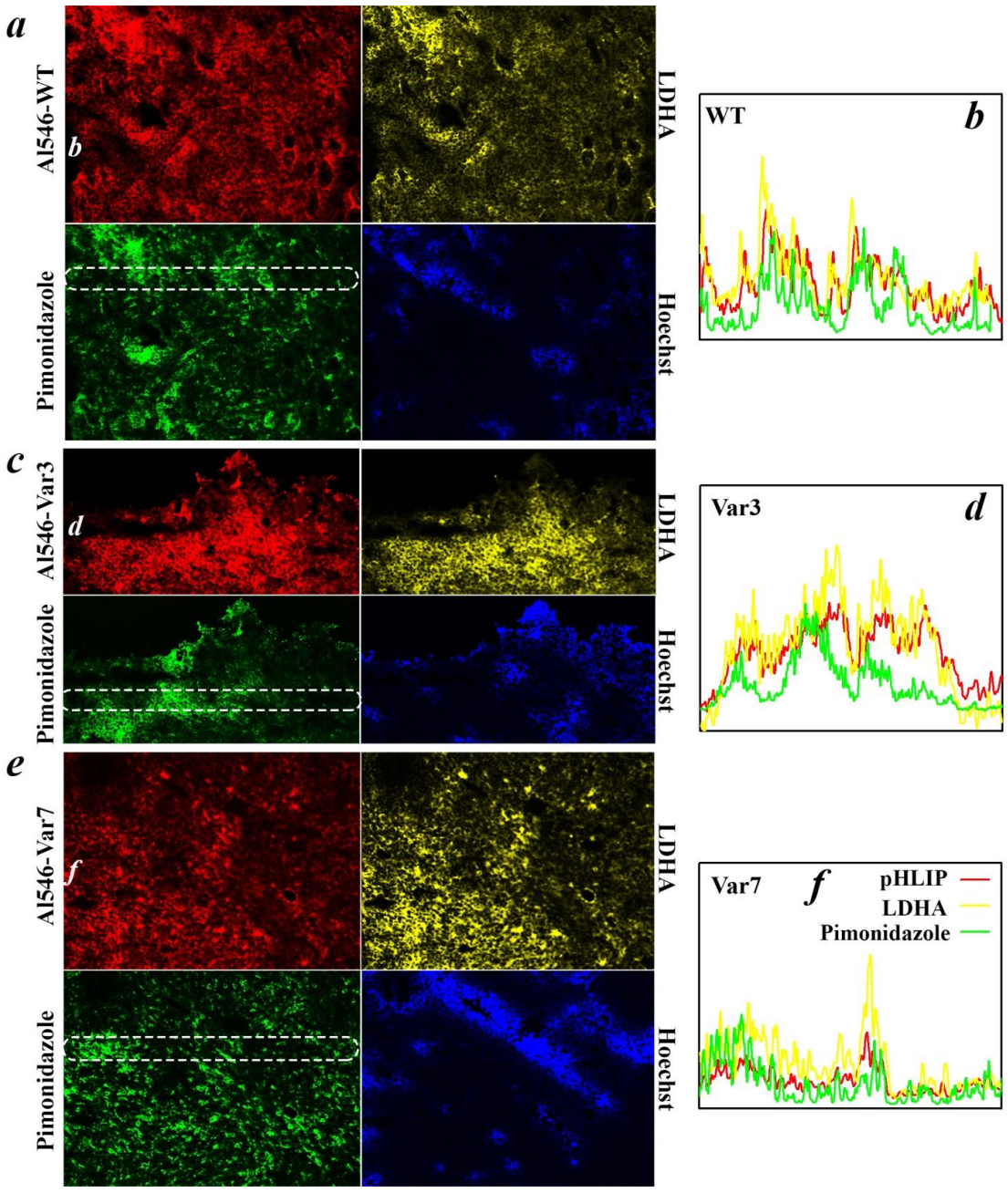

Figure 4. Immunohistochemical staining of 4T1 tumors. pHLIPs distribution (Alexa546-pHLIPs, red), LDHA staining (yellow), hypoxia (Pimonidazole, green) and blood flow (Hoechst, blue), are compared on tumor sections (*a, c, e*). Intensity profiles of the fluorescent signals in the highlighted regions are shown on *b, d, f*.

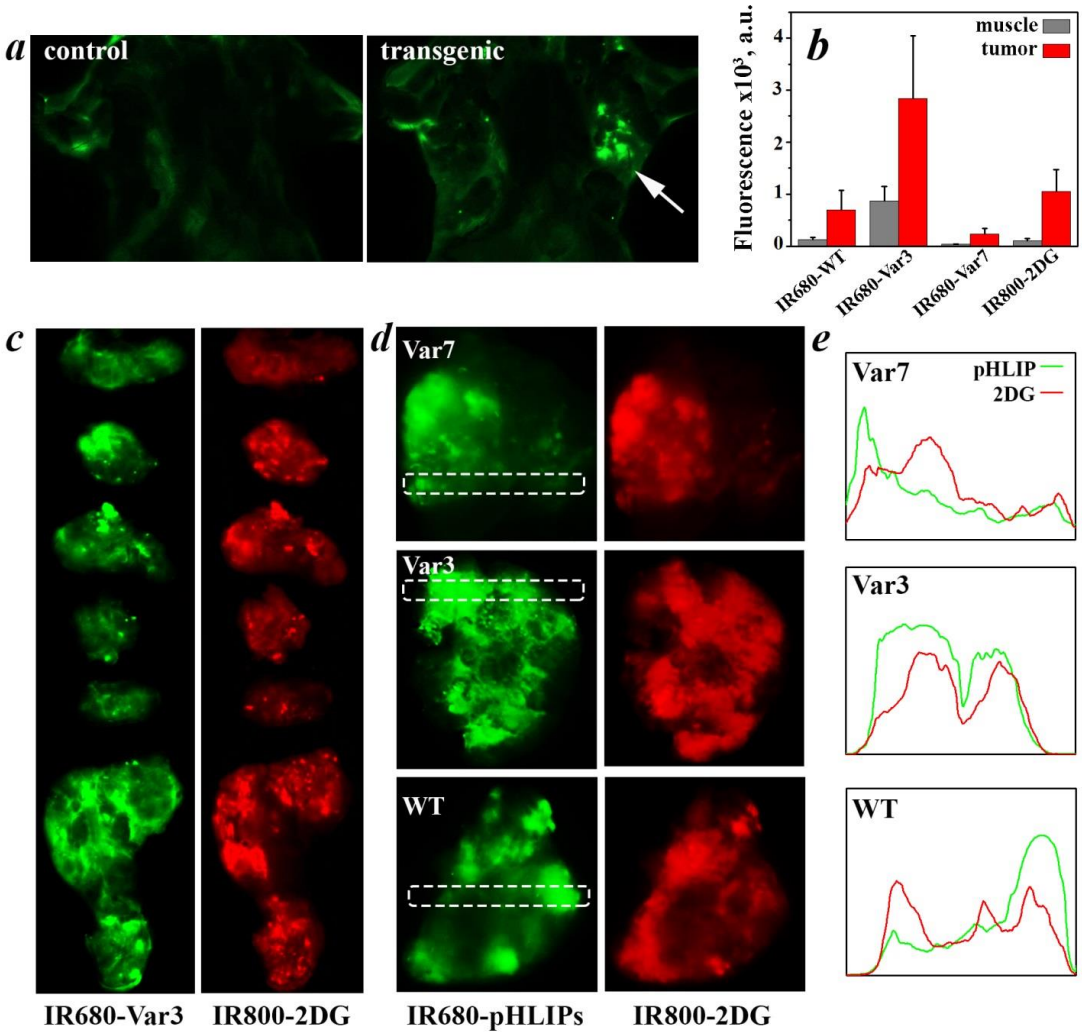

Figure 5. Tumor targeting by IR680-pHLIPs and IR800-2DG in transgenic mice. Whole-body NIR fluorescence images of control and transgenic mice were obtained at 24 hrs after i.v. administration of IR680-pHLIP, tumor is indicated by arrow (*a*). Averaged mean fluorescence of IR680-pHLIPs and IR800-2DG in tumors and muscle is calculated (*b*). Distributions of IR680-pHLIPs (green) and IR800-2DG (red) in breast tumors are compared (*c, d*). Intensity profiles of the fluorescent pHLIPs and glucose in the highlighted regions are shown on *e*.

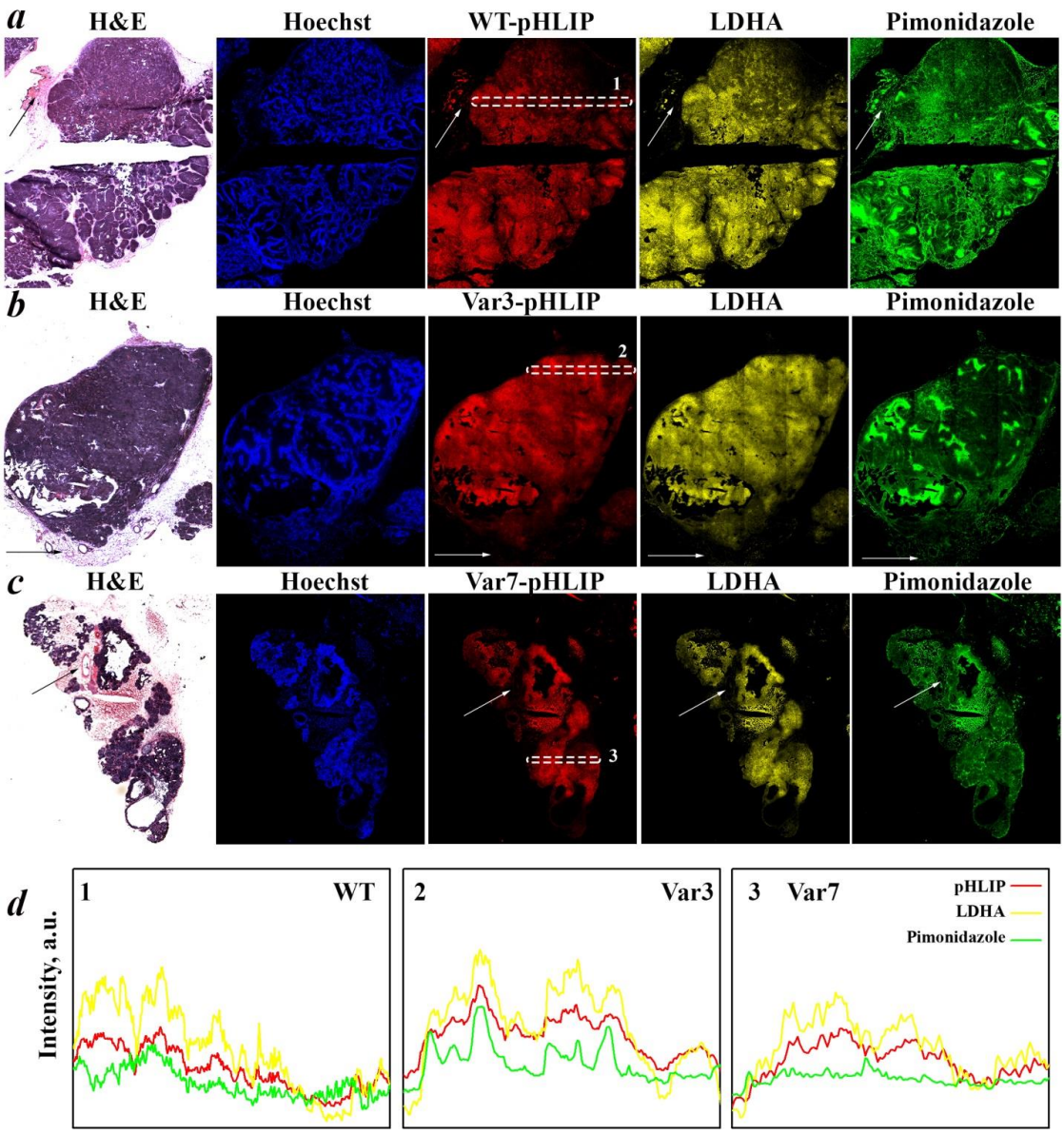

Figure 6. Immunohistochemical staining of tumors from transgenic mice. Histology (H&E), blood flow (Hoechst, blue), pHLIPs distribution (Alexa546-pHLIPs, red), LDHA staining (yellow) and hypoxia (Pimonidazole, green) are compared on tumor sections (*a, b, c*). The non-cancerous regions are indicated by arrows. Intensity profiles of the fluorescent signals in the highlighted regions are shown on *d*.

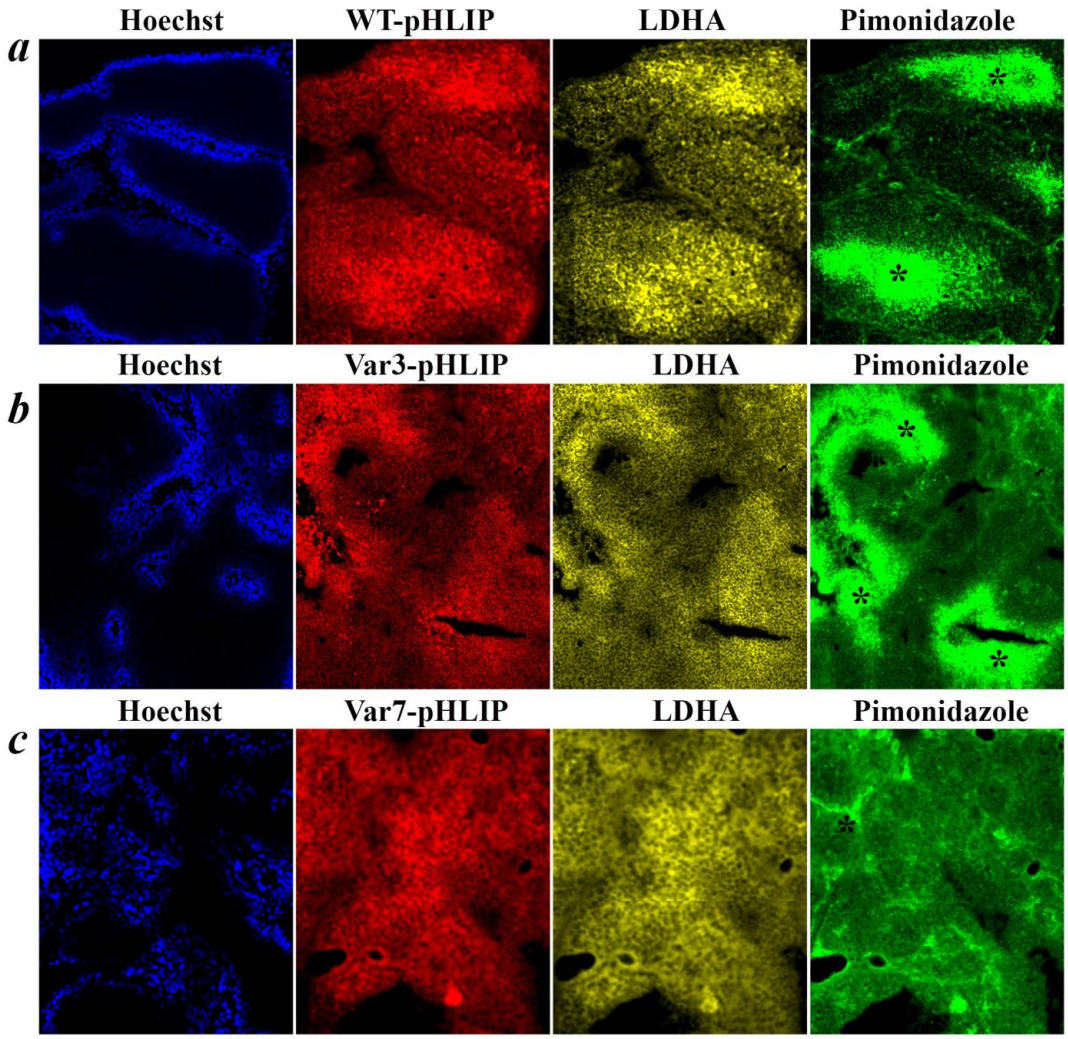

Figure 7. Magnified images of sections of breast tumors from transgenic mice. Blood flow (Hoechst, blue), pHLIPs distribution (Alexa546-pHLIPs, red), LDHA staining (yellow) and hypoxia (Pimonidazole, green) are compared on tumor sections (*a*, *b*, *c*). Hypoxic regions indicated by stars.

SUPPORTING INFORMATION

Targeting Breast Tumors with pH (Low) Insertion Peptides

Ramona-Cosmina Adochite, Anna Moshnikova, Sean D. Carlin, Renato A. Guerrieri, Oleg A. Andreev, Jason S. Lewis, Yana K. Reshetnyak

Table S1. Mean fluorescence (and St. D.) of 4T1 mammary tumors, muscle, kidney and liver. The control means mice injected with the The data are shown on Figure 2a. The p-level values (shown by asterisks) were calculated based on the two-tailed test between mean of fluorescence in tumor vs muscle, liver and kidney at various time points for different pHLIPs. The signal in tumor is statistically significantly higher compared to the signal in organs, except Var7 signal in kidney at 24 and 48 hrs.

Organs	Time post-injection	WT n= 6	Var3 n= 6	Var7 n= 6	Auto-fluorescence n = 4
Tumor	**2 h**	3856.7 ± 1058.5	4664.5 ± 720.4	3267.1 ± 689.9	
	4 h	5716.8 ± 1284.8	5809.9 ± 880.4	3514.1 ± 622.9	163.1 ± 19.4
	24 h	1287.1 ± 290.4	2773.0 ± 600.3	810.4 ± 196.2	
	48 h	999.5 ± 129.8	1229.6 ± 281.9	516.7 ± 128.9	
Muscle	**2 h**	1057 ± 137.8 (***)	963.4 ± 120.8 (***)	1150.2 ± 126.6 (***)	
	4 h	1212.0 ± 189.4 (***)	1117.9 ± 167.3 (***)	757.0 ± 34.9 (***)	146.7 ± 8.4
	24 h	294.4 ± 23.2 (***)	297.7 ± 28.6 (***)	191.2 ± 8.3 (***)	
	48 h	193.6 ± 18.1 (***)	201.1 ± 13.3 (***)	179.4 ± 16.1 (***)	
Liver	**2 h**	1671.7 ± 148.7 (***)	1670.3 ± 409.5 (***)	805.8 ± 112.4 (***)	
	4 h	1984.0 ± 27.9 (***)	1448.7 ± 317.7 (***)	623.6 ± 77.2 (***)	149.8 ± 5.8
	24 h	502.5 ± 85.5 (***)	303.4 ± 64.4 (***)	217.0 ± 21.8 (***)	
	48 h	357.2 ± 24.5 (***)	254.9 ± 37.2 (***)	193.6 ± 20.6 (***)	
Kidney	**2 h**	1235.5 ± 182.2 (***)	880.3 ± 51.2 (***)	1346.8 ± 145.8 (***)	
	4 h	1099.2 ± 254.3 (***)	1148.4 ± 326.7 (***)	1045.2 ± 144.4 (***)	164.7 ± 2.0
	24 h	544.8 ± 85.9 (***)	12887 ± 253.3 (***)	821.3 ± 122.5 (ns)	
	48 h	485.4 ± 126.5 (***)	918.5 ± 225.9 (*)	690.5 ± 259.6 (ns)	

Table S2. Contrast index calculated based on the data presented in Table 1. The data are shon on Figure 2b. Table contains Mean values and St.D.

Time post-injection	**WT n= 6**	**Var3 n= 6**	**Var7 n= 6**
2h	4.1 ± 0.9	5.6 ± 0.4	3.2 ± 0.9
4h	5.2 ± 0.6	5.9 ± 0.9	5.5 ± 0.8
24h	12.8 ± 5.7	18.8 ± 4.2	19.1 ± 7.2

Table S3. Mean fluorescence (and St.D.) are given. The ***n*** is the number of cases. The data are plotted on Figure 2a

Organs	**IR680-WT**	**IR680-Var3**	**IR680-Var7**	**IR800-2DG**
Muscle	130.8 ± 33.4 (n = 3)	867.5 ± 276.7 (n = 3)	40.04 ± 0.49 (n = 3)	99.4 ± 51.8 (n = 9)
Tumor	694.6 ± 381.7 (n = 33)	2834.2 ± 1213.1 (n = 29)	233.3 ± 106.3 (n = 33)	1050.1 ± 422.5 (n = 99)

AUTHOR INFORMATION

Corresponding Author

The correspondence should be addressed to Yana K. Reshetnyak, 2 Lippitt Rd., Kingston, RI 02881, reshetnyak@mail.uri.edu

Funding Sources

The work was supported by the RI-INBRE summer undergraduate fellowship to RG; NIH grants CA138468 to JL and YKR; CA133890 and GM073857 to OAA, YKR. Masspec was done in RI-INBRE core facility funded by NCRR /NIH P20RR016457.

ACKNOWLEDGMENT

We are very grateful to Prof. David E. Wazer, Department of Radiation Oncology, and Prof. Yihong Wang, Department of Pathology, both from the Rhode Island Hospital for helpful discussions.

ABBREVIATIONS

2DG, 2-deoxy-glucose; CCD, charge-couples device; CI, contrast index; DMF, dimethylformamide; FDG, 2-deoxy-2-fluoro-D-glucose; FITC, fluorescein isothiocyanate; HPLC, high pressure liquid chromatography; hrs, hours; IR, infrared; LHDA, lactate dehydrogenase A; MRSI, magnetic resonance spectroscopic imaging; NIH, National Institute of Health; PET, positron emission tomography; pHLIP, pH Low Insertion Peptide; RMPI, Roswell Park Memorial Institute medium; SELDI-TOF, surface enhanced laser desorption/ionization time-of-flight; SPECT, single photon emission computed tomography; Var, variant; WT, wild type.

CHAPTER 2

Published in ACS Chemical Biology on 21st of November, 2014

pHLIP-FIRE, a Cell Insertion-Triggered Fluorescent Probe for Imaging Tumors Demonstrates Targeted Cargo Delivery In Vivo

Alexander G. Karabadzhak[1], Ming An[2], Lan Yao[3], Rachel Langenbacher[2], Anna Moshnikova[4], Ramona-Cosmina Adochite[4], Oleg A. Andreev[4], Yana K. Reshetnyak[4], Donald M. Engelman[1]

[1] Department of Molecular Biophysics and Biochemistry, Yale University, New Haven, CT 06511

[2] Department of Chemistry, State University of New York, Binghamton University, Binghamton, NY 13902

[3] Department of Physics, Applied Physics and Astronomy, State University of New York, Binghamton University, Binghamton, NY 13902

[4] Department of Physics, University of Rhode Island, Kingston, RI 02881

Corresponding author

Donald M. Engelman, Department of Molecular Biophysics and Biochemistry, Yale University, 266 Whitney Ave., New Haven, CT, 06511, USA, Phone: (203) 432-5601, Fax: (203) 432-6381, e-mail: donald.engelman@yale.edu

Abstract

We have developed an improved tool for imaging acidic tumors by reporting the insertion of a transmembrane helix: the pHLIP-Fluorescence Insertion REporter (pHLIP-FIRE). In acidic tissues, such as tumors, peptides in the pHLIP family insert as α-helices across cell membranes. The cell-inserting end of the pHLIP-FIRE peptide has a fluorophore-fluorophore or fluorophore-quencher pair. A pair member is released by disulfide cleavage after insertion into the reducing environment inside a cell, resulting in de-quenching of the probe. Thus, the fluorescence of the pHLIP-FIRE probe is enhanced upon cell-insertion in the targeted tissues, but is suppressed elsewhere due to quenching. Targeting studies in mice bearing breast tumors show strong signaling by pHLIP-FIRE, with a contrast index of ~ 17, demonstrating (i) direct imaging of pHLIP insertion and (ii) cargo translocation *in vivo*. Imaging and targeted cargo delivery should each have clinical applications**.**

Introduction

Imaging technologies are an important focus for improving the diagnosis of cancer, and for guiding surgical and radiation therapies. Among the new tools, perhaps the greatest recent growth has come in the field of fluorescence imaging, with numerous new technologies now being adapted for clinical use[1, 2]. One promising approach is the targeting of tumor biomarkers with fluorescent agents, allowing surgeons to visualize tumors in real-time during an operation. This advance has the potential to improve the success of surgical interventions by giving an active real-time marker of tumor borders, which are often hard to distinguish from the surrounding healthy tissue[3]. The primary goal in imaging-agent design is a high target-to-background ratio: agents should contribute minimal background, but have high local concentrations at intended target sites. The "self" nature of targeted markers often leads to background signals too high for effective discrimination of tumors. A further complication lies in the diverse nature of human cancers. Since heterogeneous marker expression is often found within regions of a tumor, and further since no two cancers are identical, it is unlikely that a single marker can be relied upon[4].

As an alternative to biomarker targeting, we have suggested that the acidic environment within solid tumors may be exploited for targeting by the pH (Low) Insertion Peptide (pHLIP) family[5]. Malignant tumors exhibit elevated uptake and consumption of glucose, as well as metabolite buildup and hypoxia due to inadequate blood supply, leading to tumor acidosis from the Pasteur and Warburg effects[6-8]. As a result, the extracellular environment in virtually all solid tumors is acidic (pH ~ 6.0 -

6.5)[9, 10], and more aggressive tumors are more acidic [11]. Extracellular acidity may therefore be a general biomarker for targeting malignant tumors.

The original pHLIP is a 36-amino-acid peptide, and a number of versions with different properties have now been found that constitute the family of pHLIPs[5]. A pHLIP exists as a soluble, unstructured monomer with an affinity for cell membranes at physiological pH. The adsorption to a model POPC membrane at high pH is accompanied by the release of about 5-7 kcal mol^{-1} of energy[5, 12]. At low pH (pH $\leq$ ~6), pHLIP folds to form a transmembrane α-helix, inserting its C-terminus across the cell membrane. The transition proceeds with an additional release of 1.5-2 kcal mol^{-1} of energy. This pH-dependent insertion is triggered by protonation of carboxyl groups on residues in the peptide transmembrane region and peptide inserting end. The protonation effectively increases the overall hydrophobicity of pHLIP, permitting the insertion[13]. Serendipitously, the extracellular pH at which pHLIP undergoes its insertion transition corresponds closely to the extracellular pH produced in acidic solid tumors. Using peptides covalently modified with fluorescent dyes at the non-inserting N-terminus, pHLIP has been shown to target both spontaneous and implanted tumors in small animal models, although slow background clearance has limited the contrast ratios that can be attained[14-18]. The insertion energy can be used to deliver cargo molecules into cells, by biasing the equilibrium between surface and inserted forms in favor of the transport of cell-impermeable polar molecules attached to the C-terminus[19-21]. While such delivery has been explored in cells, the step of demonstrating cytoplasmic delivery in tumors in an animal had not been taken before the work we report here.

To improve contrast and to document transmembrane insertion delivery *in vivo*, we have developed the pHLIP Fluorescence Insertion REporter system (pHLIP-FIRE), with the main goal as enhancing fluorescent signal upon insertion into cells in diseased tissue. pHLIP-FIRE peptides possess neighboring lysine and cysteine residues in the cell-inserting, C-terminal end. The lysine side-chain is irreversibly covalently linked to a fluorophore via an amide bond. The neighboring cysteine side-chain is covalently linked by a disulfide bond to a fluorescence quencher or another fluorophore (for self-quenching). When these moieties are both present on the peptide, the fluorescence is quenched, but upon insertion of the C-terminus into the reducing environment of a living cell, the quenching moiety is released by disulfide reduction, leading to the dequenching of the fluorophore emission (Figure 1). The pHLIP-FIRE strategy aims to increase the contrast of fluorescence imaging *in vivo* by quenching background signals. We report tumor imaging with improved sensitivity, as well as demonstrating for the first time pHLIP insertion and cargo delivery *in vivo*.

Results and Discussion

Our strategy of pHLIP-FIRE is based on fluorescence quenching, which occurs upon close proximity of either two fluorophores (homo-quenching and H-dimer formation) or a fluorophore-quencher pair (hetero-quenching). When one of the members of a pair is released, in our case by disulfide cleavage in the cytoplasm, the result is greatly enhanced observable fluorescence. Accordingly, we designed and synthesized two pHLIP-FIRE constructs. The first construct, pHLIP-T-T, carries two TAMRA fluorophores that are self-quenched by forming an H-dimer, with one attached to pHLIP via a disulfide bond. The second construct, pHLIP-T-Q, has a TAMRA-QSY9

pair, where the quencher (QSY9) is attached to pHLIP via a disulfide bond. To control for quenching activity, a pHLIP with a single, unquenched TAMRA dye covalently linked to a C-terminal cysteine via a thioether bond was also synthesized and tested. The constructs used in this study are as follows:

pHLIP-T-T:

AAEQNPIYWARYADWLFTTPLLLLDLALLVDADEGT**K(TAMRA)C(TAMRA)**G

pHLIP-T-Q:

AAEQNPIYWARYADWLFTTPLLLLDLALLVDADEGT**K(TAMRA)C(QSY9)**G

pHLIP-T:

AAEQNPIYWARYADWLFTTPLLLLDLALLVDADEGT**C(TAMRA)**

Chemical fluorescence dequenching. The spectral properties of each pHLIP-FIRE construct were investigated in solution in the absence and presence of a reducing agent. Glutathione (GSH) is the primary reducing agent in living cells, with an intracellular concentration of up to 10 mM, depending upon the intracellular compartment and the cell cycle[22]. We used 1, 3, or 10 mM concentrations of glutathione to simulate reductive and physiologically reasonable intracellular conditions. pHLIP-FIRE dequenching was observed by absorbance and fluorescence spectroscopy. The absorbance peak of the TAMRA-TAMRA H-type dimer (in pHLIP-T-T) is blue-shifted to 524 nm from the usual monomer TAMRA absorbance maximum at 555 nm[23]. The blue-shifted TAMRA-TAMRA dimer absorbance peak was replaced by an augmented 555 nm TAMRA peak following disulfide reduction in the pHLIP-T-T peptide with 10 mM glutathione. As expected, in contrast to pHLIP-T-T, the shape of the absorbance spectrum of pHLIP-T-Q does not change significantly

after the cleavage of the S-S bond and resulting quencher separation (Figure 2a). The activation of the pHLIP-T-Q and pHLIP-T-T probes were each monitored by changes in the TAMRA fluorescence signal. After incubation with 10 mM glutathione, the pHLIP-T-Q or pHLIP-T-T fluorescence was excited at 555 nm, and emission was followed at its 580 nm maximum (Figure 2b). An increase in emission intensity was observed over time following the addition of glutathione (1, 3, or 10 mM). Fluorescence intensity was plotted as a function of time and fit using a single exponential function (Figure 2d). The fluorescence of each pHLIP-FIRE construct was significantly quenched when compared to the emission of pHLIP-T (Figure 2c). The addition of glutathione did not alter the fluorescence intensity of pHLIP-T, whereas a 7 to 18-fold increase in fluorescence intensity was observed for the pHLIP-FIRE constructs after 3 hours. Our data show the expected higher dequenching signal for pHLIP-T-T compared to pHLIP-T-Q, since two moles of TAMRA are dequenced in the T-T case. The kinetics of activation depend on the glutathione concentration: At 10 mM GSH, the rates are k = 4.7 hr^{-1} and 3.4 hr^{-1} for pHLIP-T-T and pHLIP-T-Q respectively, whereas at 1 mM GSH, the rates are k = 1.1 hr^{-1} and 0.4 hr^{-1} (Supplementary Table 1).

The pH-dependent interactions of pHLIP-FIRE peptides with artificial membranes were followed by Circular Dichroism (CD). Peptides were incubated with 100-nm POPC liposomes overnight in pH 8 phosphate buffer and the pH was dropped rapidly to pH 4 by the addition of concentrated HCl. When measured alone in solution or in the presence of liposomes at pH 8, pHLIP-FIRE exhibited CD spectra characteristic of an unstructured peptide, with a negative ellipticity peak around 200 nm. When the pH

was dropped to 4, a characteristic CD α-helical signal was observed, with two negative ellipticity peaks at 208 nm and 222 nm and a positive peak at 195 nm. The CD data show that the pHLIP-FIRE constructs exhibit the three states of pH-dependent membrane insertion characteristic of pHLIP peptides (Figure 3).

pHLIP-FIRE activation in cultured cells. pH-triggered activation of each pHLIP-FIRE probe was tested in cultured cells grown at normal pH medium (HeLa and COS-7) or adapted for low pH growth (A549). HeLa and COS-7 cells were incubated with pHLIP-FIRE peptides (1 μM) for 20 minutes at room temperature (~ 22°C) either at pH 7.4 or at pH 6.1 DPBS buffer in 96-well plates. Cells were then washed three times with DPBS buffer (pH 7.4 or pH 6.1) and DMEM (pH 7.4 or pH 6.1) was added before measurements were performed at each experimental pH. TAMRA fluorescence was measured immediately after washing (time zero used for normalization), then at multiple time points for up to two days following the incubation and wash steps. TAMRA fluorescence intensity steadily increased over two days following incubation at low pH conditions to a maximum intensity of 16-fold over the zero time point. Higher TAMRA fluorescence signals (8-16 fold increase) were observed in cells (HeLa and COS-7) incubated with pHLIP-FIRE peptides at pH 6.1 as compared to the fluorescence increase following incubation and washing at pH 7.4 (2-4 fold increase) (Figure 4). Activation of the pHLIP-FIRE at neutral pH might occur due to *i*) membrane insertion of some amount of the construct at pH 7.2-7.4, since there is an equilibrium between inserted and surface locations of the peptide, or *ii*) endocytotic uptake of the peptide adsorbed at the membrane surface, especially since the time course of the experiment is several days, or both. The fluorescence data were fitted

with a single exponential non-linear regression. For constructs at low pH the rate constants were found to be ~ 0.8 – 1.38 hr^{-1} with a positive linear slope of 0.08 – 0.23 (Figure 5), similar to rates observed in the chemical dequenching experiments with glutathione concentrations from 1 – 3 mM (Supplementary Table 1). The linear component of the fitting signal may arise from a second population of pHLIP-FIRE, in which some other mechanism is involved, such as non-specific endocytotic uptake of the constructs, producing slow kinetics. Interestingly, the linear component of non-specific uptake is higher for HeLa cells than COS-7 cells, possibly indicating that different cell types internalize the peptide via different pathways and at different rates.

The A549 cells adapted to low pH growth were incubated with pHLIP-FIRE peptides (1 μM) or the unquenched control peptide, pHLIP-T (1 μM), for 20 minutes as described above, then washed cells were kept in culture at pH 6.1. Fluorescence was measured at intervals for four days after treatment. pHLIP-T showed no significant change in fluorescence (2-fold background increase) over the course of these measurements, whereas both pHLIP-T-T and pHLIP-T-Q showed an 8- to 10-fold increase in fluorescence at 74 hours after incubation (Figure 6). pHLIP itself doesn't show signs of toxicity in cells or animals[5, 21].

Confocal Microscopy of pHLIP-T-T Activation in Cells. We used confocal microscopy to visualize pH-dependent TAMRA release and distribution inside cultured cells. The cells were treated with 1 μM of pHLIP-T-T as described above. 30 minutes before imaging, the cells were treated with Hoechst to stain the nuclei. When C-terminuis of the construct is inside the cytoplasm we expect to see TAMRA fluorescence signal throughout the cytoplasm due to release of the disulfide linked

TAMRA. Confocal microscopy shows that this is the case at pH 6.1 but not at pH 7.4. Interestedly, we observed some "punctate" fluorescence at pH 7.4, which might be attributed to endocytic uptake of the construct by HeLa (Figure 7).

Imaging *in vivo*. Because of their pH-dependent interaction with membranes, pHLIP peptides have been shown to target and persistently label cells in acidic tissues, such as cancerous tumors, *in vivo* [24, 25]. pHLIP peptides have also been successfully used to translocate cell-impermeable molecules across the membranes of cultured cells in a pH-dependent manner [19, 20]. Here, we take the next step: demonstrating targeted delivery into tumor cells *in vivo*.

Balb/c mice bearing implanted 4T1 murine breast tumors were used to assess the tumor targeting and biodistribution properties of pHLIP-FIRE in comparison with pHLIP-T. Mouse tumors were established by subcutaneous injection of 4T1 cells (8 x 10^5 cells) in the right flank of each mouse. When tumors reached 5 to 6 mm in diameter, each of the pHLIP-FIRE peptides and the unquenched control pHLIP-T were given as single injections into the tail veins of groups of mice. Peptides were injected at ~1 mg/kg, with adjustments made to deliver equimolar dosages of the varied peptide constructs. Animals were euthanized at 24 or 48 hours following injection, and necropsy was performed immediately thereafter. Tumors and major organs were excised and imaged on an FX Kodak *in vivo* image station. Imaging was performed for each animal using a uniform set of illumination and exposure parameters in order to allow accurate comparison of the resulting intensities (Figure 8 *a*, *b*). The mean TAMRA-fluorescence intensities for pHLIP-FIRE constructs and for pHLIP-T are shown (Figure 8 *c*) and their numeric values are given in Supplementary

Table 2. Strong tumor targeting was observed in each case, with very little off-target labeling detected in muscle, heart, spleen and lungs. The fluorescence intensity was the highest in tumors labeled with pHLIP-T-Q and was the lowest in muscle for the pHLIP-T-T construct. Also, we observed an elevated uptake of the pHLIP-FIRE constructs in liver and kidneys compared to pHLIP-T.

To quantify improvement in tumor discrimination using the pHLIP-FIRE constructs as a result of the lower background we compared the fluorescence intensities of tumors and non-targeted muscle tissues and calculated contrast index (C.I.), defined as the corrected tumor to background ratio:

$$\mathrm{CI} = \frac{\mathrm{Fl}_{\mathrm{tumor}} - \mathrm{Fl}_{\mathrm{auto}}}{\mathrm{Fl}_{\mathrm{muscle}} - \mathrm{Fl}_{\mathrm{auto}}}$$

where Fl_{tumor}, Fl_{norm}, and Fl_{auto} are the mean fluorescence intensities of tumors, skeletal muscle, and the autofluorescence background signal from corresponding tissues in an untreated mouse, respectively.

The contrast index was substantially greater for the pHLIP-FIRE constructs than the unquenched pHLIP-T. After 24 hrs, the mean contrast indices were 11.7, 16.6, and 7.3 for pHLIP-T-T, pHLIP-T-Q and pHLIP-T respectively (Figure 8 *d*). Thus, we achieved over 2-fold improvement in contrast using pHLIP-T-Q compared with the unquenched fluorescent probe, pHLIP-T. Because the pHLIP-FIRE signal in the muscle is close to zero after 48-hours, we could not use C.I. as a parameter for quantitative measurement of the contrast. Division by a close-to-zero value results in high deviation in the mean value, which leads to statistically weak representation. However, we can calculate the ratio of average signals in tumor and muscle. These

parameters show similar values at both 48 and 24 hrs time points. From this we conclude at least the same contrast at 48 hrs as at 24 hrs.

Here, we report a new tool, pHLIP-FIRE, for improved tumor to muscle contrast, and use it to demonstrate pHLIP delivery into tumor cells using systemic administration *in vivo*. Our strategy is similar to the "molecular beacon", where a fluorophore-quencher pair is used to detect nucleic acid hybridization[26, 27]. In each system, fluorescence quenching can be achieved by the close proximity of either two fluorophores (homo-quenching and H-dimer formation as in the case of pHLIP-T-T) or of a fluorophore-quencher pair (hetero-quenching as in the case of pHLIP-T-Q). Our approach is based on targeting of a quenched fluorescent pHLIP-FIRE construct to acidic tumors and activation of the fluorescence by translocating the cargo dye into cells, where the reducing power of the cytosol triggers the enhanced fluorescence. Testing the pH dependent interaction of pHLIP-FIRE with POPC membranes and with cultured cells demonstrated pHLIP-like pH dependent properties and fluorescence dequenching. When incubated with cells, the constructs showed 8- to 16-fold increase in fluorescence with a time course of dequenching on the order of 1-2 days. These background experiments set the stage for use *in vivo.*

Experiments using i.v. administration in mice resulted in the selective delivery and activation of the pHLIP-FIREs in tumors. Biodistribution studies of pHLIP-FIREs showed the highest accumulation in tumor sites. Slightly elevated levels of pHLIP-FIRE constructs were seen in liver and kidneys compared with the control fluorescent pHLIP construct with a single TAMRA. The activation of pHLIP-FIRE in kidneys was expected, since the kidney is acidic, and labeling of kidneys by pHLIP has often

been seen. The increase of fluorescence in liver most probably indicates a difference in the biodistribution of pHLIP-FIREs compared to pHLIP-T. Because pHLIP-FIRE constructs contain two non-polar molecules (2 TAMRA or TAMRA plus QSY9), the increased overall hydrophobicity may facilitate liver uptake. Also, liver has the highest concentration of glutathione in the body, which may lead to a higher rate of dequenching [22]. In contrast with the cell-free and cellular dequenching results, pHLIP-T-T showed lower signal intensity compared to pHLIP-T-Q and pHLIP-T *in vivo*, which we think is most probably related to the difference in pharmacokinetics of the construct and the clearance time. Future designs may explore ways to reduce or avoid these problems by enhancing the polarity of pHLIP-FIRE, for example by adding polar groups to the pHLIP moiety or choosing more polar fluorophores/quenchers. Also, use of fluorescent dyes absorbing and emitting light at longer wavelengths than TAMRA will ensure better tissue penetration of light. However, we are mostly concerned with proof of principle in the present study, and the most important point is that a significant improvement in tumor-to-background ratio was achieved. A doubling of the contrast index for pHLIP-FIREs over non-quenched pHLIP-targeted imaging probes was observed, which allows better discrimination between healthy tissues and tumors, and points the way for further improvements.

The pHLIP-FIRE system has potential applications in fluorescence-guided surgery and may also have promise as a tool in cancer diagnosis. Not only have we improved the labeling contrast, but we have also shown targeted delivery of a model cargo (TAMRA or QSY9) into tumor cells *in vivo*, encouraging the further development of pHLIP for therapeutic applications in drug delivery.

Methods

Chemical syntheses of pHLIP-constructs. Detailed accounts of the chemical syntheses and characterizations of pHLIP-T, pHLIP-T-T, and pHLIP-T-Q constructs are provided in the supplementary information. The control pHLIP-T construct was synthesized by reacting the pHLIP-Cys peptide (AAEQNPIYWA-RYADWLFTTPLLLLDLALLVDADEGTC) with tetramethyl-rhodamine, 6-maleimide. The pHLIP-FIRE constructs, pHLIP-T-T and pHLIP-T-Q, were synthesized from the pHLIP-KC peptide (AAEQNPIYWA-RYADWLFTTP-LLLLDLALLV-DADEGT**KC**G). To produce pHLIP-T-T, first the C-terminal Cys sidechain of pHLIP-KC is derivatized as an aminoethyl disulfide. Subsequent treatment with 5-TAMRA SE conjugates TAMRA to the primary amines of both the Lys sidechain and the modified Cys sidechian. Synthesis of pHLIP-T-Q requires three steps: Reaction between QSY9 succinimidyl ester and *S*-(2-pyridylthio)cysteamine (step 1) provides a QSY9 derivative that is pre-activated towards disulfide exchange with pHLIP-KC (step 2), which furnishes the C-terminal Cys sidechain with the quencher QSY9 via a disulfide bond. Subsequent treatment of the intermediate with 5-TAMRA SE (step 3) conjugates TAMRA to the neighboring Lys sidechian via an amide bond. All intermediates and products were purified to greater than 90% purity using HPLC and their identities confirmed by molecular mass (via MALDI-TOF mass spectrometry to ± 2 dalton of expected mass).

Vesicle preparation. Large Unilammelar Vesicles (LUV) were prepared by extrusion. A required stock solution of POPC (1-palmitoyl-2-oleoyl-sn-glycero-3-phosphocholine, Avanti Polar Lipids, Inc.) in chloroform was concentrated under

reduced pressure on a rotary evaporator and dried under vacuum overnight. The dried lipid film was rehydrated in 10 mM phosphate buffer at pH 8.0, vortexed, and repeatedly extruded (25 times) through a membrane with a pore size of 100 nm (Avanti Mini-Extruder).

Chemical dequenching and Circular Dichroism measurements. Fluorescence measurements were performed on an ISS Spectrofluorimeter. TAMRA was excited at 560 nm and fluorescence was recorded from 565 nm to 615 nm with the spectral widths of the excitation and the emission slits at 4 nm and 8 nm respectively. Absorbance spectra were measured on Cary 100-Bio UV-Visible Spectrophotometer. The pHLIP-FIRE constructs were dissolved in 10 mM phosphate buffer (pH 8) at 1 μM concentration. To confirm the quenching mechanism, L-Glutathione (reduced form, Cayman Chemical Company) was added to the construct solution to achieve the desired final concentrations of the reducing agent (1, 3, or 10 mM). Before each experiment glutathione powder was flushed with nitrogen and then dissolved in pH 8.0 phosphate buffer. Circular Dichroism (CD) was performed on JASCO J-810 spectropolarimeter. Spectra were recorded at 25 ºC using a 2-mm cuvette. The solution of 2 μM of pHLIP-FIRE in phosphate buffer (pH 8) was incubated with POPC vesicles at the molar lipid/peptide ratio of 200:1 and kept overnight. The pH of the samples was changed with small amounts of concentrated HCl acid.

Cell culture. Human cervix adenocarcinoma (HeLa) and human lung carcinoma (A549) cells were obtained from the American Type Culture Collection (ATCC). An African green monkey fibroblast-like cells, COS-7, were a kind gift from Maureen Gilmore-Hebert and David F. Stern (Yale). The HeLa and COS-7 cells were cultured

in DMEM supplemented with 4.5 g/L D-glucose, 10% FBS (Fetal Bovin Serum) (Gibco) and 1% penicillin. A549 cells were cultured in DMEM at pH 6.2 for several weeks to adjust the cells to a low pH environment. All the cells were grown in an incubator (Revco Elite II, Thermo Fisher Scientific) under humidified atmosphere of air and 5% CO_2 at 37 ºC.

Fluorescence dequenching experiments with cells. Cells were seeded in a UV sterilized 96-well collagen coated plate (Thermo Scientific) at a density of 5000 cells per well, and then grown close to 100% confluency level. Then the cells were treated with 100 µL of 1 µM of a pHLIP fluorescent construct in Dulbecco's Phosphate Buffer Saline (DPBS, supplied with Ca^{2+} and Mg^{2+}) at pH 7.2 or pH 6.1. Incubation was done at room temperature (22-25ºC) under normal atmosphere in the biosafety cabinet. After 20 minutes the solution was removed and the cells were washed 3 times with pH 7.2 or 6.1 DPBS, and finally pH 7.2 or 6.1 DMEM was added to the cells. The pH 7.4 DMEM (no phenol red) is supplemented with 20 mM HEPES, whereas the pH 6.1 DMEM (no phenol red) is supplemented with 20 mM HEPES and 20 mM MES. Fluorescence was measured in a Berthold Tristar LB 941 plate reader with 535 nm excitation and 590 nm emission filters, respectively. Results obtained from five wells were averaged for each condition. The data points were fitted using a single exponential function with a sloped asymptotic line $y = A \times \exp(-kt) + bx + y_0$, where *k* is the rate constant, *y* is the normalized fluorescence intensity and *b* is the linear component of the fluorescence signal. Cell viability was determined by adding a small aliquot of cell titer 96 Aqueous One solution cell proliferation MTS assay (Promega), with absorbance measured using a 490 nm filter over time. After the

experiment, the pH of the DMEM was checked and it was found to increase no more than 0.3 pH unit (most likely due to the bicarbonate content in the DMEM buffer reacting with MES and/or HEPES acid).

Confocal microscopy. HeLa cells were grown in glass bottom dishes (Electron Microscopy Science) and live cell confocal microscopy was performed on Zeiss LSM 510 NLO META using a 20X objective. Incubation times and construct concentrations are the same as described for plate reader assays. The images were taken after 24 h of incubation with the construct. The cells were incubated with 4 μg/mL Hoechst (Life Technologies) 30 minutes before imaging.

Mouse experiments. BALB/c female mice ranging in age from 5 to 6 weeks were obtained from Harlan Laboratories (Indianapolis, IN). Mouse tumors were established by subcutaneous injection of 4T1 cells ($8x10^5$ cells/0.1 ml/flank) in the right flank of each mouse. When tumors reached 5-6 mm in diameter, tail vein injections of 150 μL of 25 μM of pHLIP-T-Q (5 mice), pHLIP-T-T (5 mice), or pHLIP-T (4 mice) were performed. Animals were euthanized at 24 or 48 hours post-injections, and necropsy was performed immediately after euthanization. Tumors and major organs were collected for imaging on a FX Kodak in-vivo image station. Fluorescence intensity was obtained via analysis of images by using Kodak software. The tumor/background ratio was calculated according to the equation:

$$CI = \frac{Fl_{tumor} - Fl_{auto}}{Fl_{muscle} - Fl_{auto}}$$

where Fl_{tumor}, Fl_{norm}, and Fl_{auto} are the mean fluorescence intensities of tumor, muscle and autofluorescence signal of the same organ from untreated mice, respectively.

Acknowledgement.

We thank J. Deacon for fruitful discussions and comments on the manuscript, as well as for suggesting the name of pHLIP-FIRE. This work was supported by NIH grants CA133890 to OAA, DME, YKR; GM073857 to DME; and by SUNY, Binghamton University (BU) Research Foundation start-up funds to MA and LY, a HHMI-BU undergraduate summer fellowship to RL, and NSF grant CHE-0922815 for the Regional NMR Facility (600 MHz Instrument) at SUNY-Binghamton.

Author contributions. D.M.E., A.G.K., M.A., Y.K.R., O.A.A. designed the project and wrote the manuscript. A.G.K., M.A., L.Y, performed the experiments and analyzed data. A.G.K., R.A., A.M. performed animal experiments. M.A., R.L., L.Y. synthesized the constructs.

References

1. Gioux, S., Lomnes, S. J., Choi, H. S., and Frangioni, J. V. (2010) Low-frequency wide-field fluorescence lifetime imaging using a high-power near-infrared light-emitting diode light source, Journal of biomedical optics 15, 026005.
2. Orosco, R. K., Tsien, R. Y., and Nguyen, Q. T. (2013) Fluorescence imaging in surgery, IEEE reviews in biomedical engineering 6, 178-187.
3. Nguyen, Q. T., and Tsien, R. Y. (2013) Fluorescence-guided surgery with live molecular navigation--a new cutting edge, Nature reviews. Cancer 13, 653-662.
4. Brooks, J. D. (2012) Translational genomics: the challenge of developing cancer biomarkers, Genome research 22, 183-187.
5. Weerakkody, D., Moshnikova, A., Thakur, M. S., Moshnikova, V., Daniels, J., Engelman, D. M., Andreev, O. A., and Reshetnyak, Y. K. (2013) Family of pH (low) insertion peptides for tumor targeting, Proceedings of the National Academy of Sciences of the United States of America 110, 5834-5839.
6. Gerweck, L. E., and Seetharaman, K. (1996) Cellular pH gradient in tumor versus normal tissue: potential exploitation for the treatment of cancer, Cancer research 56, 1194-1198.
7. Warburg, O. (1956) On the origin of cancer cells, Science 123, 309-314.
8. Zhang, X., Lin, Y., and Gillies, R. J. (2010) Tumor pH and its measurement, Journal of nuclear medicine : official publication, Society of Nuclear Medicine 51, 1167-1170.

9. Tannock, I. F., and Rotin, D. (1989) Acid pH in tumors and its potential for therapeutic exploitation, Cancer research 49, 4373-4384.

10. Estrella, V., Chen, T., Lloyd, M., Wojtkowiak, J., Cornnell, H. H., Ibrahim-Hashim, A., Bailey, K., Balagurunathan, Y., Rothberg, J. M., Sloane, B. F., Johnson, J., Gatenby, R. A., and Gillies, R. J. (2013) Acidity generated by the tumor microenvironment drives local invasion, Cancer research 73, 1524-1535.

11. Chiche, J., Brahimi-Horn, M. C., and Pouyssegur, J. (2010) Tumour hypoxia induces a metabolic shift causing acidosis: a common feature in cancer, Journal of cellular and molecular medicine 14, 771-794.

12. Reshetnyak, Y. K., Andreev, O. A., Segala, M., Markin, V. S., and Engelman, D. M. (2008) Energetics of peptide (pHLIP) binding to and folding across a lipid bilayer membrane, Proceedings of the National Academy of Sciences of the United States of America 105, 15340-15345.

13. Reshetnyak, Y. K., Segala, M., Andreev, O. A., and Engelman, D. M. (2007) A monomeric membrane peptide that lives in three worlds: in solution, attached to, and inserted across lipid bilayers, Biophysical journal 93, 2363-2372.

14. Andreev, O. A., Dupuy, A. D., Segala, M., Sandugu, S., Serra, D. A., Chichester, C. O., Engelman, D. M., and Reshetnyak, Y. K. (2007) Mechanism and uses of a membrane peptide that targets tumors and other acidic tissues in vivo, Proceedings of the National Academy of Sciences of the United States of America 104, 7893-7898.

15. Segala, J., Engelman, D. M., Reshetnyak, Y. K., and Andreev, O. A. (2009) Accurate analysis of tumor margins using a fluorescent pH Low Insertion Peptide (pHLIP), International journal of molecular sciences 10, 3478-3487.

16. Cruz-Monserrate, Z., Roland, C. L., Deng, D., Arumugam, T., Moshnikova, A., Andreev, O. A., Reshetnyak, Y. K., and Logsdon, C. D. (2014) Targeting pancreatic ductal adenocarcinoma acidic microenvironment, Scientific reports 4, 4410.

17. Vavere, A. L., Biddlecombe, G. B., Spees, W. M., Garbow, J. R., Wijesinghe, D., Andreev, O. A., Engelman, D. M., Reshetnyak, Y. K., and Lewis, J. S. (2009) A novel technology for the imaging of acidic prostate tumors by positron emission tomography, Cancer Res 69, 4510-4516.

18. Viola-Villegas, N. T., Carlin, S. D., Ackerstaff, E., Sevak, K. K., Divilov, V., Serganova, I., Kruchevsky, N., Anderson, M., Blasberg, R. G., Andreev, O. A., Engelman, D. M., Koutcher, J. A., Reshetnyak, Y. K., and Lewis, J. S. (2014) Understanding the pharmacological properties of a metabolic PET tracer in prostate cancer, Proc Natl Acad Sci U S A 111, 7254-7259.

19. Reshetnyak, Y. K., Andreev, O. A., Lehnert, U., and Engelman, D. M. (2006) Translocation of molecules into cells by pH-dependent insertion of a transmembrane helix, Proceedings of the National Academy of Sciences of the United States of America 103, 6460-6465.

20. An, M., Wijesinghe, D., Andreev, O. A., Reshetnyak, Y. K., and Engelman, D. M. (2010) pH-(low)-insertion-peptide (pHLIP) translocation of membrane impermeable phalloidin toxin inhibits cancer cell proliferation, Proceedings of

the National Academy of Sciences of the United States of America 107, 20246-20250.

21. Moshnikova, A., Moshnikova, V., Andreev, O. A., and Reshetnyak, Y. K. (2013) Antiproliferative effect of pHLIP-amanitin, Biochemistry 52, 1171-1178.

22. Moron, M. S., Depierre, J. W., and Mannervik, B. (1979) Levels of Glutathione, Glutathione Reductase and Glutathione S-Transferase Activities in Rat Lung and Liver, Biochimica et biophysica acta 582, 67-78.

23. Ogawa, M., Kosaka, N., Choyke, P. L., and Kobayashi, H. (2009) H-type dimer formation of fluorophores: a mechanism for activatable, in vivo optical molecular imaging, ACS chemical biology 4, 535-546.

24. Reshetnyak, Y. K., Yao, L., Zheng, S., Kuznetsov, S., Engelman, D. M., and Andreev, O. A. (2011) Measuring tumor aggressiveness and targeting metastatic lesions with fluorescent pHLIP, Mol Imaging Biol 13, 1146-1156.

25. Andreev, O. A., Engelman, D. M., and Reshetnyak, Y. K. (2010) pH-sensitive membrane peptides (pHLIPs) as a novel class of delivery agents, Mol Membr Biol 27, 341-352.

26. Tyagi, S., and Kramer, F. R. (1996) Molecular beacons: probes that fluoresce upon hybridization, Nature biotechnology 14, 303-308.

27. Johansson, M. K., Fidder, H., Dick, D., and Cook, R. M. (2002) Intramolecular dimers: a new strategy to fluorescence quenching in dual-labeled oligonucleotide probes, Journal of the American Chemical Society 124, 6950-6956.

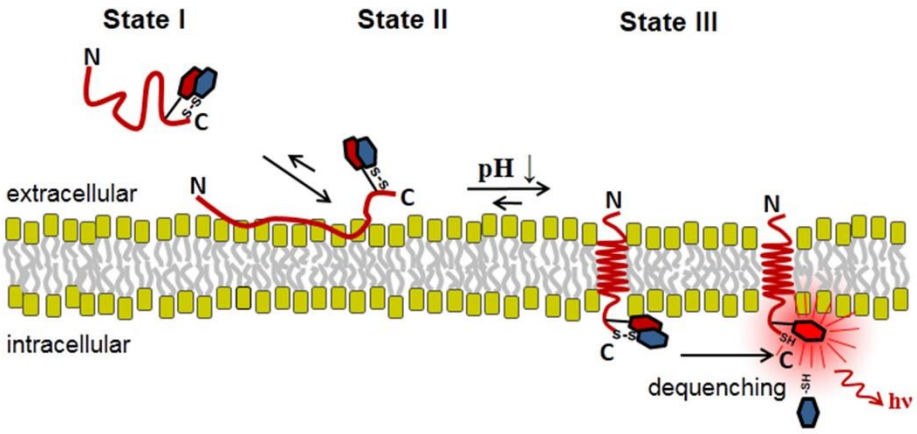

Figure 1. Activation of pHLIP-FIRE. State I: the peptide is soluble and unstructured in aqueous solution at physiological pH. State II: The peptide binds to the surface of a cell membrane in an unstructured form at physiological pH. State III: At acidic pH, the peptide forms an α-helix and inserts across the membrane, placing the self-quencing dye construct in the reducing environment of the cytoplasm. The fluorescence of the dye is activated by disulfide cleavage that disrupts the fluorophore/fluorophore or fluorophore/quencher pair, dequenching the construct and producing strong fluorescence.

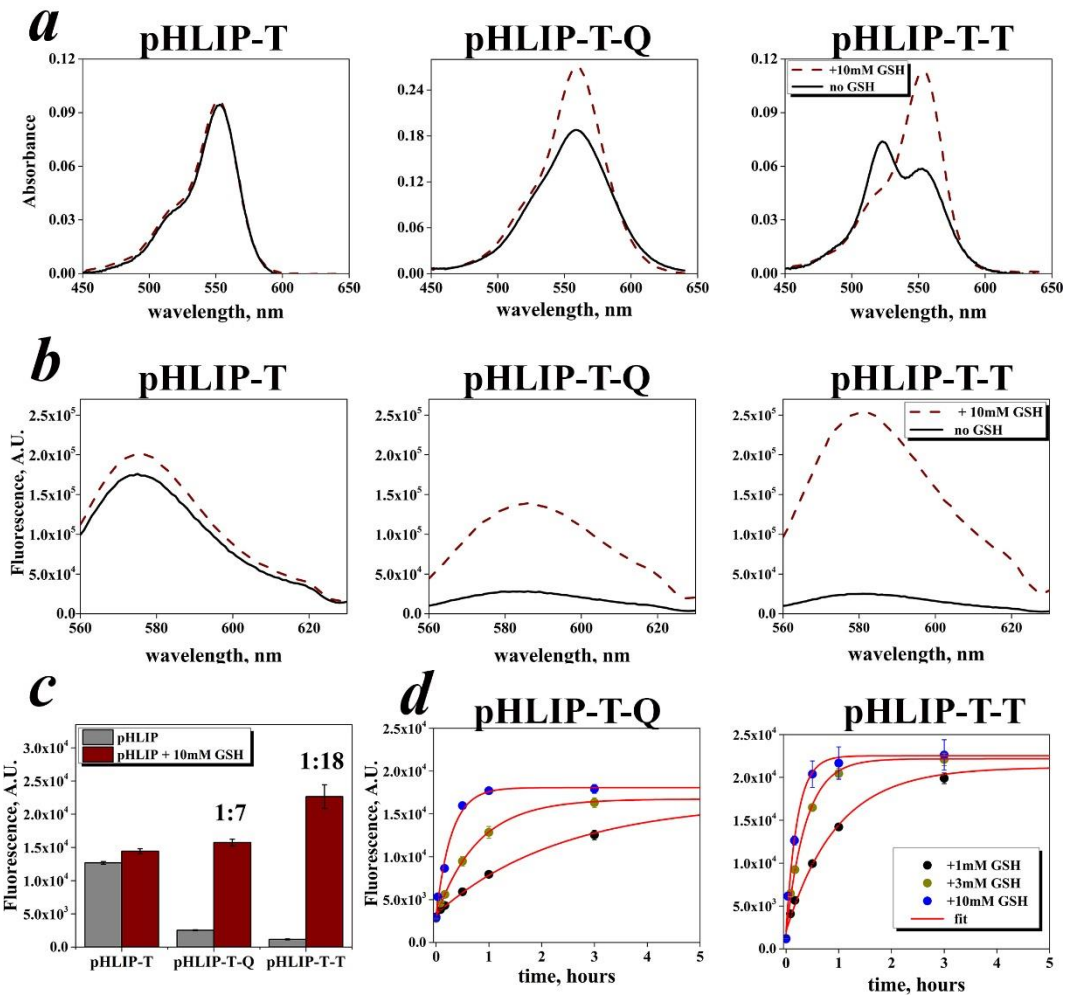

Figure 2. Chemical dequenching of pHLIP-FIRE constructs. a) Absorbance spectra of 1 μM pHLIP-T, pHLIP-T-Q and pHLIP-T-T before (solid line) and after (dashed line) treatment with 10 mM of glutathione. The red-shifted peak (dashed line) of the reduced pHLIP-T-T construct results from the conversion of H-dimer to monomeric TAMRA. b) Fluorescence spectra of 1 μM pHLIP-T, pHLIP-T-Q and pHLIP-T-T before (solid line) and after (dashed line) treatment with 10 mM of glutathione. c) TAMRA fluorescence level and dequenching capacity of quenched pHLIP-T-Q and pHLIP-T-T constructs (1 μM) and the non-quenched control pHLIP-T (1 μM) before (gray bars) and after (red bars) the addition of 10 mM glutathione. d)

Time-course of dequenching of pHLIP-T-Q or pHLIP-T-T (1 μM) after the addition of 1, 3, or 10 mM of glutathione. The dequenching rates are presented in Supplementary Table 1. Error bars, s.d. (n = 3 experiments).

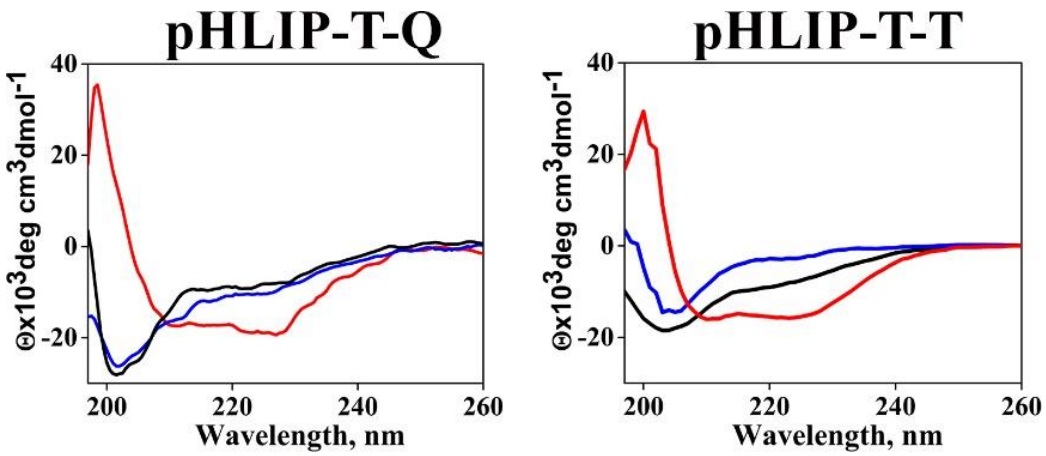

Figure 3. Peptide conformations in the three states of the pHLIP-FIRE constructs. The pHLIP-T-Q and pHLIP-T-T CD spectra. The pHLIP-FIRE peptides were studied for the presence of the three basic states of pHLIP: state I is the peptide in solution at pH 8 (black line), state II is the peptide in the presence of POPC liposomes at pH 8 (blue line), and state III is the folding and insertion of the peptide with POPC when the pH is dropped from pH 8 to pH 3.7 by the addition of an aliquot of HCl (red line). The inserted state is monitored by changes of the CD spectral signal. The concentrations of pHLIP constructs and POPC were 4 μM and 0.8 mM, respectively.

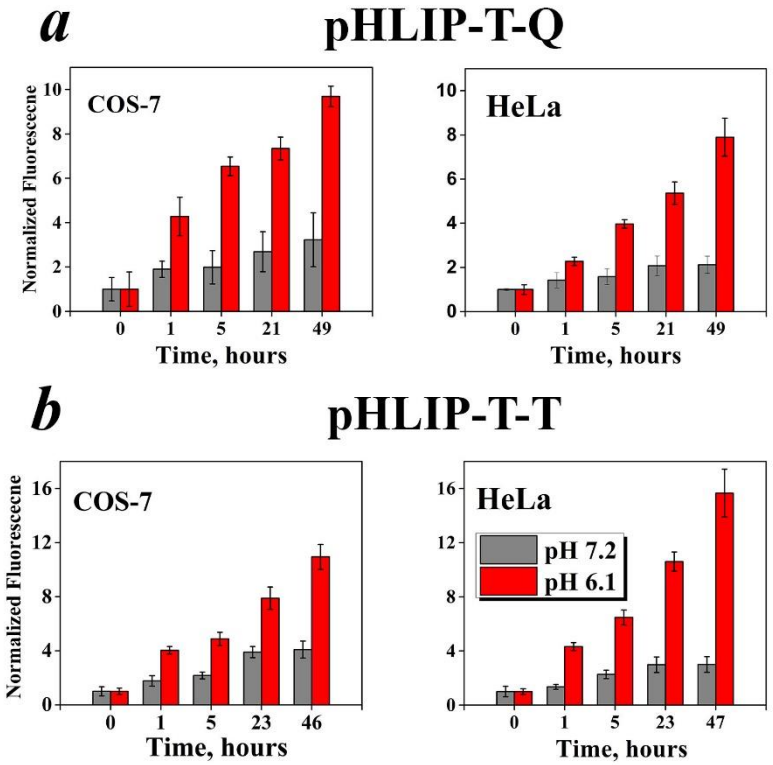

Figure 4. Changes of fluorescence intensity of TAMRA upon insertion. Insertion of pHLIP-T-Q (a) and pHLIP-T-T (b) into HeLa and COS-7 cells at pH 6.1 (red bars) and pH 7.4 (grey bars) at different time points are shown. Dequenching of the fluorophore is facilitated by the highly reducing environment inside the cells. All signals are normalized to the intensity at time zero. Error bars, s.d. (n = 6 experiments).

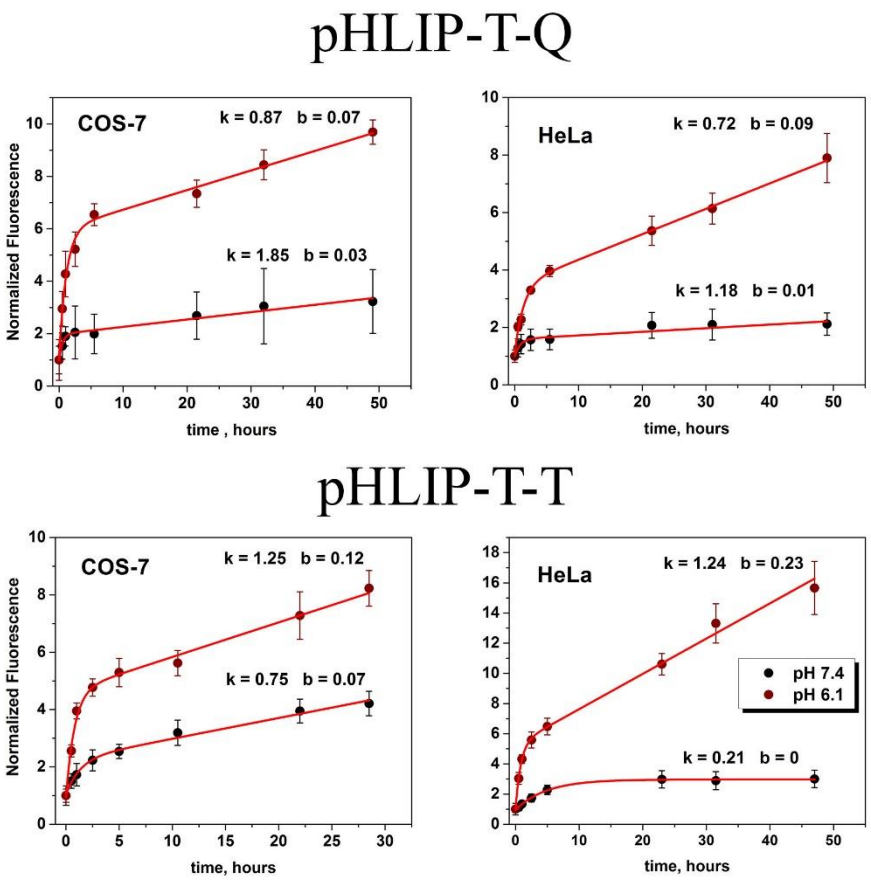

Figure 5. Kinetics of dequenching of pHLIP-FIRE fluorescence resulting from cell insertion. All data points were fitted using a single exponential function with a sloped asymptotic line $y = A \times \exp(-kt) + bx + y_0$ Error bars, s.d. (*n* = 6 experiments).

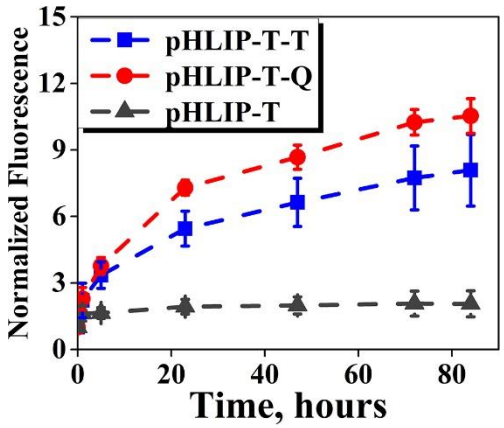

Figure 6. Incubation of pHLIP-FIRE with A549 cells at pH 6.1. Normalized TAMRA fluorescence intensities of pHLIP-T (black triangle), pHLIP-T-Q (red circle), and pHLIP-T-T (blue square). The pHLIP-T control (not quenched) showed a 2-fold increase in fluorescence. This 2-fold background increase may be due to the partial shielding effect of insertion into the cell or due to the different environmental conditions inside vs. outside of the cells. Error bars, s.d. (n = 5 experiments).

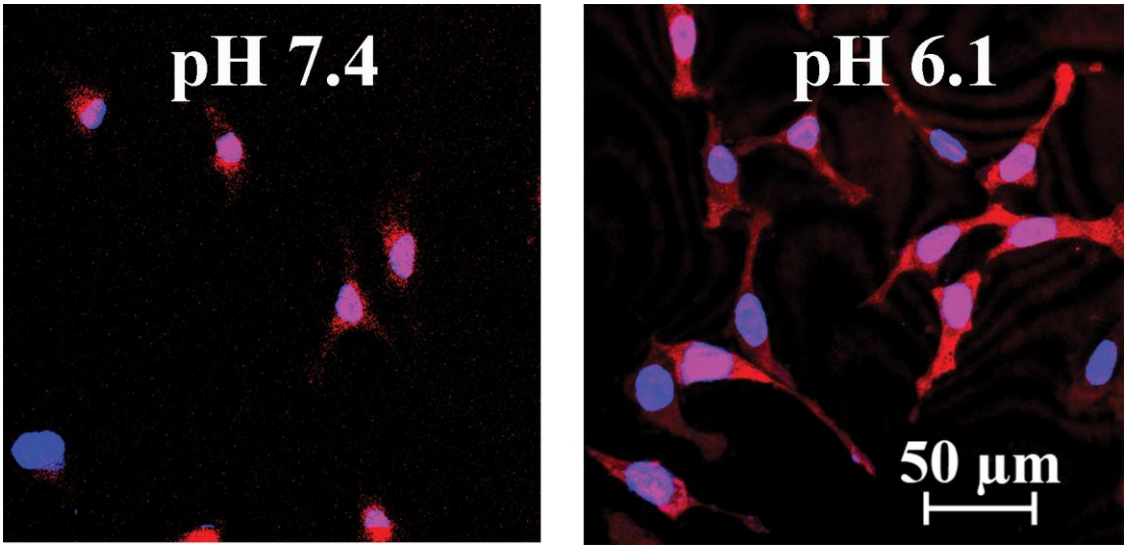

Figure 7. HeLa cells were treated with 1µM pHLIP-T-T construct for 20 min followed by 3X DPBS washing at pH 7.4 or 6.1. TAMRA fluorescence is in red, Hoechst fluorescence is in blue. The microscope image is taken at 24 hrs. after the incubation. Rhodamine excitation is at 561nm.

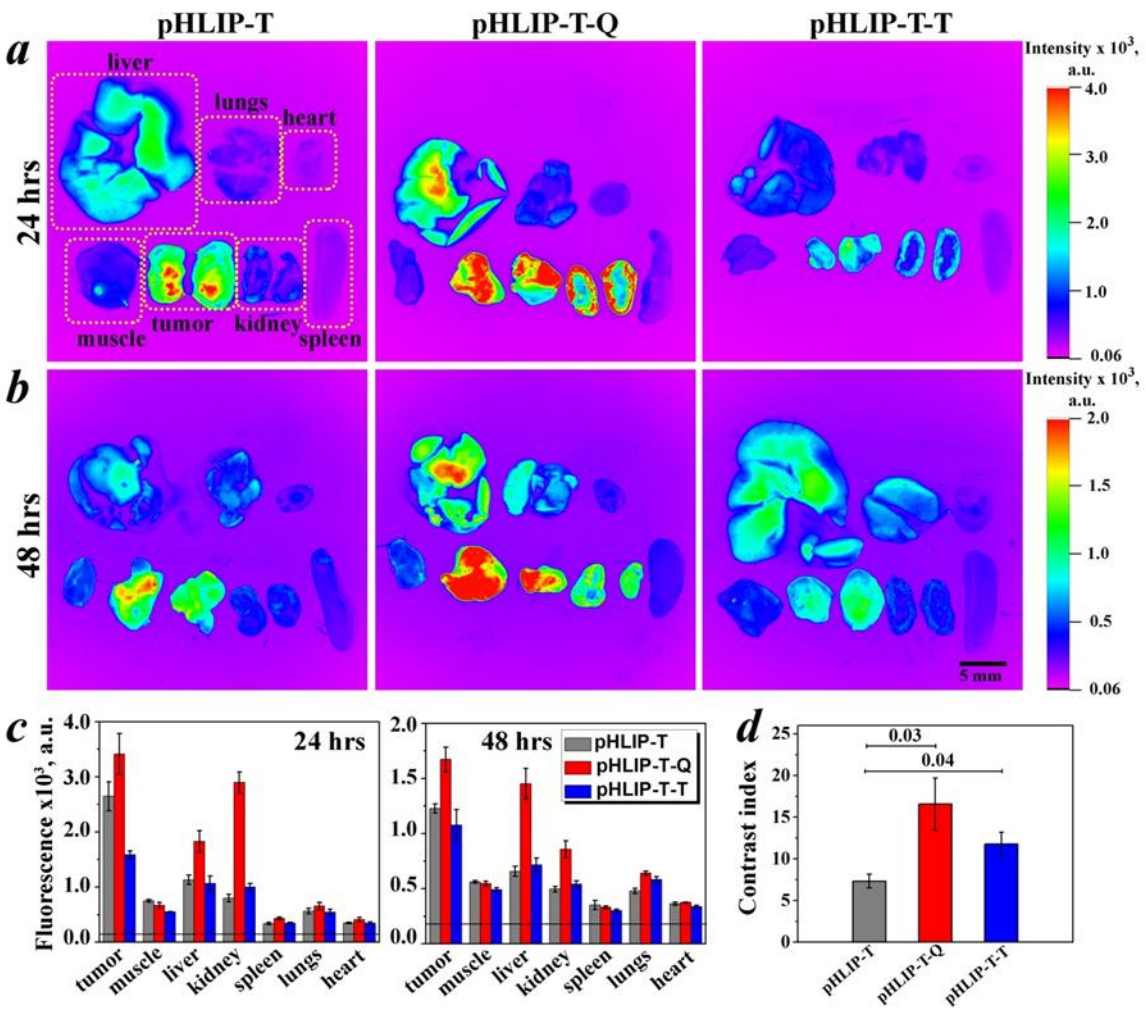

Figure 8. Biodistribution and contrast index of pHLIP-T-T, pHLIP-T-Q and pHLIP-T. Fluorescent image of organs collected at 24 h (*a*) and 48 h (*b*) time after i.v. injection of constructs. (*c*) Mean fluorescence values of tumor and organs are shown for pHLIP-T (grey bars), pHLIP-T-Q (red bars), and pHLIP-T-T (blue bars) at 24 h and 48 h after injection. The horizontal black line on the distribution panels indicates the level of instrument background fluorescence. The numeric values are presented in Supplementary Table 2. (*d*) Contrast indices for all constructs at 24 h time intervals: pHLIP-T (grey bar), pHLIP-T-Q (red bar), pHLIP-T-T (blue bar). Error bars, s.e. (n = 5 mice). *p-values* for pHLIP-T-Q and pHLIP-T-T are shown on the graph.

SUPPLEMENTARY INFORMATION

pHLIP-FIRE: a cell insertion-triggered fluorescent probe for imaging tumors demonstrates targeted cargo delivery *in vivo*

Alexander G. Karabadzhak, Ming An, Lan Yao, Rachel Langenbacher, Anna Moshnikova, Ramona-Cosmina Adochite, Oleg A. Andreev, Yana K. Reshetnyak, Donald M. Engelman

Supplementary Description of Chemical Syntheses of pHLIP-T, pHLIP-T-T and pHLIP-TQ Constructs.

pHLIP Peptides. The quenched pHLIP-FIRE constructs pHLIP-T-T and pHLIP-T-Q are synthesized from the pHLIP-KC peptide (Acetyl-NH-AAEQNPIYWARYADWLFTTPLLLLDLALLVDADEGT**KC**G-CO_2H). The pHLIP-T control construct was synthesized from the pHLIP-Cys peptide (AAEQNPIYWARYADWLFTTPLLLLDLALLVDADEGTC). The pHLIP-C and pHLIP-KC peptides were prepared by standard solid phase synthesis at the W. M. Keck Foundation Biotechnology Resources Laboratory (Yale University). The N-terminus NH_2 is capped with an acetyl group in pHLIP-KC. Crude pHLIP-KC peptide was purified using high pressure/performance liquid chromatography (HPLC). The HPLC settings are as follows: Hewlett Packard / Agilent Zorbax semi-prep 9.4 x 250 mm SB-C18 column; flow rate, 3 mL / min; phase A, water + 0.01% trifluoroacetic acid (TFA); phase B, acetonitrile + 0.01% TFA; gradient, 30 minute from 99:1 A/B to 1:99 A/B. Under these conditions, pHLIP-KC eluted at 27:73 A/B. Unless specified otherwise, these standard HPLC settings were also used to purify various intermediates and pHLIP conjugates described below.

Chemicals. 2-Aminoethanethiol (HCl salt, 98% pure) was purchased from Acros Organics, pyridyl disulfide (98% pure) from Alfa Aesar, QSY9 succinimidyl ester (QSY9 SE) from Life Technologies - Invitrogen - Molecular Probes, and 5-carboxytetramethyl-rhodamine, succinimidyl ester (5-TAMRA SE) from AnaSpec or Life Technologies - Invitrogen – Molecular Probes.

Instruments. HPLC was carried out using a Shimadzu system (consisting of two LC-6AD liquid chromatography pumps, a DGU-20A5 Prominence degasser, a CBM-20A Prominence communications bus module, a SPD-M20A Prominence diode array detector, and EZstart 7.4 software for interface and data analysis). UV-vis absorbance values (used to quantify pHLIP and pHLIP conjugates) were measured using a Beckman DU 640 spectrophotometer and a Beckman Coulter Tm Cuvette (14 mm high, 1 cm path length, 300 μL volume). H1 NMR was carried out on a Bruker AV 600 MHz Icon NMR. Mass spectrometry (MS) for product characterization was carried out using the Matrix-Assisted Laser Desorption/Ionization technique coupled with a Time of Flight mass spectrometer (MALDI-TOF). Unless specified otherwise, all MALDI-TOF MS results were obtained by the Mass Spectrometry Laboratory at the University of Illinois, Urbana-Champaign.

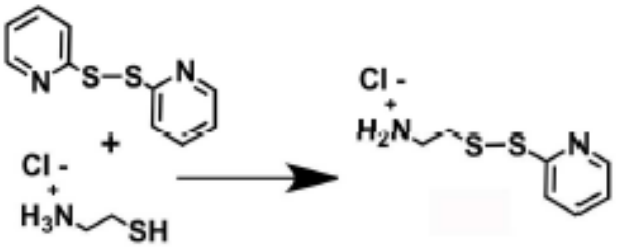

***S*-(2-pyridylthio)cysteamine hydrochloride.** The linker *S*-(2-pyridylthio)cysteamine (HCl salt) was synthesized according to the method of Ebright *et al.*1, with some

modifications. A solution of 2-aminoethanethiol hydrochloride (129 mg, 1.14 mmol, 1 eq.) in methanol (1 mL) was added to a stirring solution of pyridyl disulfide (275 mg, 1.25 mmol, 1.1 eq.) in 1.2 mL of methanol and 60 µL of acetic acid in a drop wise fashion over 10 min. The reaction mixture was stirred at r.t. under Ar in the dark for 45 min. Progress was monitored with HPLC (see above for detailed HPLC settings, the desired product *S*-(2-pyridylthio)cysteamine hydrochloride eluted at 61:39 A/B while pyridyl disulfide eluted at 25:75 A/B). The reaction mixture was concentrated under reduced pressure several times (residue re-dissolved in methanol as needed). The residue (or the collected precipitate) was re-dissolved in 2 mL methanol, and then mixed with 10 mL of cold diethyl ether to precipitate the product (repeated 3 times). The precipitate was dried under vacuum to give 95 mg of *S*-(2-pyridylthio)cysteamine (38% yield) contaminated with 2- aminoethyl disulfide (HCl salt). The mother liquor was stored at -20°C overnight to give a second batch of precipitated crystals, which were collected via filtration, re-dissolved in 1.5 mL of methanol, and mixed with 7.5 mL of diethyl ether to precipitate out 15 mg of pure *S*-(2- pyridylthio)cysteamine (HCl salt) (6% yield). 1H-NMR (DMSO-d6): δ (ppm) 3.09 (s, 4H), 7.28-7.32 (m, 1H), 7.73-7.76 (m, 1H), 7.82-7.87 (m, 1H), 8.10 (br s, 3H), 8.50-8.53 (m, 1H).

Synthesis of pHLIP-T-T. A solution of pHLIP-KC (1.2 mg, 0.26 µmole, 1 eq.) and *S*-(2-pyridylthio)cysteamine hydrochloride (0.07 mg, 0.31 µmole, 1.2 eq.) in 600 µL of

1:1 acetonitrile / aqueous (aq.) sodium phosphate buffer (100 mM, pH 8.0) was stirred at room temperature (r.t.) under Ar for 1 hr. The progress of the reaction was monitored by reverse phase HPLC (gradient: 99:1 A/B to 55:45 A/B over 10 min followed by 55:45 A/B to 10:90 A/B over 35 min): pHLIP-KC eluted at 27:73 A/B, the desired intermediate product pHLIP-KC (cysteamine disulfide) eluted at 30:70 A/B. This initial reaction is usually complete within 1h. Afterwards, a solution of 5-TAMRA-SE (0.68 mg, 1.3 μmole, 5 eq.) in 400 μL of 1:1acetonitrile / water was added and the pH of the reaction mixture was adjusted to pH 8.5 (via addition of small amounts of aq. NaOH solution). The resulting mixture was stirred at r.t. under argon for 3 hr. The desired final product pHLIP-T-T was isolated via HPLC (eluting at 25:75 A/B) in 69% yield (0.18 μmole) over two steps, quantified using UV absorption of H-type dimer of TAMRA at 550 nm (ε280=45,000 M-1cm-1). MALDI-TOF MS+ was used to confirm product identity: The molecular weight (MW) calculated for pHLIP-T-T (C256H352N52O68S2) is 5310, and the value obtained (using MALDI-TOF instrument at Yale Chemistry Department core facility) is 5311.7, matching the predicted (MW + 1) value for MH+ (molecule plus proton) of 5311.

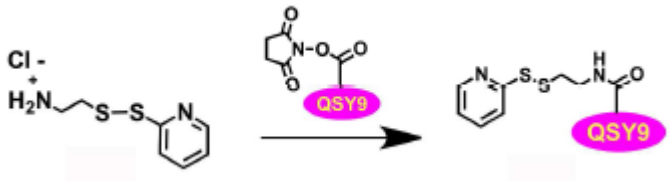

QSY9, S-(2-pyridylthio)cysteamide. A solution of *S*-(2-pyridylthio)cysteamine hydrochloride (0.24 mg, 1.08 μmole, 1.03 eq.) and triethyl amine (0.32 mg, 3.14 μmole, 3 eq.) in 0.1 mL of Ar saturated dry DMSO was used to dissolve 1 mg of

QSY9, SE (1.05 µmole, 1 eq.). The resulting mixture was vortexed, and then allowed to react at r.t. in the dark under Ar for 1 hr. Reaction

progress was monitored using HPLC (QSY9, SE eluted at 48:52 A/B whereas the desired product QSY9, S-(2-pyridylthio)cysteamide eluted at 46:54 A/B). The reaction is complete in less than one hour. Subsequently, the reaction mixture was diluted via addition of 400 µL of dry DMSO and stored at -20°C. The desired product was isolated using HPLC to provide 0.7 µmole of QSY9, S-(2-pyridylthio)cysteamide (67% yield). Quantification was performed using QSY9 absorbance at 562 nm (ε562nm in water=79,000 M-1cm-1).

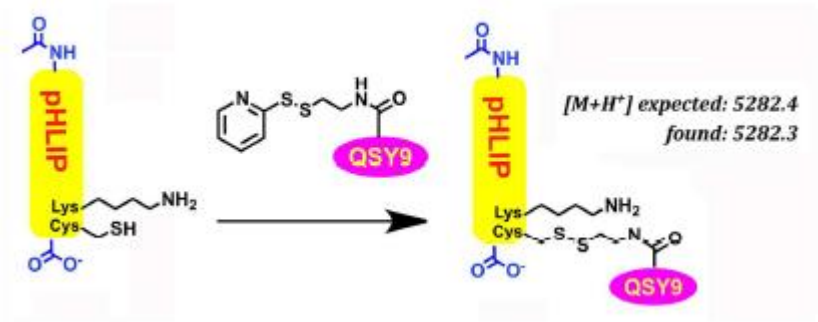

pHLIP-KC(QSY9) disulfide. To a solution of QSY9, S-(2-pyridylthio)cysteamide (655 nmole, 1.1 eq.) in 1.35 mL of Ar saturated, aq. sodium phosphate buffer (75 mM, pH 7.8) was added a solution of pHLIP-KC (2.62 mg, 594 nmole, 1 eq.) in 100 µL of Ar saturated DMSO. The reaction mixture was vortexed, and then allowed to react at r.t. in the dark under Ar for 1 hr. Reaction progress was monitored using HPLC (the desired product pHLIP-KC(QSY9) disulfide eluted at 28:72 A/B, s.m. pHLIP-KC monomer eluted at 27:73 A/B, and pHLIP-KC disulfide dimer eluted at 24:76 A/B). The reaction is near completion in less than 10 min. The pHLIP-KC(QSY9) disulfide intermediate was isolated using HPLC. Collected HPLC fractions were concentrated

under reduced pressure to remove as much acetonitrile as possible; at this point, pHLIP conjugates often precipitated out of the acidic water (pH 3); minimal amount of triethylamine was added to the aq. solution to adjust the pH to 7-10 and to redissolve pHLIP; this solution was frozen and then lyophilized to give the desired product pHLIP-KC(QSY9) in 58% yield (346 nmole), quantified using QSY9 absorbance at 562 nm (ε562nm in water=79,000 M-1cm-1). MALDI-TOF MS+ gave an observed Exact Mass of 5282.3 (for MH+), compared with the expected Exact Mass of 5282.4 for pHLIP-KC(QSY9) disulfide (C245H345N51O70S5) plus a proton.

pHLIP-T-Q. To a solution of pHLIP-KC(QSY9) disulfide (4.3 mg, 814 nmole, 1 eq.) and triethylamine (2.5 µL, 1.8 mg, 17.8 µmole, 22 eq.) in 400 µL of Ar saturated, dry DMSO was added a solution of 5-TAMRA SE (0.61 mg, 1152 nmole, 1.42 eq.) in 200 µL of Ar saturated, dry DMSO. The reaction mixture was vortexed, and then allowed to react at r.t. in the dark under Ar for 39 hr. Reaction progress was monitored using HPLC: the desired product pHLIPK(TAMRA)C(QSY9) disulfide eluted at 25.5 : 74.5 A/B whereas 5-TAMRA SE eluted at 37:63 A/B. Since some 5-TAMRA SE hydrolyzed over time, more 5-TAMRA SE was added at time 1hr (0.48 mg, 910 nmole, 1.1 eq., added directly) and time 24 hr (0.3 mg, 569 nmole, 0.7 eq., added as a solution in 50 µL dry DMSO), as well as additional triethylamine at time 21 hr (1 µL,

0.72 mg, 7.13 μmole, 8.8 eq.) and 24 hr (1.5 μL, 1.08 mg, 13.1 eq.). The final product pHLIP-TQ was isolated via HPLC in 45% yield (362 nmole), quantified using QSY9+TAMRA absorptions at 560 nm wavelength (ε560=79,000+83,000 M-1cm-1), along with 48 nanomole of the recycled starting material pHLIP-KC(QSY9). MALDI-TOF MS+ gave observed Exact Mass of 5694.4 (for MH+) or 5733.2 (for MK+), compared with the expected Exact Mass of 5694.5 or 5732.5 for pHLIP-T-Q (C270H365N53O74S5) plus a proton or a potassium ion, respectively.

pHLIP-T. pHLIP-Cys was conjugated with 6-TAMRA maleimide (Invitrogen) in DMSO at a molar ratio of 1.4:1 of dye/peptide and incubated at room temperature for about 6 h and then at 4 °C until the conjugation reaction was complete. The reaction progress was monitored and the desired pHLIP-Cys(TAMRA) thioether product was purified by reverse phase HPLC. The purity of the product was assessed by analytical HPLC.

pHLIP-FIRE dequenching rate constants *in vitro* and cultured cells

	In vitro			**Cultured cells**	
	1 mM GSH	**3 mM GSH**	**10mM GSH**	**HeLa**	**COS-7**
pHLIP-T-T	1.1 ± 0.1	2.7 ± 0.2	4.7 ±0.6	1.2 ± 0.2	1.3 ± 0.3
pHLIP-T-Q	0.4 ± 0.05	1.3 ± 0.05	3.4 ± 0.4	0.7 ± 0.1	0.9 ± 0.1

Supplementary Table 1. pHLIP-FIRE dequenching rate constants *in vitro* and in cultured cells after adding different concentrations of glutathione. Error, s.d. (n = 3 experiments for *in vitro*, n = 6 experiments for cultured cells).

Mean TAMRA fluorescence with SD calculated for each organ collected at 24h or 48h.

	pHLIP-T-Q		pHLIP-T		pHLIP-T-T	
Organ	24 hours	48 hours	24 hours	48 hours	24 hours	48 hours
Tumor	3414 ± 369	1672 ± 109	2648 ± 261	1226 ± 41	1586 ± 70	1077 ± 141
Muscle	668 ± 55	546 ± 22	752 ± 24	562 ± 22	552 ± 7	491 ± 19
Liver	1826 ± 195	1452 ± 140	1131 ± 85	658 ± 44	1064 ± 136	716 ± 60
Kidney	2895 ± 194	856 ± 76	801 ± 67	495 ± 25	997 ± 68	541 ± 29
Spleen	433 ± 21	331 ± 13	339 ± 19	352 ± 41	347 ± 13	303 ± 10
Lung	656 ± 68	641 ± 19	564 ± 51	479 ± 22	542 ± 56	583 ± 27
Heart	407 ± 41	374 ± 4	350 ± 12	363 ± 15	343 ± 25	336 ± 14

Supplementary Table 2. Numeric fluorescence values of each organ. Errors, s.d. (*n* = 5 mice).

CHAPTER 3

Submitted in Angewandte Communications

pH-Sensitive Cyclic Peptides for Tumor Targeting

Dhammika Weerakkody,[a] Anna Moshnikova,[a] Naglaa Salem El-Sayed,[b,c,d], Ramona-Cosmina Adochite,[a] Jovana Golijanin,[a] Rakesh K. Tiwari,[b,c,d] Oleg A. Andreev,[a] Keykavous Parang,[b,c,d,*] Yana K. Reshetnyak[a,*]

[a]Department of Physics, University of Rhode Island, Kingston, RI 02881, United States; [b]Chapman University School of Pharmacy, Irvine, CA 92618, United States;

[c]Department of Biomedical and Pharmaceutical Sciences, College of Pharmacy, University of Rhode Island, Kingston, RI 02881, United States; [d]Chao Family Comprehensive Cancer Center, School of Medicine, University of California, Irvine, Shanbrom Hall, 101 The City Drive, Orange, CA 92868 (USA)

Corresponding Authors

Keykavous Parang, Chapman University School of Pharmacy, Irvine, CA 92618, United States; phone: 714-516-5489; E-mail: parang@chapman.edu

Yana K. Reshetnyak, Department of Physics, University of Rhode Island, Kingston, RI 02881, United States; phone: 401-874-2054; E-mail: reshetnyak@mail.uri.edu

Abstract

Tumor development, progression, and invasiveness are associated with the elevation of acidosis. The most effective pH-sensitive tumor targeting agents should sense pH at the surface of cancer cells, where it is expected to be the lowest. We have designed, synthesized, and evaluated a series of cyclic pH-sensitive peptides containing a number of tryptophan (W) and glutamic acid (E) residues. Biophysical studies revealed the molecular mechanism of peptides action and localization within the lipid bilayer at high and low pHs. Fluorescently-labeled peptides were tested for targeting of acidic tumors in mice. The highest tumor to muscle ratio (4.3) was established for an asymmetric cyclic peptide, c[E_4W_5C], at 4 h after intravenous administration. The same asymmetric cyclic peptide can translocate polar cargo molecules of similar size across lipid bilayer in a pH- and concentration-dependent manner. We introduced a novel class of pH-sensitive agents, cyclic peptides, which could be developed for imaging of acidity in tumors and translocation of polar cargo molecules across the lipid bilayer of the membrane. These data suggest that cyclic peptides containing tryptophan and glutamic acid can be utilized as a new class of pH-sensitive cellular delivery and tumor targeting tools.

Extracellular acidity is associated with various pathological states, such as tumor, ischemia, stroke, and infection. There are a number of approaches under development for delivery of imaging and therapeutic agents to diseased tissue in a pH-dependent manner. They are based on the use of pH-sensitive polymers, liposomes, nanoparticles and small molecules.[1-7] Among peptides, family of pHLIPs, linear peptides of 25-35 residues, which insert into cellular membrane and form transmembrane helices are

used for targeting of acidic tumors of various origins and other acidic diseased tissues.[8,9]

Application of cyclic peptides in biological sciences has become a subject of major interest because of their enhanced enzymatic stability versus linear peptides.[10] Recently we reported the design and synthesis of homochiral L-cyclic peptides containing arginine (R), tryptophan (W) residues and their application for the nuclear targeting delivery of anti-HIV drugs, phosphopeptides, anticancer drugs, and siRNA.[11-14] These peptides offered several advantages including nuclear delivery of doxorubicin, endocytosis-independent uptake, low cytotoxicity, biocompatibility, hydrophobic drug entrapment through non-covalent interactions, and drug delivery through conjugation with doxorubicin.

Here we design pH-sensitive negatively charged cyclic peptides and study their interactions with the lipid bilayer of liposomal and cellular membranes *in vitro* and *in vivo*. To the best of our knowledge, this is the first report of using pH-sensitive cyclic peptides for intracellular delivery of a toxin and tumor targeting.

We introduced and investigated one linear and five cyclic peptides (Figure 1 and Table S1). All peptides contain: i) single cysteine (Cys, C) residue for conjugation purposes, ii) at least one tryptophan (Trp, W) for ability to record fluorescence signal, iii) 3-5 protonatable glutamic acid (Glu) residues to trigger pH-dependent interaction with membrane. First three peptides, *c*[$(WE)_4$WC], *c*[$(WE)_5$WC], and *c*[$(WE)_3$WC] have 3, 4, and 5 repeating units of WE, respectively, where Trp and Glu residues are alternating in the cyclic peptide. Another peptide, *c*[$(LE)_4$WC], has leucine (Leu, L) instead of Trp to investigate the role of aromatic Trp residues for peptides interaction

with the membrane. Fifth peptide, *c*[E_4W_5C], is an asymmetric; it has five Trp residues located on one side of the cycle, while four Glu residues are located on the other side of the cycle. Finally, we synthesized also linear *l*(CW$(EW)_4$) 10-residues peptide for the comparison with the cyclic peptides.

The peptides were synthesized by employing Fmoc/*t*Bu-based solid phase chemistry. As representative examples, the synthesis of *l*(CW$(EW)_4$ and *c*[$(WE)_4$CW] peptides are depicted in Scheme S1. In brief, the linear protected peptide was first assembled. Direct cleavage of peptide-attached resin generated the linear peptide. However, cleavage of side chain protecting groups from the resin in the presence of AcOH/TFE/DCM (1:2:7 v/v/v), cyclization in dilute condition using DIC/HOAt in DMF/DCM solution for 12 h, followed by the deprotection of the side chain by using cleavage cocktail (TFA:thioanisole:anisole:EDT (90:5:2:3 v/v/v/v) afforded the cyclic peptide. All peptides were purified by reverse phase HPLC.

The fluorescent techniques were employed to establish the molecular mechanism of peptides interaction with membrane and their localization within the lipid bilayer at high and low pHs. We monitored changes of tryptophan fluorescence (Figure S1, Table S2) and circular dichroism (Figure S2) spectral signals for the peptides in absence and presence of POPC liposomes at different pHs. All peptides demonstrated pH-dependent partition into the membrane. Asymmetric cyclic peptide with Trp residues located on one side of the cycle, *c*[E_4W_5C], most probably partitions into the membrane facing Trp residues inside a bilayer and exposing Glu to the extracellular space. The drop of pH leads to the protonation of carboxyl groups of Glu residues, which increases peptides hydrophobicity and promotes partition of peptides in bilayer.

As a result, positions of maximum of fluorescence spectra shift to 6-9 nm to short wavelengths (Figure 2 and Table S2). The linear peptide shows appearance of helicity in the result of pH drop (Figure S2). *c*[$(WE)_4WC$], *c*[$(WE)_5WC$] and *c*[$(WE)_3WC$] peptides show similar CD signals at pH 8, which are altered by interaction with lipid bilayer and drop of pH. The CD signal of *c*[E_4W_5C] peptide was different but was also pH-dependent. We did not observe characteristic CD signal of exiton with a minimum at 232-235 nm. Such an exciton might be formed as the result of the stacking of aromatic amino acids due to peptides aggregation/stacking.[18] Thus, we concluded that at concentrations of the peptides we used in our study, it is unlikely formation of some kind tubular structures of peptides.

To establish localization of the peptides within a lipid bilayer of the membrane, dual quenching assay[15] was used (Figure 2 and Table S3). Effective quenching of fluorescence by acrylamide would occur only for tryptophan residues exposed to polar parts of outer or inner leaflets of the bilayer. At the same time, tryptophan residues located in the middle of a membrane would be effectively quenched by 10-DN. The *c*[E_4W_5C] demonstrates the highest quenching by 10-DN and highest energy transfer at pH 8 indicating to the internal position of Trp residues in the bilayer of the membrane. All other peptides are located at the outer leaflet of the bilayer at pH 8. The peptides *c*[$(WE)_3WC$] and *c*[$(LE)_4WC$] are the most exposed to the aqueous solution showing the highest degree of quenching by acrylamide and least quenching by 10-DN. The peptide *c*[$(LE)_4WC$] might be less exposed, while it's single Trp could be oriented toward aqueous solution, while Leu residues are located deeper in the membrane.

The results of dual quenching assay allow to establish if tryptophan residues are located in the middle of a membrane or close to the polar headgroups of bilayer. However, it would not allow distinguishing between location at outer or inner leaflets of the bilayer. Therefore, we also performed FRET assay (Figure 3).[16,17] First, symmetrically-labeled by NBD dye POPC liposomes were prepared. Then, membrane-impermeable dithionite was used to modify chemically and quench fluorescence of NBD at outer leaflet of the bilayer followed by removal of dithionite by gel filtration. As a result, asymmetrically-labeled liposomes with NBD only at the inner leaflet were obtained. FRET is monitored from tryptophan residues to NBD, which occurs when both fluorophores are in a proximity to each other (within 5-15 Å). Thus, when tryptophan is located at outer leaflet of the bilayer, no significant energy transfer to NBD at inner leaflet would occur (the distance will be about 50-60 Å). The energy transfer would be detected only if tryptophan residues were located in the middle of the membrane or at inner leaflet. FRET signal would be maximal, when tryptophan is located in proximity to the headgroups of the inner leaflet. Among *c*[$(WE)_4$WC], *c*[$(WE)_5$WC], and *c*[$(WE)_3$WC] peptides, the peptide with smallest cycle, *c*[$(WE)_3$WC], shows the deeper partition into membrane and closer location to the inner leaflet, since FRET signal is the highest for it. The highest partition into bilayer at pH 3 is observed for asymmetric *c*[E_4W_5C] peptide. Linear peptide, *l*(CW$(EW)_4$), also demonstrates partition into bilayer in the result of pH drop.

By monitoring shift of the position of maximum of fluorescence spectra for the peptides in the result of pH drop, we established apparent pK of peptides partition into bilayer. The pKa for most cyclic and linear peptides varies in the range of 5.7-6.4,

while the smallest pKa value is observed for cyclic Leu-containing peptide, *c*[$(LE)_4$WC] (Figure 4).

Extracellular acidity is established already at early stages of tumor development, during the avascular phase of carcinoma in situ. As tumor continues to grow, acidosis is increasing due to the poor blood perfusion, switch of cancer cells to glycolytic mechanism of energy production even in the presence of oxygen and overexpression of carbonic anhydrases (CA). Adaptations to the highly acidic microenvironment are critical steps in the transition from an avascular pre-invasive tumor to a malignant invasive carcinoma.[25-28] Thus, targeting of tumor acidity might serve as a predictive marker for tumor invasiveness. pH is especially lower in the vicinity of the membrane of cancer cells due to the work of proton pumps and CAIX and CAXII. Also, pK of protonation of Asp and Glu residues is higher (pK~6-7) near the surface of the hydrophobic membrane compared to bulk aqueous solution, where pK~3-4.[29-32] The protonation of Asp/Glu in the range of pHs of 6-7 established for cyclic peptides is relevant to tumor environment, where pH is about 6.2-6.8.

Before animal studies, we showed no cytotoxicity induced by peptides (Figure S3). Next we proceed to *in vivo* tumor targeting experiments. The murine 4T1 xenograft model, which closely mimics stage IV of human breast cancer[19-21] was used in our study. Small 4T1 tumor (tumor volume <150 mm^3) generates a significant level of lactate and serve as a good model of an aggressive, acidic tumor.[22] All peptides were covalently conjugated with Alexa546-malemiede. The fluorescent constructs were given as a single IV injection and at 4 h after administration animals were euthanized followed by necropsy. The mean fluorescence of tumor, muscle, kidney, liver and

lungs were recorded and analysed. The highest tumor targeting was observed for linear peptide, *l*(CW(EW)$_4$), and asymmetric cyclic peptide, *c*[E$_4$W$_5$C] (Figure 5a, b and Table S4). The least targeting was observed for Leu-containing peptide, *c*(LE)$_4$CW. The signal in organs for all peptides except Leu-containing peptide was smaller than in tumor. Muscle clearance was also highest for linear, *l*(CW(EW)$_4$), and asymmetric cyclic, *c*[E$_4$W$_5$C], peptides (Figure 5c and Table S5). We exclude the possibility of passive tumor targeting by peptides, since it should be very similar for all peptides, or at least for symmetric and asymmetric peptides of the exact the same molecular weights and compositions. Also at time point of 4 h after constructs administration the clearance of organs (muscle, liver, lungs) is very significant, thus the signal in tumor cannot be attributed to the presence of the peptides in blood.

According to obtained data, the linear peptide belongs to the class of truncated pHLIP peptides, which form a helical structure in the membrane in a result of pH drop. Linear peptide we investigated here has 10 amino acids, which is a minimal number for the formation alpha and/or 3_{10} helices or mixture of both to span bilayer, with the assumption of some thinning of bilayer, as we established in other our study of truncated pHLIP peptides (paper is in preparation). Linear pHLIPs indeed show excellent tumor targeting since it is based on a pH-dependent membrane-associated folding with well controlled pKa of peptides insertion into bilayer. Among cyclic peptides, the best tumor targeting was established for asymmetric peptide, which we investigated further.

Asymmetric cyclic peptide was evaluated for its ability to move polar cargo across membrane. As a polar cargo we used amanitin, which is a cell-impermeable cyclic

peptide. It is a deadly toxin, which inhibits RNA polymerase II, if transferred across lipid bilayer of plasma membrane. The pH- and concentration-dependent cell death was observed after treatment of HeLa cells with up to 4 μM of *c*[E_4W_5C]-S-S-Amanitin (see Scheme S2, for the peptide-amanitin structures) for just 2 hours (Figure 6). The similar results were obtained with *c*[$(WE)_4WC$]-S-S-Amanitin (Figure S4). Previously we showed that amanitin alone does not induce cell death at the concentrations used and for the duration of treatment of 2 hours.[23] We also tested construct, where amanitin was conjugated to the asymmetric *c*[E_4W_5C] cyclic peptide via non-cleavable bond (Scheme S2, b). The cytotoxic effect for non-cleavable construct was reduced significantly at both pHs (Figure 6). It might indicate that the equilibrium is shifted toward peptide membrane-bound form, and cleavage of amanitin from the peptide is needed to allow amanitin to reach RNA polymerase II in the nucleus. Alternatively, if peptide-amanitin is translocated into cytoplasm, the cleavage of amanitin might be required, since affinity of the peptide-amanitin to the RNA polymerase II might be reduced compared to the affinity of free amanitin to the RNA polymerase II. Based on the obtained results, we proposed that at high/normal pH asymmetric cyclic peptide is mostly located at the outer leaflet of the bilayer. In the result of pH drop, protonation of Glu residues leads to the enhancement of peptide hydrophobicity and partition into bilayer, where it is mostly concentrated on inner leaflet, since Glu residues could be de-protonated in cytoplasm of cells. This assumption was further confirmed by quenching of fluorescence of FITC labeled with asymmetric cyclic peptide by cell impermeable Trypan Blue (Figure S5). Trypan Blue is used to quench fluorescence of FITC located in the extracellular space.[24] Our data

indicate that cells treated with the FITC-labeled peptide at low pH followed by Trypan Blue quenching show higher level of fluorescent signal compared to the cells treated with the FITC-labeled peptide at normal pH followed by Trypan Blue quenching (Figure S5).

Targeting of membrane by asymmetric cyclic peptide, *c*[E_4W_5C], has a different mechanism compared to the action of linear peptides. Our data indicate that negatively charged Glu residues of asymmetric cyclic peptide are exposed to the aqueous solution at pH 8. Trp residues most probably do not partition deep into the membrane (Figure 7 and Figure S6). It is known that indole rings of Trp residues can stably interact with the interface between bilayer lipid chains and headgroups.[31,33-36] When pH is lowered, Glu residues are protonated. The pKa of protonation is higher due to the proximity to hydrophobic membrane.[29-32] Protonation leads to the increase of hydrophobicity of the peptide, which promotes partition of the peptide into bilayer. However, due to the fact that Trp residues have higher affinity to the headgroups region compared to the central hydrophobic part of bilayer, peptide is equilibrated in the region of headgroups between inner and outer leaflets of bilayer. We and others showed that pH equilibrates fast inside a liposome.[32,37] Thus, an equal amount of the peptide molecules are distributed between both leaflets of liposomal membrane with low pH outside and inside of it (Figure S6). However, in the case of cells, pH inside both normal and cancer cell is normal (around 7.2). At the same time, extracellular pH in the vicinity of cancer cells is low (6.2-6.5). As a result, peptides reaching inner leaflet of the bilayer might expose their Glu residues to the cytoplasm, where they would be de-protonated and became charged again. It would reduce the rate of the peptide diffusion back into

the membrane and should lead to the shift of the equilibrium toward accumulation of the peptides at inner leaflet of bilayer of plasma membrane of cells (Figure 7). Thus, the cyclic peptide could be considered as a weak acid with multiple protonated groups, which diffuses across bilayer. For weak acids, the intracellular-extracellular distribution, C_i/C_e, should be calculated according to the following equation:

$$\frac{C_i}{C_e} = \frac{1 + 10^{\,pH_i - pK_a}}{1 + 10^{\,pH_e - pK_a}}$$

where pH_i and pH_e are the intracellular and extracellular pH values, respectively. Since the cyclic peptide has affinity to the membrane we consider C_i and C_e as the concentrations of the peptide on inner and outer leaflets, respectively. We established that pKa of membrane partition for asymmetric cyclic peptide is 5.7. The calculation show that at pHe = 7.4 (healthy tissue) and pHi = 7.2 the concentration ratio on inner and outer leaflets for asymmetric cyclic peptides is 0.6. However, the same ratio increases to 4.5, 7.8, and 10.9 if extracellular pHe would be 6.5, 6.2 and 6.0, respectively.

We assume that the symmetrical WE peptides have the same mechanism of action as asymmetric peptide, however they have less favorable localization of Trp and Glu residues, which reduces their ability to accumulate at inner leaflet of bilayer of cellular membranes and target acidic tumors. Leu-containing peptides are less advantageous due to their reduced affinity to the headgroup part of the bilayer and high affinity to the center of the membrane.

Our study justifies further development and testing of pH-sensitive asymmetric cyclic peptides for imaging of acidic tumors. Cyclic peptides have much higher stability in

blood compared to linear peptides and could have much faster blood clearance, which will be very advantageous for clinical imaging.

Keywords: amanitin •dual-quenching assay • fluorescence spectroscopy • microscopy and imaging • NBD-FRET assay • Trypan • Blue quenching

REFERENCES

1. H. Karanth, R. Murthy, *Journal of Pharmacy and Pharmacology*, **2007**, *59*, 469–483
2. C. J. Chu, J. Dijkstra, M. -Z. Lai, K. Hong, F.C. Szoka, *Pharmaceutical Research* **1990**, *7*, 824–834.
3. N. K. Subbarao, R. A. Parente, F.C. Szoka Jr, L. Nadasdi, K. Pongracz, *Biochemistry* **1987**, *26*, 2964–2972.
4. Z. Poon, D. Chang, X. Zhao, P. T. Hammond, *ACS Nano* **2011**, *5* 4284–4292.
5. S. Okada, S. Mizukami, T. Sakata, Y. Matsumura, Y. Yoshioka, K. Kikuchi, *Adv. Mater.* **2014**, *26*, 2989–2992.
6. K. C. Liu, Y. Yeo, *Mol. Pharm.* **2013**, *10*, 1695-1704.
7. K. Nwe, C. H. Huang, A. Tsourkas, *J. Med. Chem.* **2013**, *56*, 7862–7869.
8. O. A. Andreev, D. M. Engelman, Y. K. Reshetnyak, Targeting diseased tissues by pHLIP insertion at low cell surface pH, *Front Physiol.* **2014**, *5*, 97.
9. D. Weerakkody, A. Moshnikova, M. S. Thakur, V. Moshnikova, J. Daniels, D.M. Engelman, O.A. Andreev, Y.K. Reshetnyak, *Proc Natl Acad Sci U. S. A.*, **2013**, *110*, 5834–5839.
10. M. Katsara, T. Tselios, S. Deraos, G. Deraos, M. T. Matsoukas, E. Lazoura, J. Matsoukas, V. Apostolopoulos, *Curr. Med. Chem*. **2006**, *13*, 2221–2232.
11. D. Mandal, A. Nasrolahi Shirazi, K. Parang, *Angew. Chem. Int Ed Engl 2011*, 50, 9633–9637.
12. A. Nasrolahi Shirazi, R. K. Tiwari, D. Oh, A. Banerjee, A. Yadav, K. Parang, *Mol. Pharm*. **2013**, *10*, 2008–2020.

13. A. Nasrolahi Shirazi, D. Oh, R. K. Tiwari, B. Sullivan, A. Gupta, G. D. Bothun, K. Parang, *Mol. Pharm*. **2013**, *10*, 4717–4727.

14. A. N. Shirazi, K. L. Paquin, N. G. Howlett, D. Mandal, K. Parang, *Molecules* **2014**, *19*, 13319–13331.

15. G. A. Caputo, E. London, *Biochemistry* **2003**, *42*, 3265-3274.

16. J. C. McIntyre, R. G. Sleight, *Biochemistry* **1991**, *30*, 11819–11827.

17. A. Clausell, F. Rabanal, M. Garcia-Subirats, M. Asuncion Alsina, Y. Cajal, *J. Phys. Chem. B*, **2006**, *110*, 4465–4471.

18. R. S. Roy, H. N. Gopi, S. Raghothama, R. D. Gilardi, I. L. Karle, P. Balaram, *Biopolymers* **2005**, *80*, 787.

19. K. Tao, M. Fang, J. Alroy, G.G. Sahagian, *BMC Cancer* **2008**, *8*, 228.

20. J. Yang, S. A. Mani, J. L. Donaher, S. Ramaswamy, R.A. Itzykson, C. Come, P. Savagner, I. Gitelman, A. Richardson, R.A. Weinberg, *Cell*, **2004**, *117*, 927–939.

21. B. L. Eckhardt, B. S. Parker, R. K. van Laar, C. M. Restall, A. L. Natoli, M. D. Tavaria, K .L. Stanley, E. K. Sloan, J. M. Moseley, R. L. Anderson, *Mol. Cancer Res.* **2005**, *3*, 1–13.

22. I. Serganova, A. Rizwan, X. Ni, S. B. Thakur, J. Vider, J. Russell, R. Blasberg, J. A. Koutcher, Metabolic imaging: a link between lactate dehydrogenase A, lactate, and tumor phenotype. *Clin. Cancer Res.* **2011**, *17*, 6250–6261.

23. A. Moshnikova, V. Moshnikova, O. A. Andreev, Y. K. Reshetnyak, *Biochemistry* **2013**, *52*, 1171–1178.

24. J. Nuutila, E. M. Lilius, *Cytometry A*, **2005**, *65*, 93–102.

25. J. W. Wojtkowiak, D. Verduzco, K. J. Schramm, R. J. Gillies, *Mol. Pharm.* **2011**, *8*, 2032–2038.

26. B. P. Mahoney, N. Raghunand, B. Baggett, R. J. Gillies, *Biochemical Pharmacology* **2003**, *66*, 1207–1218.

27. R. A. Gatenby, R. J. Gillies, *Nature Reviews Cancer* **2008**, *8*, 56–61.

28. G. LaMonte, X. Tang, J. L.-Y. Chen, J. Wu, C.-K. C. Ding, M. M. Keenan, C.

29. A. T. Petkova, J. G. Hu, M. Bizounok, M. Simpson, R. G. Griffin, J. Herzfeld, *Biochemistry* **1999**, *38*, 1562–1572.

30. T. K. Harris, G. J. Turner, Structural basis of perturbed pKa values of catalytic groups in enzyme active sites, *IUBMB Life* **2002**, *53*, 85–98.

31. A. C. Johansson, E. Lindahl, Amino-acid solvation structure in transmembrane helices from molecular dynamics simulations, *Biophys. J.* **2006**, *91*, 4450–4463.

32. A. G. Karabadzhak, D. Weerakkody, D. Wijesinghe, M. S. Thakur, D.M. Engelman, O.A. Andreev, V.S. Markin, Y.K. Reshetnyak, *Biophys. J.* **2012**, *102*, 1846–1855.

33. J. A. Killian, G. von Heijne, *Trends Biochem Sci.* **2000**, *25*, 429-434.

34. S. H. White, W. C. Wimley, *Annu Rev. Biophys. Biomol. Struct*. **1999**, *28*, 319–365.

35. P. C. van der Wel, N. D. Reed, D. V. Greathouse, R. E. Koeppe, 2nd, *Biochemistry* **2007**, *46*, 7514–7524.

36. J. L. MacCallum, W. F. Bennett, D. P. Tieleman, *Biophys J.* **2008**, *94* 3393–3404.

37. K. Elamrani, A. Blume, *Biochimica et Biophysica Acta*, **1983**, *727*, 22–30.

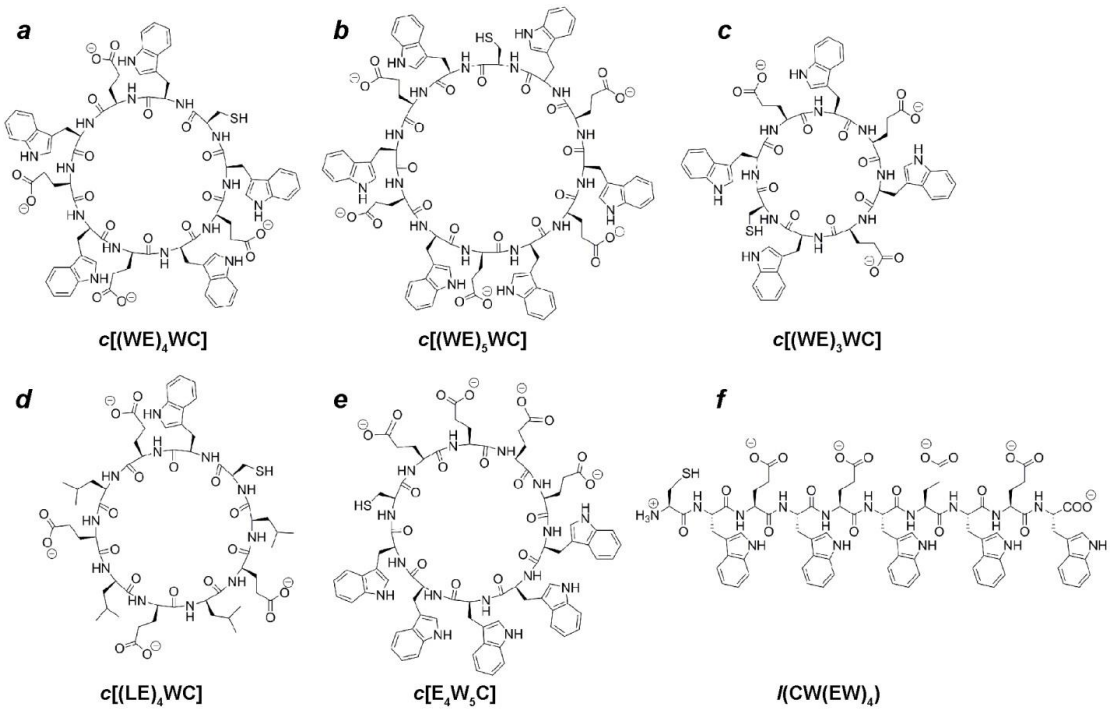

Figure 1. Chemical structures of cyclic peptides.

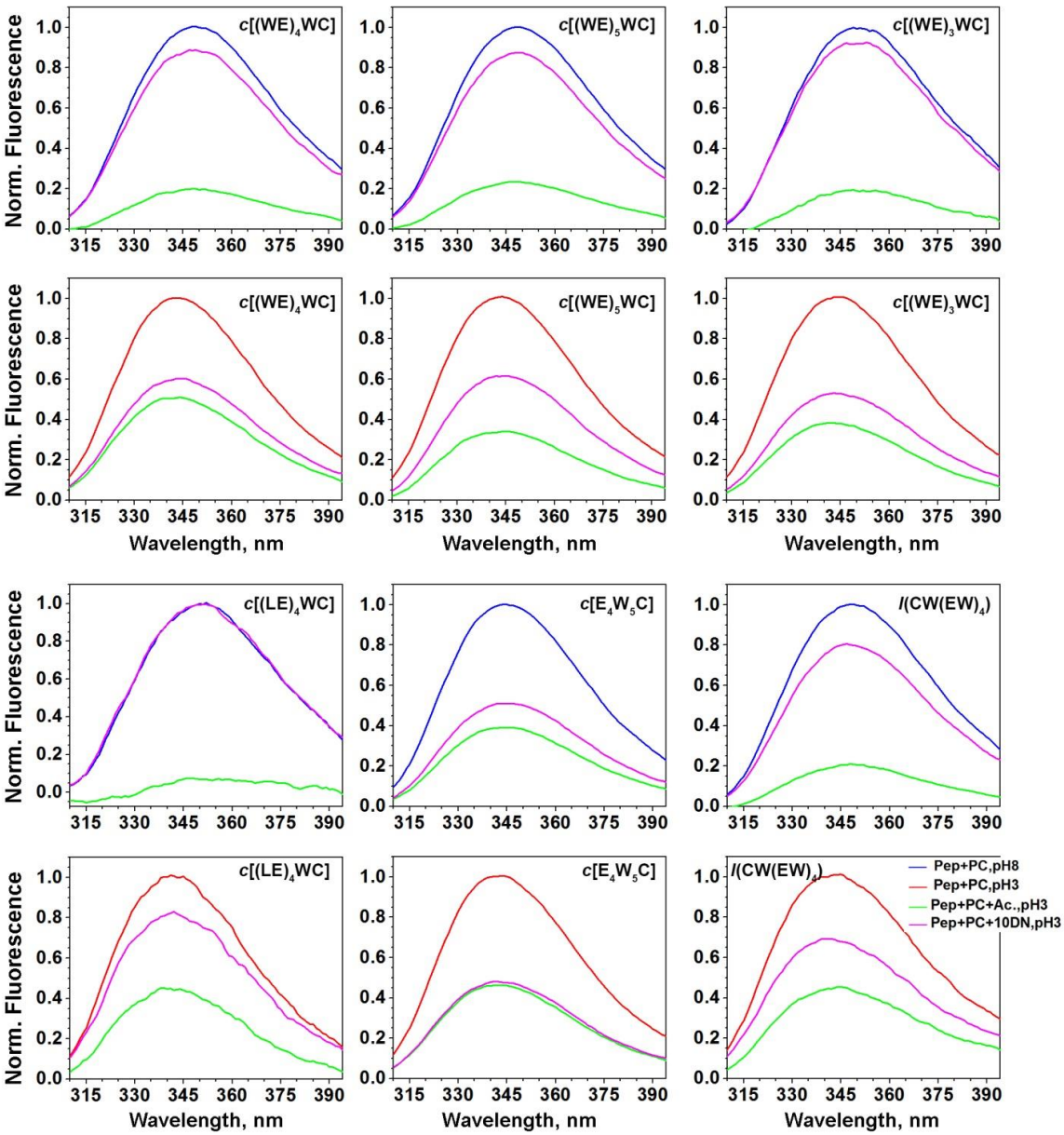

Figure 2. Quenching of fluorescence of peptides in the presence of POPC liposomes at pH 8 (blue lines) or at pH 3 (red lines) by acrylamide (green lines) and 10-DN (magenta lines) are shown. The percentage of quenching is given in Table S3.

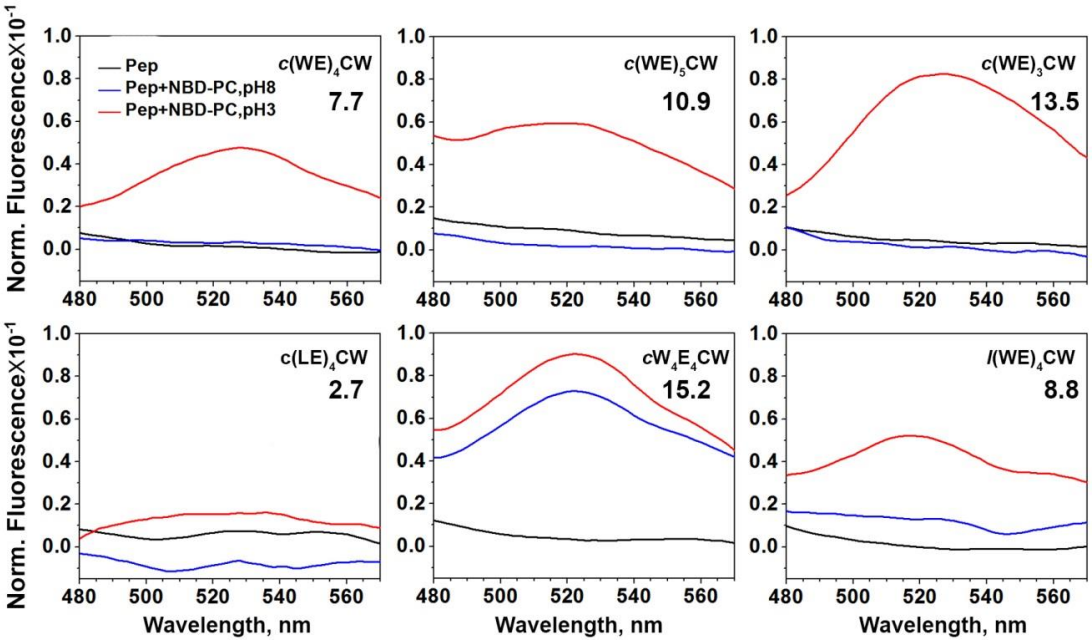

Figure 3. NBD fluorescence spectra of peptides in phosphate buffer at pH 8 (black lines) and in presence of asymmetrically labeled POPC liposomes containing NBD at inner leaflet at pH 8 (blue lines) and at pH 3 (red lines) are shown. The numbers indicate an increase of FRET at pH 3 compared to the peptide fluorescence in phosphate buffer at pH 8.

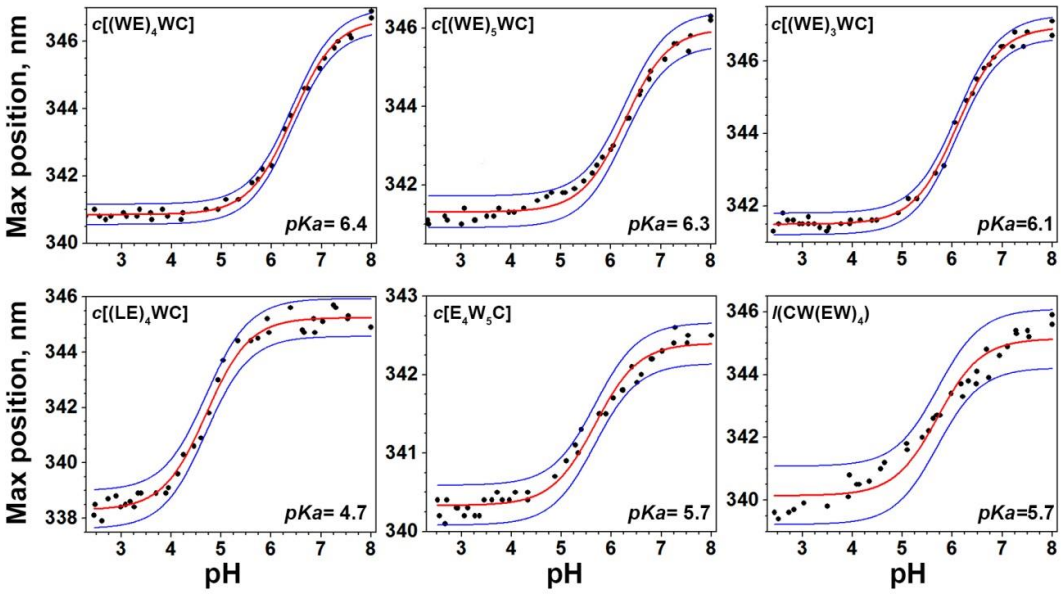

Figure 4. The changes of tryptophan fluorescence are used to follow the partition of the peptides into POPC liposomes as a function of pH. Fitting curve (red lines) and 95% confidence interval (blue lines) are shown.

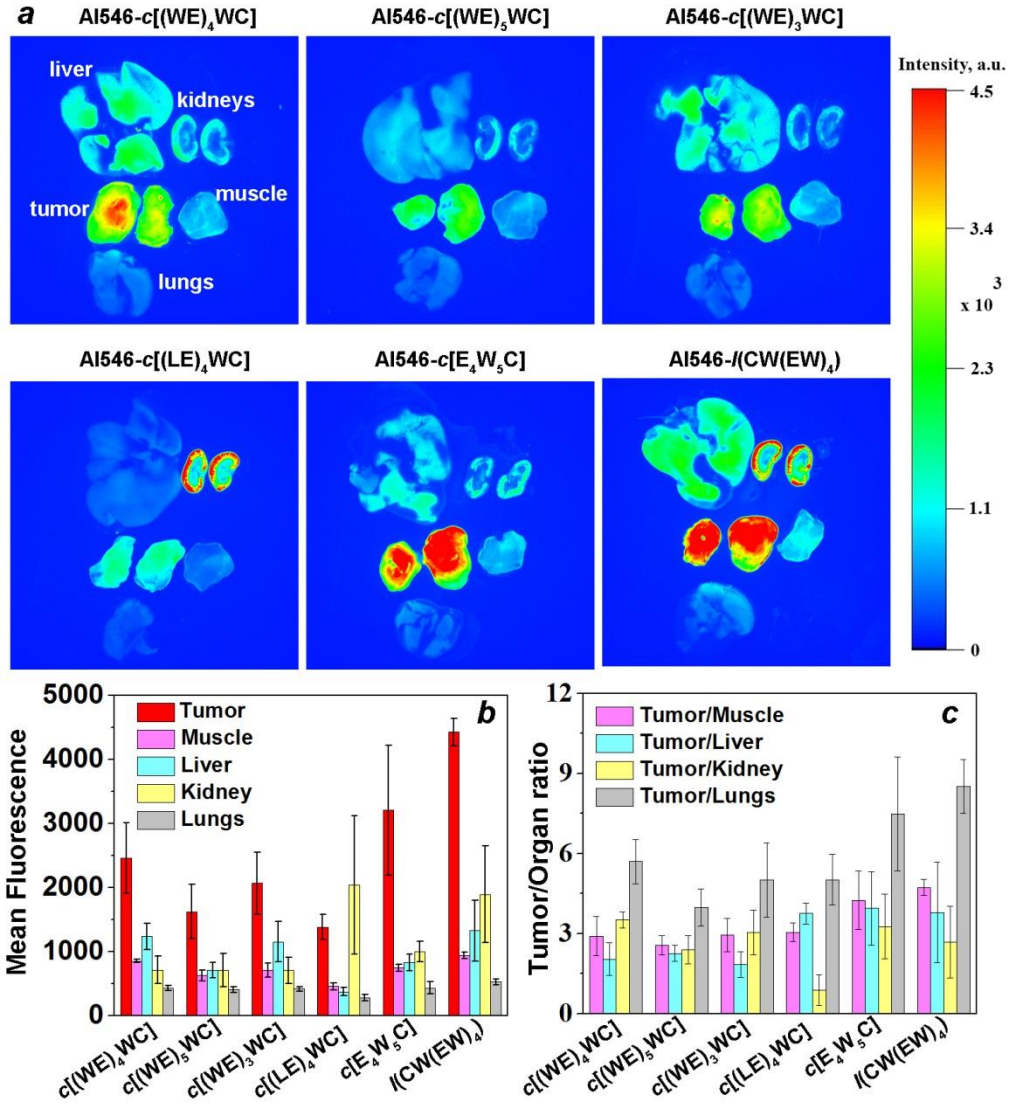

Figure 5. *Ex vivo* fluorescence imaging of tumor, muscle, lungs, liver and kidneys collected at 4 h after IV administration of Alexa546-peptides (**a**); values of mean fluorescence of organs with St.d. (**b**) and Tumor/organ ratios (**c**) are shown. The values are given in Tables S4 and S5 of Supplementary Materials.

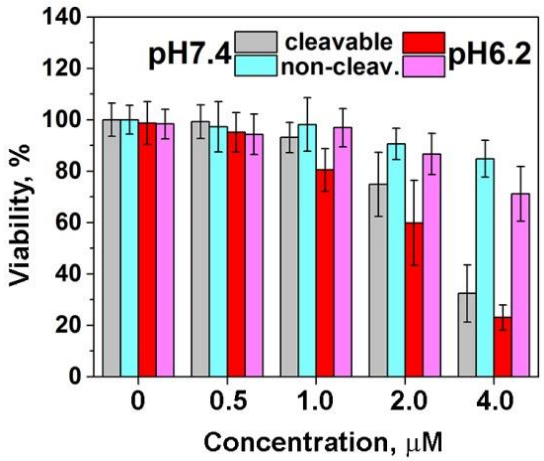

Figure 6. Concentration- and pH-dependent inhibition of HeLa cells proliferation was monitored at 48 h after incubation of cells with cleavable asymmetric *c*[E_4W_5C]-S-S-amanitin and non-cleavable *c*[E_4W_5C]-amanitin constructs for 2 h at normal (pH 7.4) and low (pH 6.2) pHs followed by constructs removal and keeping cells in DMEM with 10% FBS at pH 7.4. The total number of points averaged for each concentration is six.

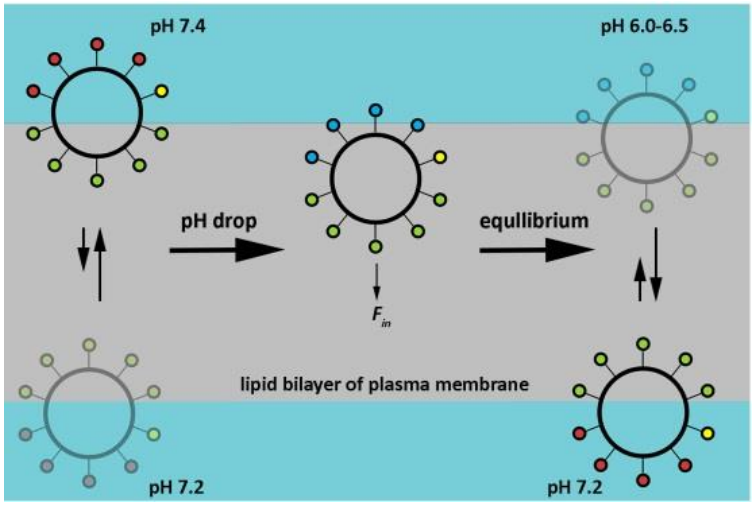

Figure 7. The peptides distribution between outer and inner leaflet of the lipid bilayer of plasma membrane. At neutral and high pHs, Glu residues are negatively-charged (red circles). Trp residues (green circles) interact with polar headgroups. Cys residue (yellow circle) could be directed into bilayer or away depending on hydrophobic or hydrophilic cargo is conjugated with it. More cyclic peptides could be found on the outer bilayer of plasma membranes of cells compared to the inner bilayer due to the small pH gradient (pHe = 7.4 and pHi = 7.2). Drop of a pH leads to the protonation of Glu residues (blue circles), which enhances peptides hydrophobicity and induces partition into bilayer.

SUPPORTING INFORMATION

pH-Sensitive Cyclic Peptides for Tumor Targeting

Dhammika Weerakkody,[a] Anna Moshnikova,[a] Naglaa Salem El-Sayed,[b,c,d], Ramona-Cosmina Adochite,[a] Jovana Golijanin,[a] Rakesh K. Tiwari,[b,c,d] Oleg A. Andreev,[a] Keykavous Parang,[b,c,d,]* Yana K. Reshetnyak[a,]*

EXPERIMENTAL SECTION

1. Peptide Synthesis

1.1. Materials. The peptide synthesis materials including Fmoc-L-amino acid building blocks, preloaded amino acids on 2-chlorotrityl resin as the solid support, and 2-(1*H*−benzotriazol-1-yl)-1,1,3,3-tetramethyluronium hexafluorophosphate (HBTU) used for coupling reagents were purchased from Chem-Impex Int'l Inc., Wood Dale, IL. Piperidine and *N*-methylmorpholine were purchased from Sigma-Aldrich Chemical Co. (Milwaukee, WI). The other chemicals such as *N*,*N*-diisopropylethylamine (DIPEA), cleavage cocktail reagents trifluoroacetic acid (TFA), 1-hydroxy-7-azabenzotriazole (HOAt), *N,N′*-diisopropylcarbodiimide (DIC), acetic acid (AcOH), 2,2,2-trifluoroethanol (TFE), anisole, thioanisole, ethanedithiol (EDT), and anhydrous solvents such as *N*,*N*-dimethylformamide (DMF), dichloromethane (DCM), hexane, acetic acid (AcOH), and 2,2,2-trifluoroethanol (TFE) were purchased from Fisher Scientific, Pittsburg, PA.

1.2. Methodology. The peptides were synthesized by employing the *N*-(9-fluorenyl)methoxycarbonyl (Fmoc)-solid phase chemistry using PS3 automated

peptide synthesizer (Rainin Instrument Co., Inc.) at room temperature. The peptide sequence was assembled on preloaded amino acid on 2-chlorotriyl resin using coupling, activating, and deprotecting reagents using HBTU, *N*-methylmorpholine (0.4 M), and piperidine in DMF (20% v/v), respectively. The amino acids in the peptide sequence were coupled using coupling reagents and activating reagent in DMF for 1 h followed by washing with DMF 3 times. The deprotection were carried using piperidine (20%, v/v) in DMF for 2 times, 10 minute for each time, followed by washing with DMF (3 times). The appropriate sequence of linear protected peptide was assembled using the synthesizer. *N*- to *C*-terminal cyclization of peptide were achieved by cleavage of protected peptidyl resin by stirring the peptidyl resin in freshly prepared cleavage cocktail of AcOH/ TFE/DCM (1:2:7, v/v/v) for 1 h at room temperature followed by washing the resin with TFE:DCM (2:8 v/v, 2 times). The collected filtrate was evaporated using a rotary evaporator followed by azeotropic removal of acetic acid by addition of hexane and dichloromethane to afford high viscous liquid or solid-protected linear peptide. The crude linear protected peptide was dissolved in excess of solvents DMF:DCM (4:1 v/v) followed by the addition of HOAt/DIC (1:1.1 equiv) for cyclization for 12-48 h confirmed by MALDI TOF-TOF mass spectrometry. The solvent was evaporated under high reduced pressure in a rotatory evaporator at 40-45 ^{o}C to remove DMF. The final cleavage of side chain protection from the peptide were carried out after confirming the peptide cyclization by MALDI mass spectrometer data by shaking the cyclized peptide mixture in cleavage cocktail reagent R (TFA/thioanisole/anisole/EDT (90:5:2:3 v/v/v/v, 10-15 mL) for 2-4 h followed by precipitation of peptide using cold ether, centrifugation at

2500 rpm and washing with excess of cold ether at 25 ^{o}C for 5 min. The crude peptide was purified with semi preparative reversed phase high performance liquid chromatography (RP-HPLC) by using Hitachi L-2455 on a C18 Phenomenex Prodigy reversed-phase column (10 μm, 250 cm x 21.2 cm). The pure peptide was eluted at 15.0 mL/min using a gradient of binary solvent system using water and acetonitrile with 0.1% TFA for 0-100% over 60 min. The pure collected peptide fractions were pooled and lyophilized to provide solid powder in purity of ≥98 %. All peptides were characterized by using high resolution time of flight AXIMA-performance MALDI TOF-TOF mass spectrometer (Shimadzu). The above mentioned protocol was applied for the synthesis of all cyclic peptides. As representative examples, the synthesis of cyclic, *c*[(WE)$_4$CW], and linear, *l*(CW(EW)$_4$), peptides is described here and provided in Scheme S1, respectively.

1.2.1. Synthesis of *c*[(WE)$_4$CW]. The linear peptide sequence was synthesized on PS3 automated synthesizer as described above in the scale of 0.3 mmol. H-Trp(Boc)-2-chlorotrityl resin (384.6 mg, 0.3 mmol, 0.78 mmol/g) was swelled in DMF, followed by coupling and deprotection cycles to assemble respective amino acids on the peptidyl resin using respective amino acids, such as Fmoc-Glu(OtBu)-OH (382.9 mg, 0.9 mmol), Fmoc-Trp(Boc)-OH (473.9 mg, 0.9 mmol), Fmoc-Cys(Trt)-OH (527.1 mg, 0.9 mmol), and HBTU (341 mg, 0.9 mmol) as the coupling reagent (Scheme S1). Fmoc group of *N*-terminal in the peptidyl resin was removed using deprotection cycle, and the resin was transferred to 100 ml round bottom flask. The linear protected peptide was cleaved by shaking peptidyl resin in cleavage cocktail AcOH/TFE/ DCM (1:2:7 v/v/v, 50 ml) for 1 h followed by washing the resin using TFE:DCM (2:8 v/v,

10 mL, 2 times). The combined filtrate was evaporated to dryness with the subsequently addition of hexane (50 mL × 3) and DCM (10 mL × 3) to remove acetic acid, which provided solid white crude protected peptide ready for cyclization. The cyclization was carried out by dissolving the solid peptide in anhydrous DMF/DCM (250 mL, 4:1 v/v) under nitrogen using DIC (155.0 μL, 0.99 mmol) and HOAt (122.5 mg, 0.9 mmol) with stirring at room temperature for 24 h. The cyclized product was confirmed by taking small aliquot of the reaction mixture and cleavage with reagent R and using MALDI. After cyclization was confirmed, the solvents were evaporated under high reduced pressure, and the side chain protections were removed by addition of cleavage cocktail of reagent R, TFA/thioanisole/anisole/EDT (15 mL, 90:5:2:3 v/v/v/v), and shaking at room temperature for 3 h. The peptide was precipitated, centrifuged, and washed with cold diethyl ether to yield the crude white solid peptide. The peptide was dissolved in H_2O/ CH_3CN with 0.1% TFA and purified using RP HPLC. Then, the pure fractions were collected, concentrated and lyophilized to afford pure solid white powder of *c*[$(WE)_4$WC] peptide. MALDI-TOF (m/z) [$C_{78}H_{83}N_{15}O_{18}S$]: calcd, 1549.5761; found, 1572.2693 [M + Na]$^+$; *c*[$(WE)_5$WC]: MALDI-TOF (m/z) [$C_{94}H_{100}N_{18}O_{22}S$]: calcd, 1864.6980; found, 1865.3943 [M + H]$^+$; *c*[$(WE)_3$WC]: MALDI-TOF (m/z) [$C_{62}H_{66}N_{12}O_{14}S$]: calcd, 1234.4542; found, 1234.7385 [M]$^+$; *c*[$(LE)_4$WC]: MALDI-TOF (m/z) [$C_{58}H_{87}N_{11}O_{18}S$]: calcd, 1257.5951; found, 1258.2421 [M + H]$^+$; *c*[E_4W_5C]: MALDI-TOF (m/z) [$C_{78}H_{83}N_{15}O_{18}S$]: calcd, 1549.5761; found, 1549.1430 [M]$^+$.

1.2.2. Synthesis of *l*(CW$(EW)_4$). The linear peptide was assembled as described above using H-Trp(Boc)-2-chlorotrityl resin (384.6 mg, 0.3 mmol 0.78 mmol/g) in

reaction vessel (Scheme S1). The peptide sequence was assembled using the appropriate amino acid building blocks Fmoc-Glu(OtBu)-OH (382.9 mg, 0.9 mmol), Fmoc-Trp(Boc)-OH (473.9 mg, 0.9 mmol), Fmoc-Cys(Trt)-OH (527.1 mg, 0.9 mmol), and HBTU (0.9 mmol, 341 mg) as the coupling reagent. The final *N*-terminal Fmoc group was deprotected. The peptide was cleaved from the resin and side chain was deprotected by reaction of the peptidyl resin with freshly prepared cleavage cocktail reagent R, TFA/thioanisole/anisole/EDT (15 mL, 90:5:2:3 v/v/v/v), for 3 h at room temperature. The linear protected peptide was precipitated, centrifuged, and purified by using RP-HPLC as mentioned above to yield *l*(CW(EW)$_4$). MALDI-TOF (m/z) [$C_{78}H_{85}N_{15}O_{19}S$]: calcd, 1567.5867; found, 1606.1204 $[M + K]^+$.

Concentration of peptides was calculated spectrophotometrically by measuring absorbance at 280 nm. The extinction coefficients, ε_{280}, M^{-1} cm^{-1}, for the peptides are the following: *c*[(WE)$_4$WC] = 28,000; *c*[(WE)$_5$WC] = 33,600; *c*[(WE)$_3$WC] = 2,400; *c*[(LE)$_4$WC] = 5,600; *c*[E_4W_5C] = 28,000; *l*(CW(EW)$_4$) = 28,000.

1.2.3. Labeling of Peptides with Fluorescent Dyes. Peptides were conjugated with Alexa546- and Fluorescein-5-maleimide (Life Technologies) in DMF at a ratio of 1.2:1 and incubated at room temperature for about 6 hours and then at 4 °C until the conjugation reaction was completed. 50 mM of sodium phosphate /150 mM NaCl buffer pH7.0 (saturated with argon) was added to the reaction mixture (1/10 of the total volume). The reaction progress was monitored by the reverse phase HPLC. The products were purified by the reverse phase HPLC, lyophilized and characterized by SELDI-TOF mass spectrometry. The concentration of the constructs was determined

by absorbance at 556 and 494 nm using molar extinction coefficients of 93,000 $M^{-1} \cdot cm^{-1}$ for Alexa546 and 68,000 $M^{-1} \cdot cm^{-1}$ for Fluorescein-5 (FITC).

1.2.4. Synthesis of Peptide-Amanitin Constructs. We conjugated symmetric *c*[$(WE)_4$WC] and asymmetric *c*[E_4W_5C] peptides with alpha-amanitin (Sigma-Aldrich) via cleavable S-S bond. Furthermore, asymmetric *c*[E_4W_5C] peptide was labeled with amanitin via non-cleavable bond. The conjugation Scheme consists of 2 steps: i) NH_2 group of amanitin (see Scheme S2, a) was conjugated with NHS group of the cleavable crosslinker, SPDP, *N*-succinimidyl 3-(2-pyridyl-dithio)-propionate (Scheme S2, b) or the non-cleavable crosslinker, GMBS, *N*-γ-maleimidobutyryl-oxysuccinimide ester (Scheme S2, c) (both crosslinkers were from (Thermo Scientific) in 50 mM sodium phosphate/150 mM NaCl buffer pH 7.6 at a ratio 1:20 at room temperature for 4 h to get SPDP-amanitin or GMBS-amanitin. The products were purified by the reverse phase HPLC on Zorbax SB-C18 column (9.4 x 250mm, 5-Micron). SPDP-amanitin was eluted using a gradient: 0-25%, 40 min (water and acetonitrile with 0.05% TFA) and lyophilized. *c*[$(WE)_4$WC] and *c*[E_4W_5C] peptides were incubated with SPDP-amanitin or GMBS-amanitin in 100 mM sodium phosphate/150 mM NaCl buffer pH 7.8 (saturated with argon) at a ratio 1:1 at room temperature for 1 h to obtain amanitin-SPDP-peptides (Scheme S2, d and f) or amanitin-GMBS-peptide (Scheme S2, e), respectively. The products were purified by the reverse phase HPLC on Zorbax SB-C18 column (9.4 x 250mm, 5-Micron) using gradient 10-55%, 40 min (water and acetonitrile with 0.05% TFA). The products were lyophilized and characterized by SELDI-TOF mass-spectrometry. The calculated and obtained masses for the peptides are the following: *c*[E_4W_5C]-SPDP-amanitin:

SELDI-TOF (m/z) [$C_{120}H_{139}N_{25}O_{33}S_3$]: calcd, 2553.9129; found 2555.5263 $[M + H]^+$; *c*[E_4W_5C]-GMBS-amanitin: SELDI-TOF (m/z) [$C_{125}H_{144}N_{26}O_{35}S_2$]: calcd, 2632.9279; found 2634.5723 $[M + H]^+$, and 2657.8214 $[M + Na]^+$; *c*[$(WE)_4WC$]-SPDP-amanitin: SELDI-TOF (m/z) [$C_{120}H_{139}N_{25}O_{33}S_3$]: calcd, 2553.9129; found 2554.5000 $[M + 1]^+$.

2. Liposome Preparation. Large unilamellar vesicles (LUVs) were prepared by extrusion. POPC, 1-palmitoyl-2-oleoyl-sn-glycero-3-phosphocholine (Avanti Polar Lipids), or a mixture of POPC with 0.5% of 18:1 NBD-PE, 1,2-dioleoyl-*sn*-glycero-3-phosphoethanolamine-N-7-nitro-2-1,3-benzoxadiazol-4-yl ammonium salt (Avanti Polar Lipids) were dissolved in chloroform, desolvated on a rotary evaporator, and dried under high vacuum for several hours. The phospholipid film was then rehydrated in 10 mM phosphate buffer pH 8.0, vortexed until the lipid bilayer was completely dissolved, and repeatedly (15-21 times) extruded through the membranes with 50 nm pore sizes to obtain LUVs.

3. Steady-State Fluorescence and CD. Freshly prepared peptides and POPC vesicles were mixed to have 5 μM of a peptide and 1.25 mM of lipids in the final solution. Steady-state fluorescence measurements were carried out on a PC1 spectrofluorometer (ISS, Inc.) under temperature control at 25 °C. Tryptophan fluorescence was excited at 280 nm (there is no Phe or Tyr in the peptides) and recorded with the excitation and emission slits set at 1 nm. The polarizers in the excitation and emission paths were set at the "magic" angle (54.7^o from the vertical orientation) and vertically (0^o), respectively. Steady state CD measurements were carried out in MOS 450

spectropolarimeter (Bio-Logic, Inc.) with the same concentrations of peptide and lipids as it were used in fluorescence measurements.

4. pH-Dependence. pH-dependent partitioning of the peptides into a lipid bilayer of membrane was investigated by the shift of the position of the fluorescence spectral maximum for the peptides in the presence POPC liposomes induced by a drop of pH from 8 to 2.5 by addition of HCl. The peptides were incubated overnight with 50-nm POPC liposomes (final concentration of the peptides and POPC in solution was 5 μM and 1 mM, respectively), and pH decrease was achieved by the addition of aliquots of 4, 2, 1 and 0.1 M HCl. pH was measured by micro-electrode probe (Thermo Electron Corporation, Orion Ross Micro pH electrode). Fluorescence spectra were recorded at each pH value. The spectra were analyzed by the decomposition algorithms using on-line PFAST toolkit (Protein Fluorescence and Structural Toolkit: http://pfast.phys.uri.edu/) to establish the position of the emission maximum. Finally, the positions of the fluorescence spectral maxima (λ_{max}) were plotted versus pH, and the Henderson–Hasselbalch equation was used to fit the data (using Origin 8.5 software):

$$\lambda_{max} = \lambda_{1\,max} + \frac{(\lambda_{1\,max} - \lambda_{2\,max})}{1 + 10^{(pH - pKa)}}$$

where $\lambda_{1_{max}}$ and $\lambda_{2_{max}}$ are the beginning and end of the transition, and *pK*a – is the midpoint of the transition.

5. Dual Quenching. POPC liposomes without and with 10% of the lipids replaced by 10-doxylnonadecane (10-DN) (Avanti Polar Lipids) were prepared in 10 mM citrate-

phosphate buffer pH 8.0. Peptides and POPC liposomes were mixed to generate final concentrations of 7 μM peptide and 2.1 mM POPC without and with 10-DN. In some of the samples, the pH was lowered to pH 4 by addition of aliquot of 2 M citric acid, and other samples were kept at pH 8. To the samples of POPC liposomes containing no 10-DN, acrylamide (Sigma-Aldrich) was added to have a final concentration of 235 mM in solution. Concentration of peptides in all samples was kept constant. To observe quenching of tryptophan fluorescence by 10-DN or acrylamide, the tryptophan fluorescence was recorded as described above. The appropriate POPC blanks were measured and subtracted from the measured spectra before analysis. The percentage of quenching was calculated.

6. NBD-FRET. First, symmetrically NBD-labeled POPC liposomes containing 0.5% of NBD-PE were prepared. Next, 1.2 ml of 6 mM of symmetrically NBD-labeled POPC liposomes were incubated with 150 μl of 1 M freshly prepared membrane-impermeable dithionite in buffer at pH 8.0 to chemically deactivate of NDB only at outer leaflet of bilayer and obtain asymmetrically NBD-labeled POPC liposomes. The decrease of NBD fluorescence occurring in the result of quenching of NBD by dithionite was monitored at excitation of 463 nm and emission at 530 nm. The dithionite quenching leads to the reduction of about 60-65% of NBD fluorescence signal corresponding to the NBD on the outer leaflet of the bilayer. Next, POPC solution was passed through a G-10 sephadex (Sigma-Aldrich) column to remove the excess of dithionite. Asymmetrically labeled POPC liposomes were incubated with peptides at concentrations indicated above, and FRET from tryptophan residues to

NBD at inner leaflet of bilayer was monitored at 280 nm excitation wavelength, and emission was recorded from 310 to 580 nm.

7. Cell Lines. Human cervix adenocarcinoma (HeLa) cells were acquired from the American Type Culture Collection. Cells were cultured in Dulbecco's Modified Eagle's Medium (DMEM) supplemented with 10% fetal bovine serum (FBS), 10 μg/mL of ciprofloxacin in a humidified atmosphere of 5% CO_2 and 95% air at 37°C. The pH 6.2 medium was prepared by mixing 13.3 g of dry DMEM with 0.15 g of sodium bicarbonate in 1 L of deionized water.

8. Cytotoxic Assay. HeLa cells were loaded in the wells of 96-well plates (~5,000 cells per well) and incubated overnight. Growth medium was replaced with the medium without FBS pH 6.2 or pH 7.4 containing increasing amounts of constructs (5, 10, 20, and 40 μM). The same volume of DMEM medium supplemented with 20% FBS, pH 7.4 was added after 2 h of treatment. After 48 h of incubation a colorimetric reagent (CellTiter 96 AQ_{ueous} One Solution Assay, Promega) was added for 1 h followed by measuring absorbance at 490 nm to assess cell viability. All samples were prepared in triplicate.

9. Proliferation Assay. HeLa cells were loaded in the wells of 96-well plates (~5,000 cells per well) and incubated overnight. Growth medium was replaced with the medium without FBS pH 6.15 or pH 7.4 containing increasing amounts of peptide-amanitin construct (0.5, 1, 2, and 4 μM). The construct was removed after 2 h. After 48 h of incubation in standard growth medium, a colorimetric reagent (CellTiter 96

AQ_{ueous} One Solution Assay, Promega) was added for 1 h followed by measuring absorbance at 490 nm to assess cell viability. All samples were prepared in triplicate.

10. Fluorescent Microscopy. HeLa cells (8,000 cells per dish) were seeded in the center of a 35-mm dish with a 10-mm glass-bottom window coated with collagen (MatTek Corp). Next day cells were incubated with 5 μM of FITC-labeled *c*[E_4W_5C] peptide for 30 min in DMEM medium without FBS at pH 7.4 or 6.2. Cells were washed 5 times at pH 7.4 and 0.4% Trypan Blue was added for 5 min (1/10 of the total volume). Fluorescent images were acquired with a Retiga CCD camera (Qimaging) mounted to an inverted Olympus IX71 microscope (Olympus America, Inc.).

11. Ex Vivo Fluorescence Imaging. All animal studies were conducted according to the animal protocol AN04-12-011 approved by the Institutional Animal Care and Use Committee at the University of Rhode Island, in compliance with the principles and procedures outlined by NIH for the Care and Use of Animals. 4T1 breast tumors were established by subcutaneous injection of 4T1 cells (8×10^5 cells/0.1 mL/flank) in the right flank of adult female BALB/c mice (about 19-22 g weight) obtained from Harlan Laboratories. When tumors reached about 6 mm in diameter single tail vein injections of 100 μl of 40 μM Alexa546-peptides were performed. Control mice bearing tumor used to establish an auto fluorescence signal did not receive fluorescent peptides. At 4 h post-injection euthanization and necropsy was performed followed by *ex vivo* imaging of tumor, kidneys, liver, lungs and muscle. Mean fluorescence intensity of tumor and organs was calculated using Kodak software.

TABLES

Table S1. Properties of the synthesized peptides.

Peptide	Calculated M.W.	Found M.W.	Retention time in HPLC	% purity
***c*[(WE)$_4$WC]**	1549.5761	1572.2693 [M + Na]$^+$	35.2-36.7	99
***c*[(WE)$_5$WC]**	1864.6980	1865.3943 [M +H]$^+$	35.8-37.2	99
***c*[(WE)$_3$WC]**	1234.4542	1234.7385 [M]$^+$	35.0-36.0	99
***c*[(LE)$_4$WC]**	1257.5951	1258.2421 [M + H]$^+$	35.2-36.3	95
***c*[E$_4$W$_5$C]**	1549.5761	1549.1430 [M]$^+$	36.6-37.7	99
***l*(CW(EW)$_4$)**	1567.5867	1606.1204 [M + K]$^+$	32.3-33.2	99

Table S2. The spectral parameters of the peptides in phosphate buffer at pH 8, in the presence of POPC liposomes at pH 8 and pH 3 are presented. The parameters were obtained from analysis of the fluorescence spectra shown in Figure 2: the maximum position of the fluorescence spectrum λ_{max}, in nm; ***S*** – the normalized area under the spectra (normalization was done on the area under the spectrum for peptides at pH 8 in absence of POPC liposomes, black lines on Figure 2).

Peptide	λ_{max}, **nm**			***S***	
	Pep, pH8	**Pep-PC, pH8**	**Pep-PC, pH3**	**Pep-PC, pH8**	**Pep-PC, pH3**
***c*[(WE)$_4$WC]**	350.5±0.2	347.5±1.2	341.1±0.9	1.1±0.1	1.6±0.2
***c*[(WE)$_5$WC]**	350.3±0.2	346.7±1.2	341.2±0.4	1.5±0.3	2.1±0.3
***c*[(WE)$_3$WC]**	351.0±0.2	349.1±0.7	341.7±0.2	0.9±0.1	1.7±0.3
***c*[(LE)$_4$WC]**	348.7±0.3	348.2±0.6	339.6±1.2	1.1±0.0	1.1±0.1
***c*[E$_4$W$_5$C]**	350.6±0.2	342.8±0.4	340.2±0.4	2.4±0.3	2.4±0.5
***l*(CW(EW)$_4$)**	353.0±0.7	346.6±0.7	339.8±0.6	2.3±0.4	1.6±0.4

Table S3. The percentage of peptides fluorescence quenching by addition of acrylamide (AC) or 10-DN at pH 8 and pH 3 in the presence of POPC liposomes are shown. The values were obtained from analysis of the fluorescence spectra shown in Figure 3.

	Pep-PC+AC pH8	**Pep-PC+ 10-DN pH8**	**Pep-PC+AC pH3**	**Pep-PC+ 10-DN pH3**
***c*[(WE)$_4$WC]**	82	11	50	40
***c*[(WE)$_5$WC]**	78	13	68	40
***c*[(WE)$_3$WC]**	83	6	63	47
***c*[(LE)$_4$WC]**	96	0	59	17
***c*[E$_4$W$_5$C]**	61	49	54	52
***l*(CW(EW)$_4$)**	81	20	56	31

Table S4. Mean NIR fluorescence with standard deviation calculated for each organ collected at 4 h after Alexa546-peptide administration. The data are shown on Figure 6b.

	Tumor	**Muscle**	**Liver**	**Kidney**	**Lungs**
Al546-*c*[(WE)$_4$WC]	2459.1±552.3	850.6±27.9	1235.9±206.5	711.3±212.6	427.7±39.7
Al546-*c*[(WE)$_5$WC]	1621.6±422.1	626.5±84.4	710.4±122.5	705.7±260.4	403.1±43.7
Al546-*c*[(WE)$_3$WC]	2066.2±486.5	706.7±107.1	1150.5±314	704.4±205.1	416.6±35.5
Al546-*c*[(LE)$_4$WC]	1380±193.7	453.3±53.8	370.6±65.7	2039.0±1080.7	279.1±47.7
Al546-*c*[E$_4$W$_5$C]	3204.8±1011.7	745.9±55.5	825.1±130.5	996.2±160.8	429.4±93.5
Al546-*l*(CW(EW)$_4$)	4426.8±214.5	936.5±52.1	1323.9±478.4	1891.9±756.5	522.9±42.4

Table S5. Tumor/Organ ratios calculated based on the data presented in Table S1. The data are shown on Figure 6c.

	Tumor/Muscle	**Tumor/Liver**	**Tumor/Kidney**	**Tumor/Lung**
Al546-*c*[(WE)$_4$WC]	2.91±0.73	2.04±0.61	3.51±0.3	5.70±0.83
Al546-*c*[(WE)$_5$WC]	2.56±0.36	2.26±0.31	2.39±0.54	3.98±0.69
Al546-*c*[(WE)$_3$WC]	2.94±0.63	1.85±0.48	3.04±0.85	5.02±1.4
Al546-*c*[(LE)$_4$WC]	3.05±0.36	3.76±0.4	0.88±0.58	5.02±0.96
Al546-*c*[E$_4$W$_5$C]	4.25±1.09	3.95±1.38	3.27±1.21	7.48±2.14
Al546-*l*(CW(EW)$_4$)	4.73±0.31	3.80±1.88	2.68±1.34	8.52±1.00

Schemes

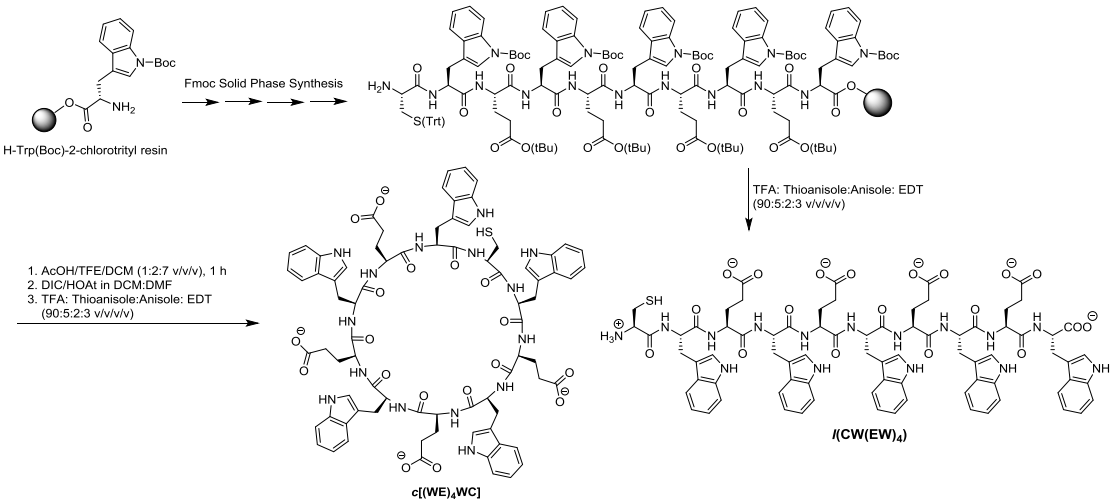

Scheme S1. Synthesis of *l*(CW(EW)$_4$) and *c*[(WE)$_4$CW] peptides.

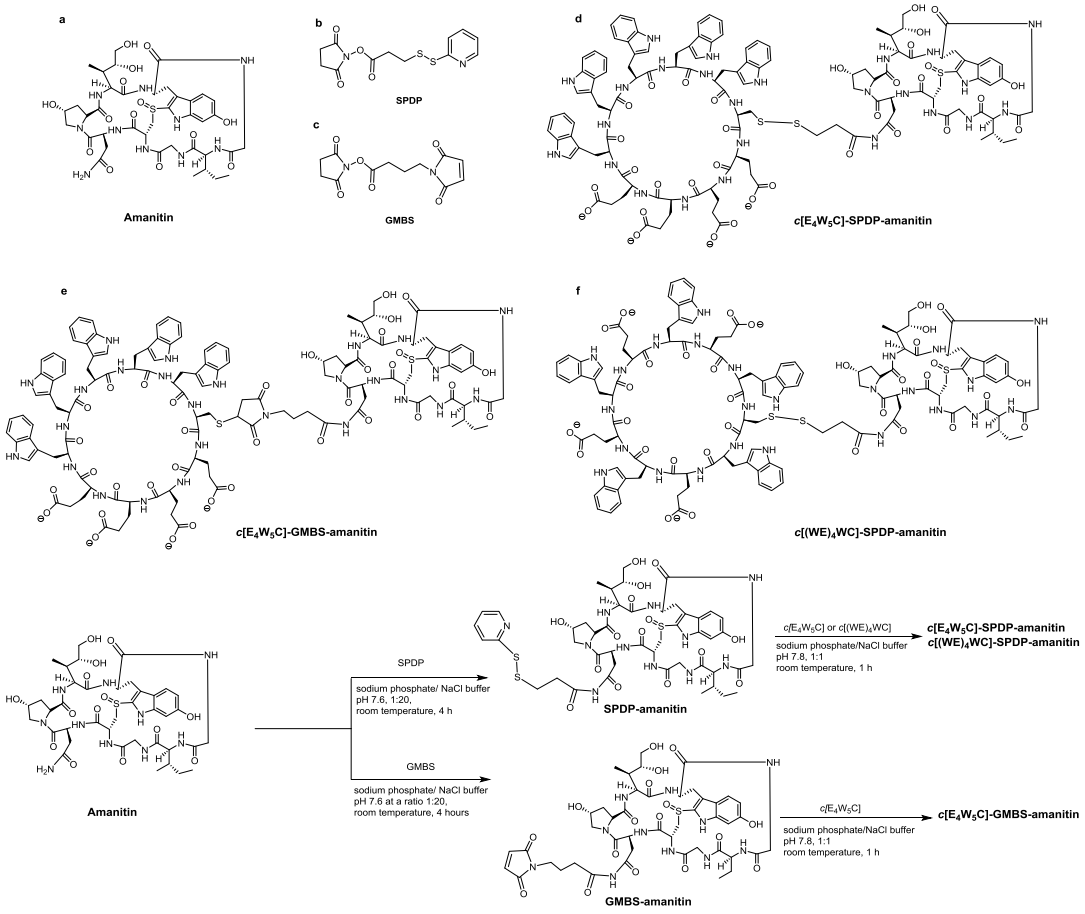

Scheme S2. Structures of amanitin (***a***), SPDP (***b***) and GMBS (***c***) crosslinkers. Schematic presentation of structures of *c*[E_4W_5C] peptide conjugated with alpha-amanitin via cleavable S-S (***d***) and non-cleavable (***e***) bonds using SPDP and GMBS crosslinkers, respectively, (***f***) *c*[$(WE)_4WC$]-SPDP-amanitin conjugated with alpha-amanitin via cleavable S-S bond using SPDP linker.

Figures

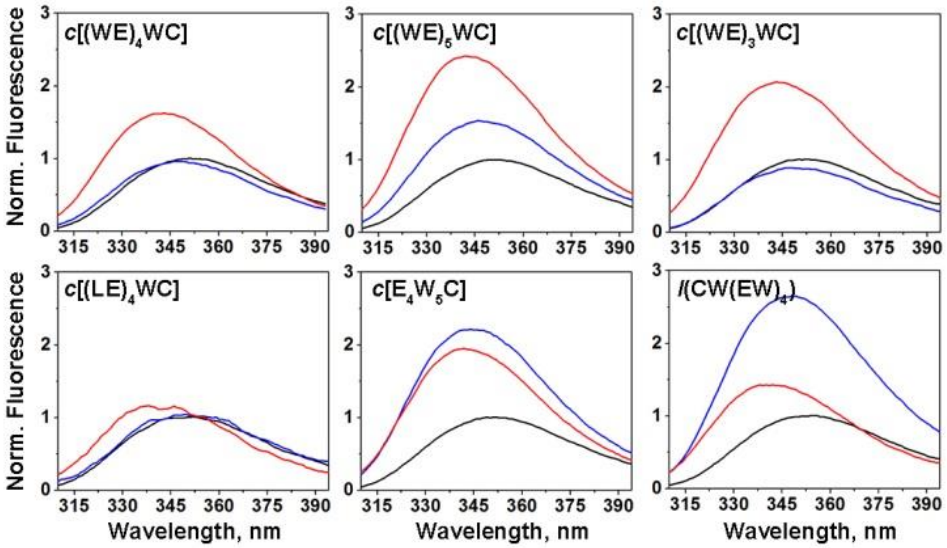

Figure S1. The emission of peptides in phosphate buffer at pH 8 (black lines) and in the presence of POPC liposomes at pH 8 (blue lines) and pH 3 (red lines) are shown. The spectral parameters are given in Table S2.

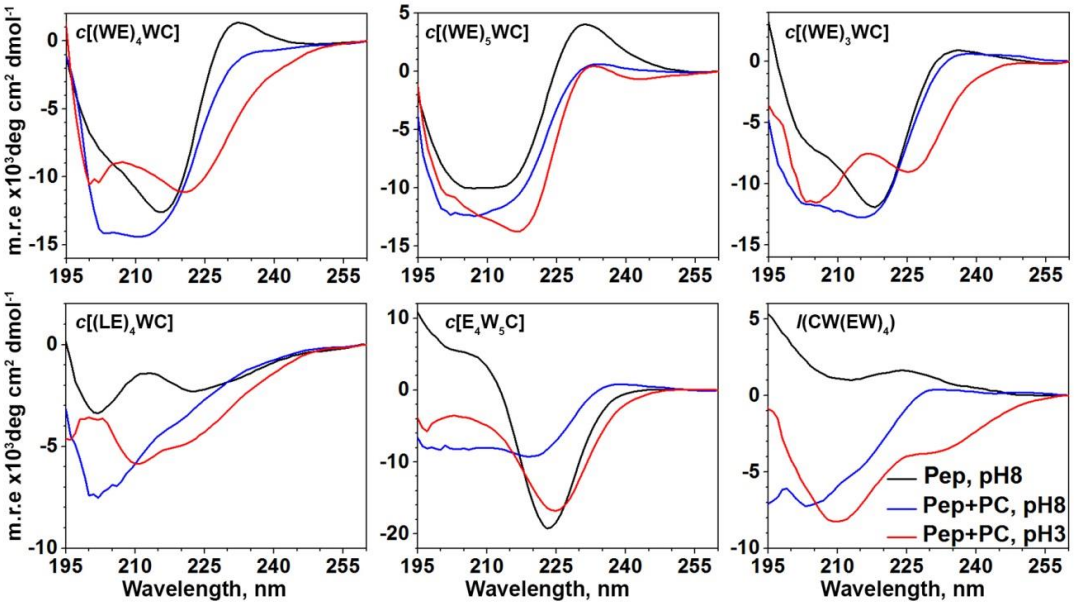

Figure S2. The circular dichroism of peptides in phosphate buffer at pH 8 (black line) and in presence of POPC liposomes at pH 8 (blue line) and pH 3 (red line) are shown.

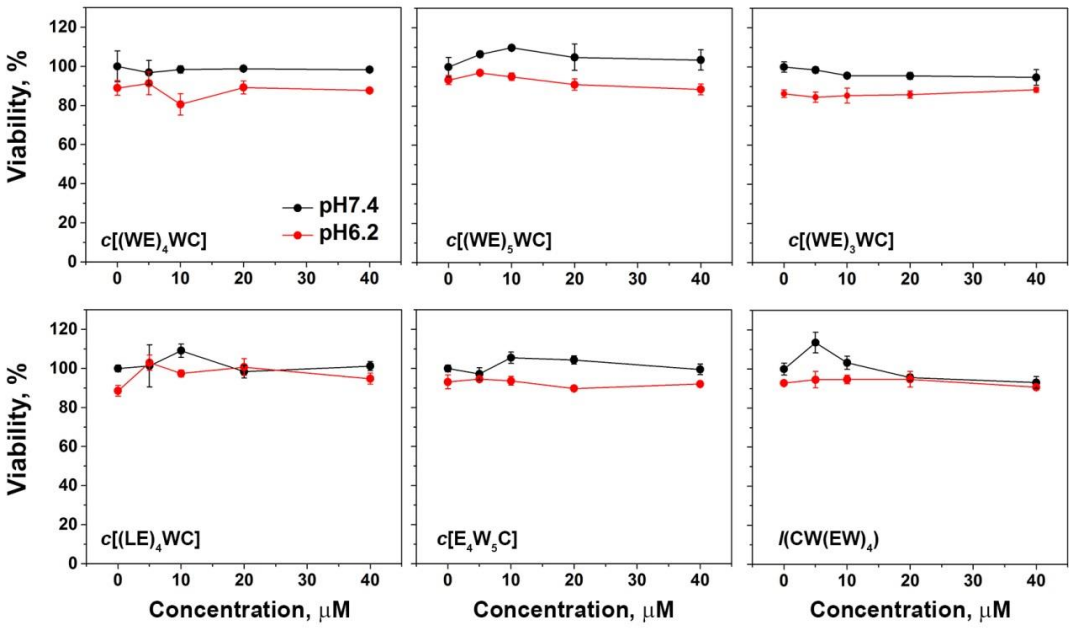

Figure S3. HeLa cells were treated with increasing concentrations of peptides without FBS at pH 6.2 (red lines and circles) or pH 7.4 (black lines and circles). The same volume of DMEM medium supplemented with 20% FBS, pH 7.4 was added after 2 hrs of treatment. After 48 hours of incubation MTS assay was performed to access cell viability.

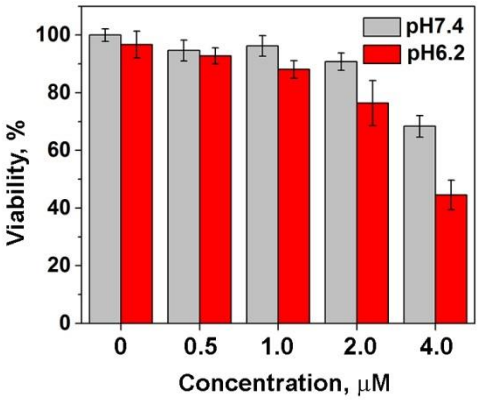

Figure S4. Concentration- and pH-dependent inhibition of HeLa cells proliferation was monitored at 48 h after incubation of cells with cleavable *c*[(WE)$_4$WC]-S-S-Amanitin construct for 2 hours at normal (pH 7.4) and low (pH 6.2) pHs followed by constructs removal and keeping cells in DMEM with 10% FBS at pH 7.4. The total number of points averaged for each concentration is six.

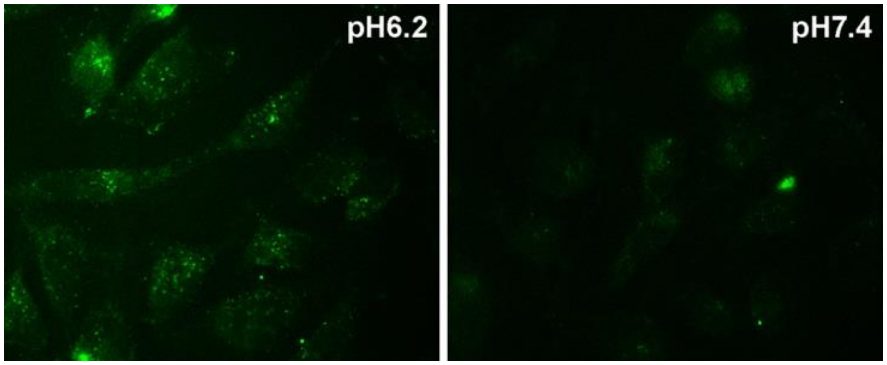

Figure S5. FITC-labeled asymmetric cyclic peptide, *c*[E$_4$W$_5$C], was treated with cells for 30 min at pH 7.4 or 6.2, followed by washing at pH 7.4 in both cases, addition of Trypan Blue for 5 min and live cell imaging. Cells treated with FITC-peptide at low pH, washed at normal pH and incubated with Trypan Blue show higher level of fluorescence signal compared to the cells treated with FITC-peptide at normal pH, washed at normal pH, and incubated with Trypan Blue.

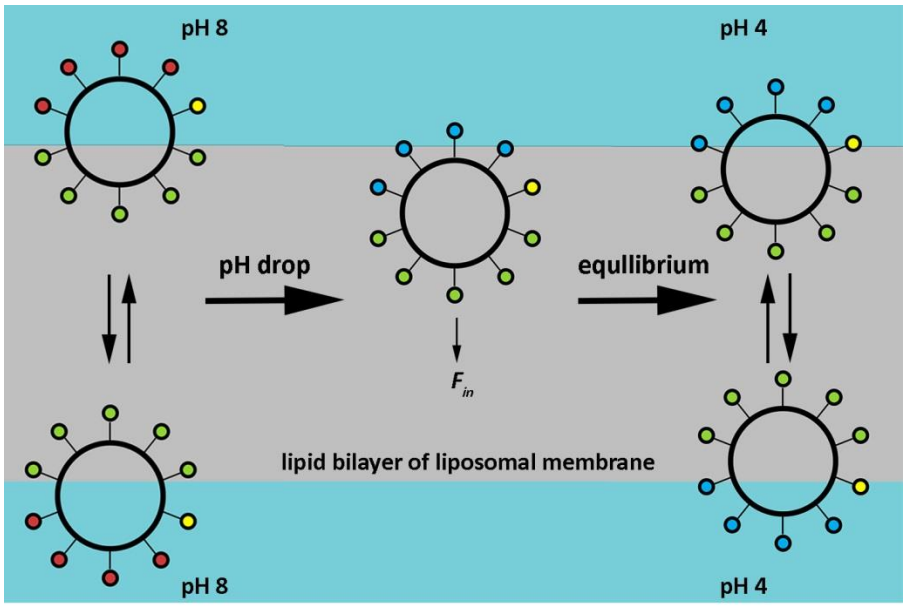

Figure S6. The peptides distribution between outer and inner leaflet of the lipid bilayer in liposomes. At neutral and high pHs, Glu residues are negatively-charged (red circles). Trp residues (green circles) interact with polar headgroups. Cys residue (yellow circle) could be directed into bilayer or away depending on hydrophobic or hydrophilic cargo is conjugated with it. Drop of a pH leads to the protonation of Glu residues (blue circles), which enhances peptides hydrophobicity and induces partition into bilayer. In the case of liposomes, pH equilibrates fast, thus low pH will be outside and inside of liposome. It would lead to the equilibration of concentration of cyclic peptides with protonated Glu residues between inner and outer leaflets of the bilayer.

CHAPTER 4

Submitted in Journal of Molecular Biology

Comparative study of tumor targeting and biodistribution of pH (Low) Insertion Peptides conjugated with various fluorescent dyes

Ramona-Cosmina Adochite[1], Anna Moshnikova[1], Jovana Golijanin[1], Oleg A. Andreev[1], Yana K. Reshetnyak[1,*]

[1]Physics Department, University of Rhode Island, 2 Lippitt Road, Kingston, RI 02881 USA

KEYWORDS: Imaging, tumor acidity, fluorescent dyes, targeting of submillimeter metastatic lesions.

Corresponding Authors

Yana K. Reshetnyak, Department of Physics, University of Rhode Island, Kingston, RI 02881, United States; phone: 401-874-2054; E-mail: reshetnyak@mail.uri.edu

ABSTRACT

An enhanced use of glycolysis and production of carbonic and lactic acids, actively contribute to the extracellular acidosis, promoting tumor development, progression and invasiveness. Thus, extracellular acidity might serve as a general marker for detection and targeting of aggressive tumors. pH (Low) Insertion Peptides (pHLIPs) pertain to the class of pH-sensitive agents able of sensing pH at the cellular surface and delivery of imaging and/or therapeutic agents to the cancer cells in tumors. Here, we investigated targeting of highly metastatic 4T1 mammary carcinoma and biodistribution of different pHLIP variants conjugated with various fluorescent dyes with the main purpose to identify the best pHLIP-based constructs for clinical applications. All fluorescent pHLIPs exhibited good targeting of breast tumors with minimal accumulation in muscle at 24 hours post-injection. The highest tumor targeting with low accumulation in liver, kidney and muscle was observed for Alexa546-pHLIPs. Also, we showed that Alexa546-Var3 targets ~500 μm sized metastatic lesions in lungs. Fluorescent pHLIP-based agents could be used for diagnosis and treatment (surgical resection) of primary tumors and submillimeter metastatic lesions.

Introduction

A common specific feature of tumor microenvironment is a hypoxia and an extracellular acidosis [1]. The acidification of extracellular space leads to reverse of a pH transmembrane gradient in cancer cells [2,3]. Previous research showed that the acidic extracellular pH, promotes invasion and metastasis of cancer cells [4,5]. The highly proliferative cancer cells (metabolically active cells) are the most acidic. Thus, targeting of tumor acidity might be developed as an important predictive clinical marker of tumor aggressiveness and invasiveness. However, a sharp proton concentration gradient exists near the surface of cancer cells. Thus, the best approach will be to access acidity in close proximity to cancer cells in tumors.

We have introduced family of pH Low Insertion Peptides (pHLIPs), which represents a unique class of water-soluble membrane polypeptides capable to undergo a pH-dependent membrane-associated folding [6,7]. pHLIP peptides possess dual delivery capabilities, making use of the energy of folding to translocate polar cargo molecules across phospholipid bilayer of membrane and/or tether molecules to the cell surface [8]. Also, the process of peptide folding within a membrane ensures a high cooperativity of the transition, which cannot be achieved by simple diffusion [9,10,11]. Since pHLIPs are in equilibrium between membrane bound and non-bound configurations at normal pH they are capable of sensing pH at the cell surface. As soon as pH drops (even on a half of pH unit), the Asp and Glu residues are protonated enhancing affinity of peptides to membrane, which triggers folding in membrane and release of energy. Depending on pHLIP sequence protonatable residues could be differently located on membrane surface, which directly affects the rate of the protonation events at various

pHs, and thus pK of peptides insertion into the membrane. We have introduced family of pHLIP peptides with pK of insertion varying from 4.5 to 6.5 and confirmed that tumor targeting is indeed pH-dependent [5,7]. Three pHLIP variants, WT, Var3 and Va7 were selected as lead candidates for pH-specific delivery of imaging and therapeutic agents to tumors of different origins [7]. We showed previously targeting of tumors by fluorescently-labeled WT-, Var3- and Var7-pHLIP as well by the pHLIP-Fluorescence Insertion REporter (pHLIP-FIRE) [12,13,14]. One of the very attractive potential clinical applications of fluorescent pHLIPs might be a fluorescence-guided surgical resection of tumors. The proliferative cancer cells will light up most of all targeted by the fluorescent-pHLIPs. However, in addition to the peptide sequence variation, fluorescent dyes (which are usually about one third of pHLIP peptides mass) can affect and alter tumor targeting and biodistribution of pHLIPs. In the present study, we compared targeting of mammary tumors and biodistribution of different pHLIP variants conjugated with eight fluorescent dyes with the main purpose to identify the best pHLIP-based constructs for various clinical uses. Also, we demonstrated staining of sub-millimeter metastatic lesions in lungs by Alexa546-Var3.

Materials and Methods

Conjugation of pHLIP peptides with fluorescent dyes

pHLIP variants were prepared by solid-phase peptide synthesis using Fmoc (9-fluorenylmethyloxycarbonyl) chemistry and purified by reverse phase chromatography by CS Bio. pHLIP variants were conjugated with Alexa546-, Alexa647-, Alexa750-, Cy5.5-, Dy680-, DyP680-maleimide (Life Technologies) and IR680-, IR800-maleimide (LiCor Biosciences) in DMF (dimethylformamide) at a ratio of 1:1 and

incubated at room temperature for about 8 hours and then at 4ºC until the conjugation was completed. The reaction progress and purity was monitored by reverse phase HPLC to ensure absence of free dyes in the final solution. The products were lyophilized and characterized by SELDI-TOF mass spectrometry. The concentration of constructs was determined by absorbance using the following molar extinction coefficients: ε_{556}=104,000 $M^{-1}\cdot cm^{-1}$ (for Alexa546-pHLIPs), ε_{650}=239,000 $M^{-1}\cdot cm^{-1}$ (for Alexa647-pHLIPs), ε_{753}=290,000 $M^{-1}\cdot cm^{-1}$ (for Alexa750-pHLIPs), ε_{673}=209,000 $M^{-1}\cdot cm^{-1}$ (for Cy5.5-pHLIPs), ε_{672}=165,000 $M^{-1}\cdot cm^{-1}$ (for IR680-pHLIPs), ε_{778}=300,000 $M^{-1}\cdot cm^{-1}$ (for IR800-pHLIPs), ε_{684}=140,000 $M^{-1}\cdot cm^{-1}$ (for Dy680-pHLIPs) and ε_{684}=180,000 $M^{-1}\cdot cm^{-1}$ (for DyP680-pHLIPs).

Absorption and fluorescence measurements

Absorbance and fluorescence measurements were carried out on a Genesys 10S UV-Vis (Thermo Scientific) spectrophotometer and a SpectraMax M2 (Molecular Devices) spectrofluorometer, respectively. The excitation wavelengths were the following for different constructs: 550 nm for Alexa546-pHLIPs; 650 nm for Alexa647-pHLIPs, 673 nm for Cy5.5-pHLIPs; 680 nm for IR680-pHLIPs, Dy680-pHLIPs and DyP680-pHLIPs; 750 nm for Alexa750-pHLIPs and 780 nm for IR800-pHLIPs.

Cell lines

The *4T1* and 4T1-GFP mouse mammary tumor cell lines were obtained from the American Type Culture Collection and cultured in RPMI medium supplemented with 10% fetal bovine serum, 10 μg/mL of ciprofloxacin in a humidified atmosphere of 5% CO_2 and 95% air at 37°C.

Tumor mouse models

Mammary tumors were established by subcutaneous injection of 4T1 cells ($8x10^5$ cells/0.1 ml/flank) in the right flank of adult female BALB/c mice (about 19-22 g weight) obtained from Harlan Laboratories. For the metastatic tumor model, $1x\ 10^6$ 4T1-GFP cells/50 μl were injected subcutaneously in the mammary fat pad. After approximately 3 weeks, the primary tumor metastasized in the lungs. All animal studies were conducted according to the animal protocol AN04-12-011 approved by the Institutional Animal Care and Use Committee at the University of Rhode Island, in compliance with the principles and procedures outlined by NIH for the Care and Use of Animals.

Fluorescent imaging of organs and tissue

When tumors reached approximately 5-6 mm in diameter tail vein injections of 100 μL of 40 μM of fluorescent-pHLIPs were performed. Animals were euthanized at 2, 4, 24 and 48 hours post-injection, and necropsy was performed immediately after euthanization. Tumors and major organs of BALB/c mice were collected for imaging on a FX Kodak in-vivo image station. Fluorescence intensity was obtained via analysis of images by using Kodak software. The contrast index (CI) was calculated according to the equation:

$$CI = \frac{F_{tumor} - F_{backg}}{F_{muscle} - F_{backg}}$$

where F_{tumor} , F_{muscle} and F_{backg} are the mean fluorescence intensities of tumor, muscle and background signal of the same organ from untreated mice, respectively.

Fluorescent images of metastatic lesions in lungs were acquired at 4 and 10x magnification using an Olympus IX71 inverted fluorescence microscope.

Results

The focus of our work was targeting of mammary tumors by three pHLIP variants recently selected for pre-clinical development [7,10]:

WT: ACEQNPIYWARYADWLFTTPLLLLDLALLVDADEGT

Var3: ACDDQNPWRAYLDLLFPTDTLLLDLLW

Var7: ACEEQNPWARYLEWLFPTETLLLEL

Each peptide had a single Cys residue at the N-terminus for conjugation with fluorescent dyes. We used fluorophores emitting at visible and near-infrared wavelengths: Alexa546, Alexa647, Alexa750, Cy5.5, Dy680, DyP680, IR680, IR800 (see Table 1). The molecular weights and HPLC retention times, reflecting the hydrophobicity of the investigated fluorescent constructs, are also given in Table 1. The absorption and emission spectra of fluorescent constructs are shown in Supplementary Figure 1. The fluorescence was measured in absence and presence of POPC liposomes to mimic behavior of the fluorescent constructs in membrane-unbound and membrane-bound forms.

With the selected fluorescent dye, Alexa750, we also investigated performance of the following pHLIP sequences, where the N-terminal end of the peptides contains six negatively-charged Asp residues for the enhancement of constructs solubility:

Var3M: ACDDDDDDPWQAYLDLLFPTDTLLLDLLW

Var7M: ACDDDDDDPWQAYLDLFPTDTLALDLW

In addition we studied biodistribution of the constructs, where Alexa546 and Cy5.5 fluorescent dyes were attached to the single Cys residue at the membrane-inserting C-terminus of the Var3 pHLIP peptide:

Var3-C: ADDQNPWRAYLDLLFPTDTLLLDLLCW

To test tumor targeting by fluorescent pHLIPs we selected the highly tumorigenic and invasive 4T1 mammary carcinoma model, which mimics stage IV of human breast cancer [33-35], and is known to be acidic [13] and targeted very well by pHLIPs [10]. This transplantable cancer cell line can spontaneously metastasize from the primary tumor in the mammary gland to multiple distant sites [15,16]. Fluorescent pHLIPs were administrated intravenously and at different time points ranging from 2 to 48 hours, animals were euthanized, tumor, kidney, liver and muscle were collected and imaged immediately. The representative fluorescent images of tissue and organs obtained at 4 hours after the constructs administration are shown on Figure 1. Very good tumor targeting was observed by all fluorescent-PHLIPs. The fluorescent images obtained at different time points were used to calculate changes of the mean surface fluorescence intensity in tissue and organs (Figure 2 and Supplementary Table 1), tumor to organ ratios (Figure 3 and Supplementary Table 2) and contract index (CI) (Figures 4 and Supplementary Table 3).

Different fluorescent pHLIPs demonstrate different kinetic profiles (Figure 2 and Supplementary Table 1). The highest tumor targeting was observed at 2 or 4 hours post-injection with subsequent decay of the signal. Most fluorescent pHLIPs have low liver accumulation except of Cy5.5-pHLIPs, which are the most hydrophobic construct among the investigated. We also performed study with Cy7.5-Var3, which is

more hydrophpobic, and observed significant liver accumulation (data not shown). Surprisingly, Alexa546-pHLIPs, which are second the most hydrophobic constructs after Cy5.5-pHLIPs, showed very low liver, kidney and muscle accumulation with the highest tumor targeting. Tumor to muscle ratio for Alexa546-Var3 was increasing from ~ 5 to 9 within 24 hrs (Figure 3 and Supplementary Table 2). With the shift to near infrared (NIR) wavelengths of excitation and emission for Alexa647-, IR680- and Dy680-pHLIPs more kidney targeting was monitored. Alexa750- and IR800-pHLIPs demonstrate the highest signal in the kidney and liver. We compared performance of Dy680 and its pegylated version, DyP680. The DyP680-pHLIPs are more polar compared to Dy680-pHLIPs. The most noticeable difference was observed in targeting of the kidney: DyP680-pHLIPs demonstrate about twice higher accumulation in the kidney than Dy680-pHLIPs, which could be related to the renal clearance. In overall the contrast index was enhanced for pegylated versions of the constructs compared to non-pegylated counterparts (Figure 4 and Supplementary Table 3).

The contrast index was calculated only for two time points, 2 and 4 hours, since fluorescent signal in muscle at 24 and 48 hrs post-injection was at the level of the background fluorescence (Figure 4 and Supplementary Table 3). We did not observe any significant difference between various pHLIP sequences, except of Alexa546-Var3, which showed statistically significant higher CI compared to Alexa546-WT and – Var7. The highest contrast (around 6) was observed for Alexa546-, Dy680- and DyP680 at 2 hrs post-injection. At 4 hrs the highest contrast of >8 was found for Cy5.5-pHLIPs. The lowest CI was detected for IR680-pHLIPs.

We tested ability of pHLIPs to deliver imaging agents into the cell by conjugating Alexa546 and Cy5.5 dyes to the C-terminal part of Var3 peptide, which inserts into the lipid bilayer of membrane. We selected the most hydrophobic dyes to avoid complications with their translocation across cellular membrane. Our data indicate that CI was very similar for the constructs, where Alexa546 or Cy5.5 were conjugated to the N- or C-terminus. We can conclude that pHLIP is capable of delivering of imaging agents not only to the cell surface but also across membrane into a cell. However, the polarity of imaging agent will affect the process of its cellular delivery. Also, we evaluated performance of modified Var3M and Var7M, where several Asp residues were inserted at the N-terminus of the peptides. The statistically significant improvement was observed only for Alexa750-Var7M compared to Alexa750-Var7.

The Alexa546-Var3 construct was selected for testing of targeting of submillimeter metastatic lesions in lungs. Since 4T1 cells implanted into mice have stable expression of GFP the lesions were identified by GFP fluorescence on the excised fresh lungs tissue by fluorescence microscopy (Figure 5). The GFP signal has excellent co-localization with Alexa546-Var3 fluorescent indicating that 400-500 μm sized metastatic lesions are acidic and targeted by fluorescent pHLIP.

Discussion

The approach for targeting of tumors, which we develop, is based on the marking of tumor acidity associated with tumor development, progression, aggressiveness and invasiveness. We have shown previously, that peptides of pHLIP family deliver optical, PET and SPECT imaging agents to the primary tumors and metastatic lesions in a pH-dependent manner [10,17,18]. Here we carried out a systematic investigation of

targeting of 4T1 mammary tumors, kidney, liver and muscle at different time points after single intravenous administration of various pHLIPs conjugated with eight different fluorescent dyes. Since the most NIR fluorescent dyes are large cyclic molecules (about 1 kDa in mass) they can affect and alter biodistribution of pHLIPs (about 4 kDa in mass). All fluorescent pHLIPs show slow tumor targeting, which ranged within hours after constructs administration. It is advantageous for drug delivery, since it could enhance pHLIP-drug circulation in blood. The best tumor targeting was observed for pHLIP variants (WT, Var3 and Var7) conjugated with Alexa546 at both N- or C-termini of the peptides to tether dye to the membrane of cancer cells in the extracellular or intracellular spaces, respectively. Accumulation of the Alexa546-pHLIPs in other organs and tissue was about 4 times less than in tumor. Thus, Alexa546 potentially can alter biodistribution of pHLIPs in a favorable way, and might be used with pHLIP-drug constructs. According to our data, Var3 demonstrates the highest tumor targeting in the most cases. We also showed targeting of submillimeter metastatic lesions in lungs by Alexa546-Var3, which opens opportunity of imaging and treating of metastasis employing pHLIP-technology.

The fluorescent pHLIPs also could have important implication for staining and visualization of cancer cells during surgical procedures [19]. Fluorescence -guided surgery has the promise to improve surgical procedures by determining tumor margins using tumor-specific targeting and by increasing the visual information available to the surgeon [20]. This technique, can possibly lead to complete resection of the tumor tissue with improved survival. On the foundation of the hallmarks of cancer, there is a variety of tumor-specific agents that are available for imaging of cancer [21]. To obtain

target-specific fluorescence imaging, the contrast agent has to be sent to the tumor site, and has to be kept by the target while nonbound agents are cleared from the circulation [17,22]. Mostly, NIR dyes are suited better for tissue staining, since auto fluorescence signal in NIR is much lower compared to visible light. The biodistribution is less critical, however the highest possible contrast between cancerous and normal tissue is the key. Var3 conjugated either with N- or C-terminus with Alexa546 or Cy5.5 show the highest tumor accumulation and highest contrast between tumor and normal tissue. Among NIR dyes, Alexa750, IR800 or Dy680 and DyP680 might be used for surgical procedures.

FIGURE LEGENDS

Figure 1. **Distribution of the fluorescent pHLIPs in 4T1 mammary tumors (cut in half), muscle, kidney and liver**. Fluorescent images of tissue and organs were obtained at 4 hrs after single i.v. administration of WT, Var3 and Var7 peptides conjugated with fluorescent dyes.

Figure 2. Time-dependent distribution of the fluorescent-pHLIPs in 4T1 mammary tumors, kidney, liver and muscle quantified by the *ex-vivo* mean fluorescence. The data in each row were normalized to the intensity in tumor of the corresponding fluorescent-WT at 2 hours. The numeric values of non-normalized fluorescent intensities are presented in the Supplementary Table 1.

Figure 3. Tumor to organ ratios calculated for 2, 4 and 24 hrs time points. The numeric values of tumor to organ ratios are presented in the Supplementary Table 2.

Figure 4. Contrast index (CI) calculated at 2 and 4 hrs time points. The p-level values were computed based on the two-tailed test. The numeric values of CI are presented in the Supplementary Table 3.

Figure 5. **Targeting of submillimeter metastatic lesions in lungs**. 4T1-GFP cells were injected subcutaneously in the mammary pad of the mouse. After 3 weeks, the primary tumor metastasized in the lungs. The Alexa546-Var3 was given as a single i.v. tail vein injection. At 4 hrs post-injection animals were euthanized, the lungs were excised and imaged immediately on the fluorescent microscope.

REFERENCES

1. Damaghi, M., Wojtkowiak, J.W., Gillies, R.J. (2013). pH sensing and regulation in cancer. Front. Physiol. 4, 370.

2. Gerweck,L.E., Seetharaman,K.(1996). Cellular pH gradient in tumor versus normal tissue: potential exploitation for the treatment of cancer. *Cancer Res.* 56, 1194–1198.

3. Raghunand,N.,Altbach,M.I.,VanSluis,R.,Baggett,B.,Taylor,C.W.,Bhujwalla, Z. M.,et al.(1999). Plasmalemmal pH-gradients in drug-sensitive and drug- resistant MCF-7 human breast carcinoma xenografts measured by 31P magnetic resonance spectroscopy. *Biochem.Pharmacol.* 57, 309–312.doi:10.1016/S0006- 2952(98)00306-2

4. Estrella, V., Chen, T., Lloyd, M., Wojtkowiak, J.W., Cornnell, H.H., Ibrahim-Hashim, A., Bailey, K., Balagurunathan, Y. Rothberg, J.M., Sloane, B.F., Johnson, J., Gatenby, R.A., Gillies, R.J. (2013). Acidity generated by the tumor microenvironment drives local invasion. Cancer Res. 73, 1524-35.

5. Wojtkowiak JW, Rothberg JM, Kumar V, Schramm, K.J., Haller, E., Proemsey, J.B., Lloyd, M., Sloane, B.F., Gillies, R.J. (2012). Chronic autophagy is a cellular adaptation to tumor acidic pH microenvironments. Cancer Res. 72,3938-47.

6. Andreev, O. A.; Engelman, D. M.; Reshetnyak, Y. K. (2010). pH-sensitive membrane peptides (pHLIPs) as a novel class of delivery agents. *Mol. Membr. Biol. 27,* 341-52.

7. Andreev, O. A.; Engelman, D. M.; Reshetnyak, Y. K. (2014). Targeting diseased tissues by pHLIP insertion at low cell surface pH. *Front. Physiol. 5*, 97.

8. Andreev, O.A., Engelman, D.M., Reshetnyak, Y.K. (2009). Targeting acidic diseased tissue: new technology based on use of the pH(Low) Insertion Peptide (pHLIP). Chim. Oggi. 27, 34-37.

9. Weerakkody, D.; Moshnikova, A.; Thakur, M. S.; Moshnikova, V.; Daniels, J.; Engelman, D. M.; Andreev, O. A.; Reshetnyak, Y. K. (2013). Family of pH (low) insertion peptides for tumor targeting. *Proc. Natl. Acad. Sci. 110*, 5834-9.

10. Karabadzhak, A. G.; Weerakkody, D.; Wijesinghe, D.; Thakur, M. S.; Engelman, D. M.; Andreev, O. A.; Markin, V. S.; Reshetnyak, Y. K. (2012). Modulation of the pHLIP transmembrane helix insertion pathway. *Biophys. J. 102*, 1846-55.

11. Andreev, O. A.; Karabadzhak, A. G.; Weerakkody, D.; Andreev, G. O., Engelman, D. M., Reshetnyak, Y. K. (2010). pH (low) insertion peptide (pHLIP) inserts across a lipid bilayer as a helix and exits by a different path. *Proc. Natl. Acad. Sci. 107*, 4081-6.

12. Adochite, R.C., Moshnikova, A., Carlin, S.D., Guerrieri, R.A., Andreev, O.A., Lewis, J.S., Reshetnyak, Y.K. (2014). Targeting breast tumors with pH (Low) Insertion Peptides. Mol. Pharm. 11, 2896-2905.

13. Karabadzhak, A.G., An, M., Yao, L., Langenbacher, R., Moshnikove, A., Adochite, R.C., Andreev, O.A., Reshetnyak, Y.K., Engelman, D. M. (2014). pHLIP-FIRE, a cell insertion-triggered fluorescent probe for imaging tumors demonstrates targeted cargo delivery *in vivo. ACS Chem. Biol. 9, 2545-2553.*

14. Cruz-Monserrate, Z.; Roland, C. L.; Deng, D.; Arumugam, T.; Moshnikova, A.; Andreev, O. A.; Reshetnyak, Y. K.; Logsdon, C. D. (2014). Targeting pancreatic ductal adenocarcinoma acidic microenvironment. *Sci Rep 4*, 4410.

15. Pulaski, B. A.; Ostrand-Rosenberg, S.; (2001). Mouse 4T1 Breast Tumor Model. Current Protocols in immunology, 39:20.2:20.2.1–20.2.16.

16. Yang, S.; Zhang, J.; Huang, X.; (2012). Mouse Models for Tumor Metastasis, Methods Mol Biol., 928, 221-228.

17. Vavere, A. L.; Biddlecombe, G. B.; Spees, W. M.; Garbow, J. R.; Wijesinghe, D.; Andreev, O. A.; Engelman, D. M.; Reshetnyak, Y. K.; Lewis, J. S. (2009). A novel technology for the imaging of acidic prostate tumors by positron emission tomography. *Cancer Res, 69*, 4510-6.

18. Macholl, S.; Morrison, M. S.; Iveson, P.; Arbo, B. E.; Andreev, O. A.; Reshetnyak, Y. K.; Engelman, D. M.; Johannesen, E. (2012). In vivo pH imaging with (99m)Tc-pHLIP. *Mol Imaging Biol*, *14*, (6), 725-34.

19. Segala, J.; Engelman, D.M.; Reshetnyak, Y.K.; Andreev, O.A. (2009). Accurate analysis of tumor margins using a fluorescent pH Low Insertion Peptide (pHLIP),*Int J Mol Sci*, 10: 3478-87.

20. Keereweer, S.; Van Driel, P. B.; Snoeks, T. J.A.; Kerrebijn, J. D.F.; Baatenburg de Jong, R. J.; Vahrmeijer, A. L.; Sterenborg, H. J. C.; Lowik, C. W. G. M.; (2013). Optical Image-Guided cancer Surgery: Challenges and Limitations, Clin Cancer Res, 19, 3745.

21. Keereweer S, Kerrebijn JD, van Driel PB, Xie B, Kaijzel EL, Snoeks TJ, et al. (2011), Optical image-guided surgery–where do we stand?, Mol Imaging Biol;13:199–207.

22. Frangioni JV. (2003). In vivo near-infrared fluorescence imaging. Curr Opin Chem Biol; 7:626–34.

Tables

Table 1. Spectral properties (position of maximum of absorbance, λ_{ab}, and emission, λ_{em}), molecular weights and HPLC retention times of the fluorescent-pHLIP constructs are shown.

Spectral Properties								
	Al546	**Al647**	**Al750**	**Cy5.5**	**IR680**	**IR800**	**Dy680**	**DyP680**
λ_{ab}, nm **λ_{em}, nm**	556 572	650 670	753 778	630/673 720	672 702	778 797	680 707	680 707
Molecular Weights								
WT	5146	5362	5462	4853	5140	5303	5084	5866
Var3	4256	4472	4572	3963	4250	4413	4194	4976
Var7	4100	4316	4416	3807	4094	4257	4038	4820
Var3-C	4313	-	-	4020	-	-	-	-
HPLC Retention Times								
WT	29.2	24.8	25.3	29.4	25.5	25.0	26.2	24.9
Var3	27.6	23.3	23.6	28.4	24.3	23.4	25.0	23.7
Var7	25.7	21.6	22.0	26.9	22.8	21.6	23.9	22.0
Var3-C	27.5	-	-	29.8	-	-	-	-

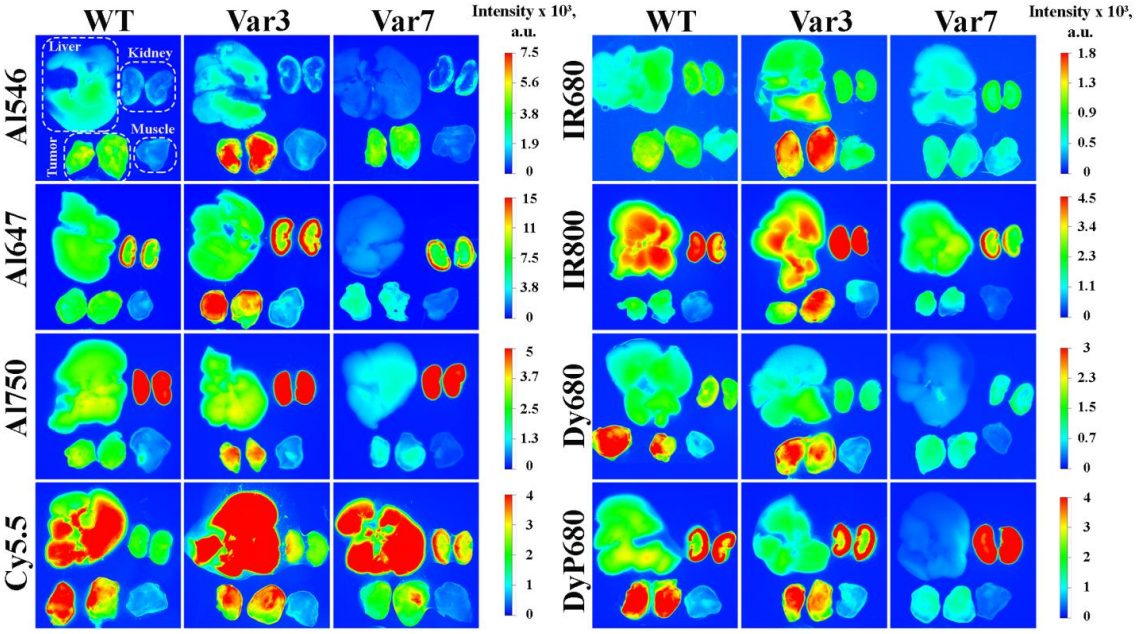

Figure 1. Distribution of the fluorescent pHLIPs in 4T1 mammary tumors (cut in half), muscle, kidney and liver. Fluorescent images of tissue and organs were obtained at 4 hrs after single i.v. administration of WT, Var3 and Var7 peptides conjugated with fluorescent dyes.

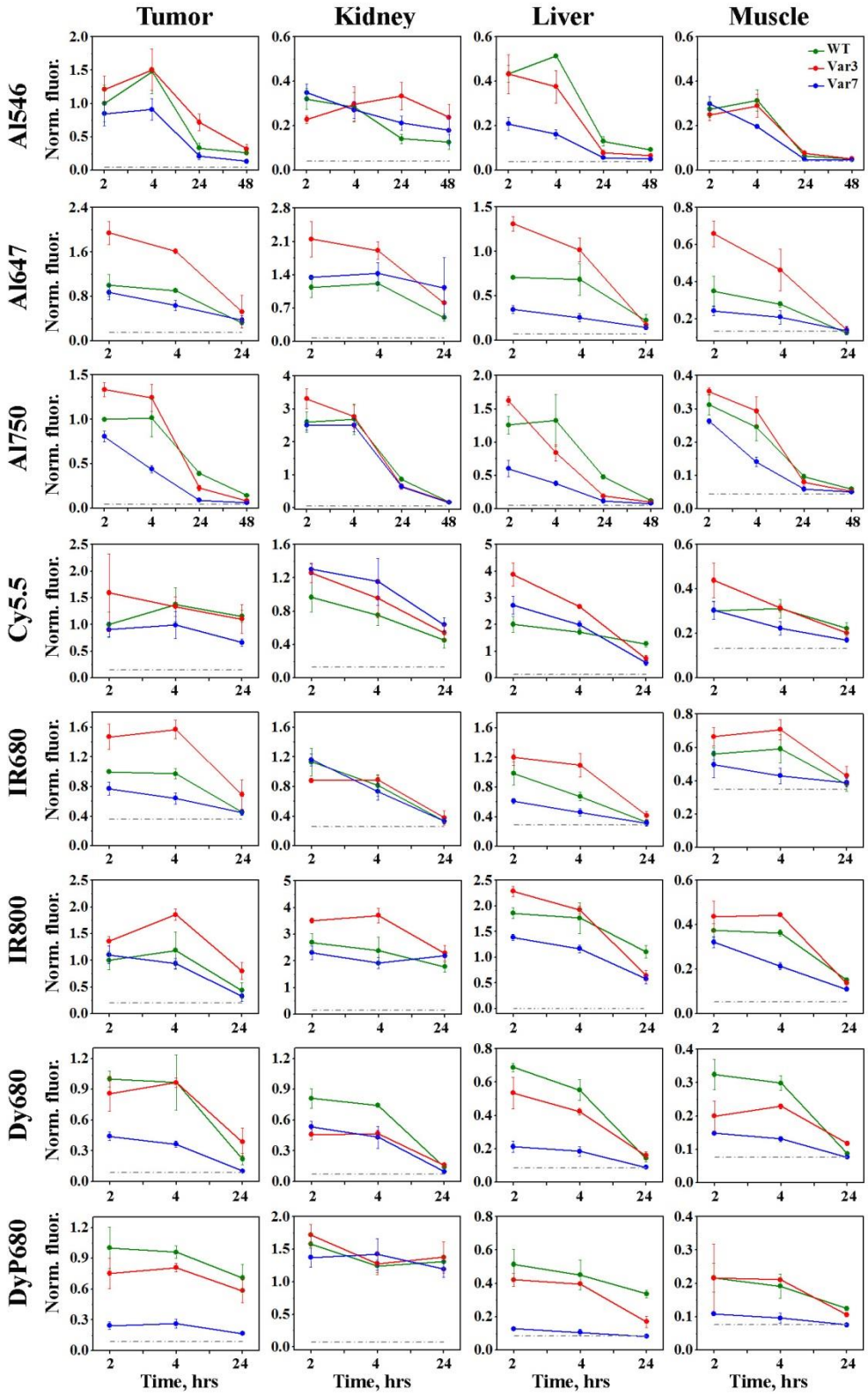

Figure 2. Time-dependent distribution of the fluorescent-pHLIPs in 4T1 mammary tumors, kidney, liver and muscle quantified by the *ex-vivo* mean

fluorescence. The data in each row were normalized to the intensity in tumor of the corresponding fluorescent-WT at 2 hours. The numeric values of non-normalized fluorescent intensities are presented in the Supplementary Table 1.

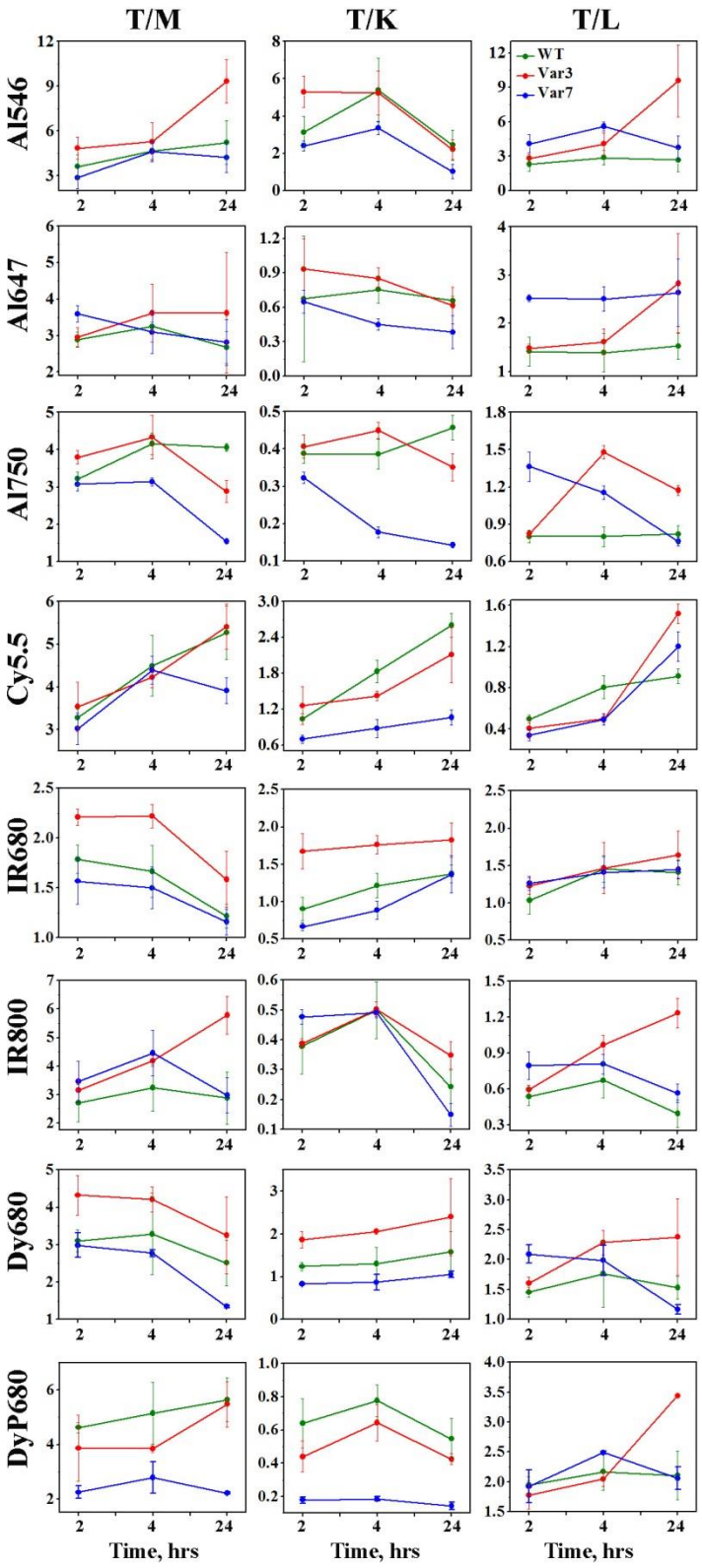

Figure 3. Tumor to organ ratios calculated for 2, 4 and 24 hrs time points. The numeric values of tumor to organ ratios are presented in the Supplementary Table 2.

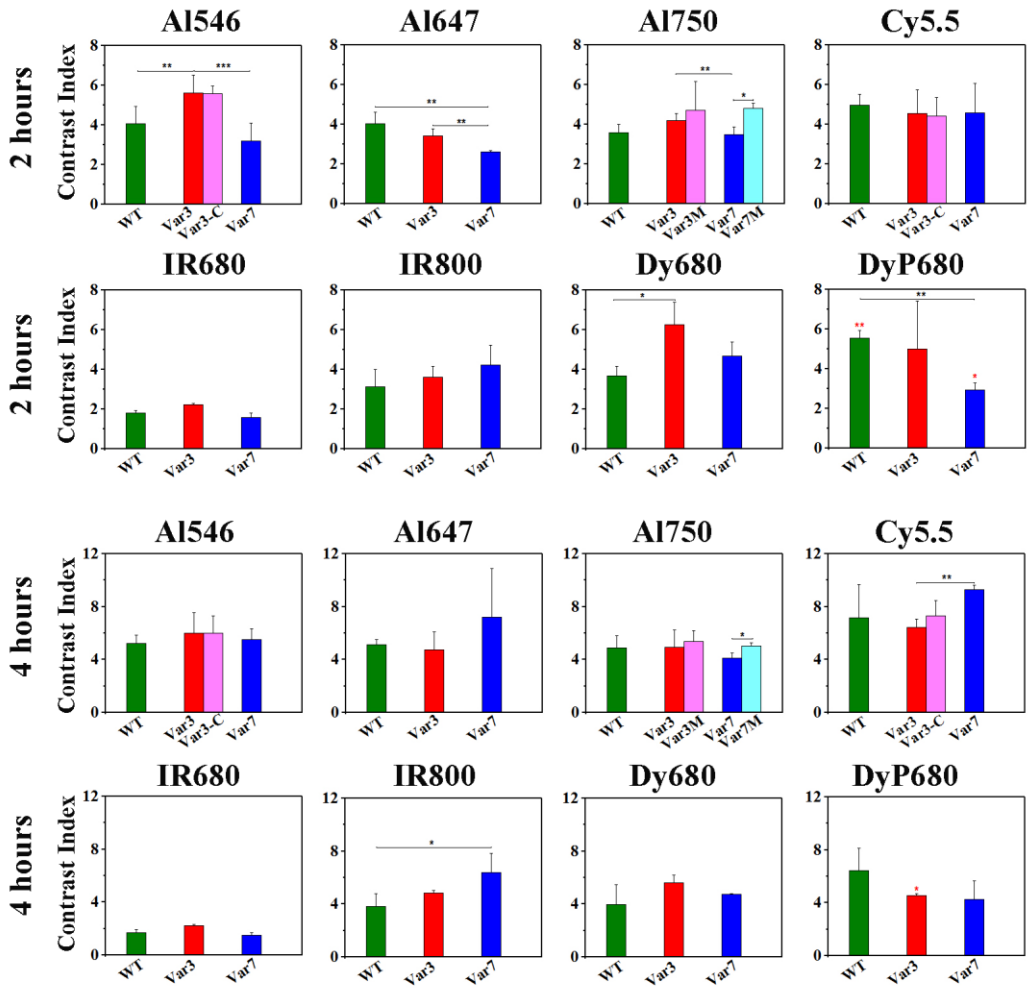

Figure 4. Contrast index (CI) calculated at 2 and 4 hrs time points. The p-level values were computed based on the two-tailed test. The numeric values of CI are presented in the Supplementary Table 3.

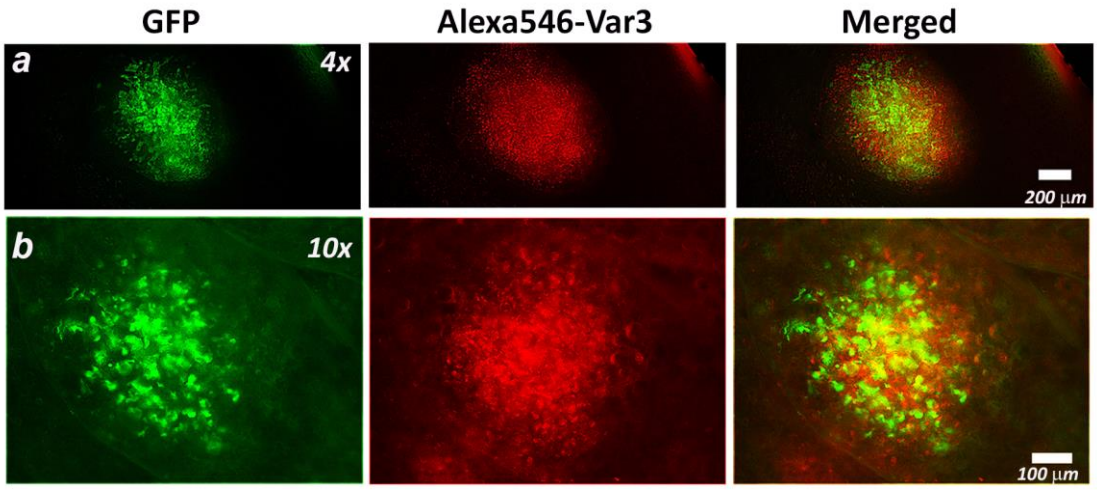

Figure 5. Targeting of submillimeter metastatic lesions in lungs. 4T1-GFP cells were injected subcutaneously in the mammary pad of the mouse. After 3 weeks, the primary tumor metastasized in the lungs. The Alexa546-Var3 was given as a single i.v. tail vein injection. At 4 hrs post-injection animals were euthanized, the lungs were excised and imaged immediately on the fluorescent microscope.

SUPPLEMENTARY DATA

Comparative study of tumor targeting and biodistribution of pH (Low) Insertion Peptides conjugated with various fluorescent dyes

Ramona-Cosmina Adochite[1], Anna Moshnikova[1], Jovana Golijanin[1], Oleg A. Andreev[1], Yana K. Reshetnyak[1,*]

Table S1. Mean surface fluorescence obtained from the organs and tissue at different time points after single i.v. administration of the fluorescent constructs. Values for the control represent baseline autofluorescence signal from animals with no injection of fluorescent constructs. The number of animals for each time point and each construct is indicated by *n*.

Alexa546-pHLIPs						
Organs	**Time post-injection**	**WT *n*=6**	**Var3 *n*=6**	**Var3-C n=3**	**Var7 *n*=6**	**Control**
Muscle	**2 hrs**	1057.0 ±137.8	963.4 ± 120.8	281.6 ± 23.3	1150.2 ± 126.6	156.3
	4 hrs	1212.0 ± 189.4	1117.9 ± 167.3	283.8 ± 52.6	756.9 ± 34.9	
	24 hrs	249.4 ± 23.2	297.7 ± 28.6	209.5 ± 18.6	191.2 ± 8.34	
	48 hrs	193.6 ± 18.0	201.0 ± 13.3		179.4 ±16.1	
Tumor	**2 hrs**	3856.7 ± 1058.5	4664.5 ± 720.4	834.6 ± 86.6	3267.1 ± 690.0	170.2
	4 hrs	5716.8 ± 1284.8	5809.9 ± 880.4	847.3 ± 162.2	3514.1 ± 622.9	
	24 hrs	1287 ± 290.4	2772.9 ± 600.3	1168.5 ± 299.8	810.4 ± 196.2	
	48 hrs	999.5 ± 129.8	1229.6 ± 281.9		516.7 ± 128.9	
Liver	**2 hrs**	1671.7 ± 148.7	1670.3 ± 409.5	380.3 ± 39.2	805.8 ± 112.4	144.2
	4 hrs	1984.0 ± 27.9	1448.7 ± 317.7	288.4 ± 11.8	623.6 ± 77.2	
	24 hrs	502.5 ± 85.6	303.4 ± 64.4	229.5 ± 17.6	217.0 ± 21.8	
	48 hrs	357.2 ± 24.6	254.9 ± 37.2		193 ± 20.6	
Kidney	**2 hrs**	1235.5 ± 182.2	880.3 ± 51.2	326.8 ± 83.1	1346.8 ± 145.8	156.4
	4 hrs	1099.2 ± 254.3	1148.4 ± 326.7	327.7 ± 41.3	1045.2 ± 144.4	
	24 hrs	544.8 ± 85.9	1288.7 ± 253.3	291.9 ± 17.9	821.3 ± 122.5	
	48 hrs	485.4 ± 126.5	918.5 ± 225.9		690.5 ± 259.6	
Alexa647-pHLIPs						
Organs	**Time post-injection**	**WT *n*=3**	**Var3 *n*=3**	**Var7 *n*=3**		**Control**

Muscle	**2 hrs**	2617.5 ± 616.0	4940.6 ± 527.6	1818.8 ± 200.0	980.7
	4 hrs	2093.2 ± 111.4	3467.6 ± 839.4	1569.0 ± 275.9	
	24 hrs	932.8 ± 49.0	1054.8 ± 121.0	1016.0 ± 171.7	
Tumor	**2 hrs**	7498.5 ± 1480.5	14565.3 ± 1577.3	6556.0 ± 1013.2	1125.5
	4 hrs	6798.8 ± 221.9	12099.6 ±255.7	4781.5 ± 675.1	
	24 hrs	2480.1 ± 290.3	3948.6 ± 2212.7	2832.5 ± 588.2	
Liver	**2 hrs**	5311.2 ± 97.9	9832.4 ± 622.3	2598.1 ± 335.6	525.6
	4 hrs	5137.2 ± 1330.5	7615.7 ± 1028.3	1921.6 ± 351.0	
	24 hrs	1680.4 ± 490.3	1327.4 ± 298.0	1091.4 ± 175.4	
Kidney	**2 hrs**	8516.0 ± 1611.7	16126.9 ± 2787.4	10112.8 ± 391.6	552.6
	4 hrs	9135.8 ± 1167.8	14325.3 ± 1332.3	10696.1 ± 1726.5	
	24 hrs	3778.7 ± 550.7	6081.2 ± 2036.8	8461.9 ± 4773.8	

Alexa750-pHLIPs

Organs	**Time post-injection**	**WT** ***n*=3**	**Var3** ***n*=3**	**Var7** ***n*=3**	**Control**
Muscle	**2 hrs**	889.8 ± 87.2	1002.6 ± 30.7	749.4 ± 21.4	127.3
	4 hrs	700.2 ± 117.8	836.3 ± 123.7	401.0 ± 40.8	
	24 hrs	275.5 ± 10.1	228.0 ± 24.5	169.0 ± 10.8	
	48 hrs	168.7 ± 7.3	150.4 ± 4.2	144.8 ± 0.3	
Tumor	**2 hrs**	2847.7 ± 40.1	3800.4 ± 226.1	2301.2 ± 172.6	135.4
	4 hrs	2897.5 ± 610.4	3542.2 ± 431.8	1256.4 ± 110.8	
	24 hrs	1118.9 ± 76.5	650.9 ± 88.8	260.7 ± 10.3	
	48 hrs	414.6 ± 23.7	236.8 ± 15.7	180.8 ± 16.9	
Liver	**2 hrs**	3577.2 ± 375.5	4618.6 ± 183.6	1722.5 ± 350.7	140.3
	4 hrs	3776.3 ± 1111.3	2401.4 ± 344.5	1087.8 ± 13.4	
	24 hrs	1370.9 ± 104.7	553.2 ± 46.8	342.7 ± 19.3	
	48 hrs	363.1 ± 36.6	286.9 ± 11.6	226.8 ± 21.7	
Kidney	**2 hrs**	7413.1 ± 881.7	9417.1 ± 862.6	7146.2 ± 419.3	143.5
	4 hrs	7664.2 ± 1328.6	7891.6 ± 984.4	7131.0 ± 552.1	
	24 hrs	2459.8 ± 164.2	1869.1 ± 197.4	1836.9 ± 236.7	
	48 hrs	491.2 ± 50.3	487.5 ± 74.6	429.2 ± 16.6	

Alexa750-pHLIP-Mutants

Organs	**Time post-injection**	**Var3M** ***n*=3**	**Var7M** ***n*=3**	**Control**
Muscle	**2 hrs**	886.2 ± 197.3	628.3 ± 24.2	146.9
	4 hrs	774.2 ± 255.2	430.1 ± 47.1	
Tumor	**2 hrs**	3444.6 ± 311.3	2451.8 ± 162.1	144.1
	4 hrs	3355.9 ± 796.2	1562.9 ± 240.4	
Liver	**2 hrs**	3954.1 ± 46.2	1389.4 ± 129.5	144.2
	4 hrs	2313.2 ± 373.7	902.0 ± 79.4	
Kidney	**2 hrs**	9114.2 ± 529.2	9691.2 ± 176.0	146.5
	4 hrs	8615.9 ± 657.4	8275.0 ± 499.0	

Cy5.5-pHLIPs

Organs	**Time**	**WT**	**Var3**	**Var3-C**	**Var7**	**Control**

	post-injection	*n*=3	*n*=3	*n*=3	*n*=3	
Muscle	**2 hrs**	634.1 ± 83.7	918.8 ± 162.6	1035.1 ± 63.4	638.0 ± 86.3	276.1
	4hrs	652.3 ± 88.4	660.5 ± 36.6	719.4 ± 113.4	467.3 ± 63.0	
	24hrs	466.5 ± 54.2	424.2 ± 30.8	411.3 ± 4.4	356.7 ± 16.5	
Tumor	**2 hrs**	2094.8 ± 497.0	3343.2 ± 1526.1	3627.7 ± 441.5	1900.3 ± 293.5	316.9
	4hrs	2882.6 ± 660.6	2798.5 ± 395.2	3482.0 ± 502.7	2076.3 ± 531.5	
	24hrs	2419.5 ± 226.1	2312.5 ± 556.1	2371.9 ± 186.9	1390.8 ± 141.9	
Liver	**2 hrs**	4209.2 ± 603.7	8118.0 ± 901.8	7828.1 ± 1161.2	5706.9 ± 719.4	259.5
	4hrs	3587.1 ± 127.3	5589.0 ± 129.6	5916.4 ± 843.6	4177.2 ± 278.0	
	24hrs	2666.9 ± 229.0	1513.1 ± 248.1	1844.5 ± 437.3	1180.8 ± 197.8	
Kidney	**2 hrs**	2024.9 ± 349.3	2641.0 ± 249.2	2926.5 ± 223.8	2729.3 ± 137.4	263.9
	4hrs	1576.9 ± 253.7	1998.0 ± 485.3	2322.7 ± 335.8	2416.3 ± 588.9	
	24hrs	947.9 ± 198.0	1135.4 ± 193.9	1116.7 ± 28.6	1335.8 ± 174.5	

IR680-pHLIPs

Organs	Time post-injection	WT *n*=3	Var3 *n*=3	Var7 *n*=3	Control
Muscle	**2 hrs**	523.3 ± 32.9	619.2 ± 50.7	463.5 ± 73.9	324.1
	4 hrs	551.6 ± 80.0	659.5 ± 56.9	401.0 ± 44.6	
	24 hrs	353.6 ± 37.5	401.9 ± 53.1	363.4 ± 23.2	
Tumor	**2 hrs**	931.9 ± 18.8	1370.8 ± 158.3	718.9 ± 83.5	333.1
	4 hrs	906.3 ± 66.0	1462.7 ± 114.7	597.8 ± 69.8	
	24 hrs	426.7 ± 5.5	645.5 ± 185.8	719.7 ± 34.1	
Liver	**2 hrs**	917.9 ± 144.1	1119.3 ± 97.7	569.2 ± 33.3	270.3
	4 hrs	626.3 ± 52.6	1020.2 ± 150.4	427.7 ± 47.2	
	24 hrs	305.8 ± 35.3	389.4 ± 53.3	291.5 ± 33.0	
Kidney	**2 hrs**	1053.0 ± 171.0	821.8 ± 30.6	1081.4 ± 76.1	241.7
	4 hrs	758.6 ± 137.3	830.5 ± 52.5	682.6 ± 107.8	
	24 hrs	353.6 ± 37.5	352.4 ± 89.0	311.6 ± 34.1	

IR800-pHLIPs

Organs	Time post-injection	WT *n*=3	Var3 *n*=3	Var7 *n*=3	Control
Muscle	**2 hrs**	630.6 ± 53.2	736.4 ± 116.0	542.9 ± 43.0	127.3
	4 hrs	612.6 ± 25.1	747.9 ± 10.5	359.1 ± 27.7	
	24 hrs	255.6 ± 19.7	231.6 ± 21.1	185.1 ± 14.6	
Tumor	**2 hrs**	1684.9 ± 292.6	2289.3 ± 146.0	1858.2 ± 271.3	135.4
	4 hrs	1996.4 ± 581.3	3129.0 ± 176.4	1585.9 ± 165.8	
	24 hrs	737.5 ± 241.1	1349.9 ± 267.3	554.9 ± 156.6	
Liver	**2 hrs**	3133.4 ± 179.7	3849.9 ± 164.7	2337.0 ± 107.9	140.3
	4 hrs	2969.8 ± 512.7	3238.8 ± 127.2	1964.7 ± 129.2	
	24 hrs	1863.4 ± 201.1	1089.6 ± 165.0	972.4 ± 149.9	
Kidney	**2 hrs**	4529.1 ± 547.1	5908.6 ± 128.3	3885.1 ± 420.8	143.5
	4 hrs	4015.6 ± 861.0	6235.9 ± 470.1	3238.1 ± 345.6	
	24 hrs	2998.4 ± 314.5	3863.7 ± 478.2	3696.5 ± 114.7	

Dy680-pHLIPs					
Organs	**Time post-injection**	**WT *n*=3**	**Var3 *n*=3**	**Var7 *n*=3**	**Control**
Muscle	**2 hrs**	754.9 ± 106.3	465.4 ± 103.5	345.6 ± 4.7	172.3
	4 hrs	694.3 ± 50.6	533.2 ± 18.3	305.5 ± 16.4	
	24 hrs	203.6 ± 4.8	274.6 ± 15.8	178.9 ± 9.2	
Tumor	**2 hrs**	2326.0 ± 183.6	1998.2 ± 394.4	1029.3 ± 100.8	219.0
	4 hrs	2246.3 ± 627.8	2243.3 ± 103.9	847.4 ± 73.5	
	24 hrs	511.7 ± 129.3	897.0 ± 314.3	241.1 ± 7.8	
Liver	**2 hrs**	1600.0 ± 60.7	1243.7 ± 218.2	495.5 ± 77.8	210.9
	4 hrs	1284.6 ± 142.6	984.2 ± 47.5	431.2 ± 65.6	
	24 hrs	331.8 ± 46.2	373.0 ± 49.8	207.5 ± 20.6	
Kidney	**2 hrs**	1886.5 ± 227.5	1066.6 ± 119.8	1242.9 ± 119.1	160.2
	4 hrs	1728.6 ± 45.4	1088.9 ± 73.8	1004.5 ± 250.7	
	24 hrs	327.9 ± 29.1	375.4 ± 39.5	229.8 ± 22.6	
DyP680-pHLIPs					
Organs	**Time post-injection**	**WT *n*=3**	**Var3 *n*=3**	**Var7 *n*=3**	**Control**
Muscle	**2 hrs**	829.6 ± 165.3	828.6 ± 389.7	416.5 ± 22.7	172.3
	4 hrs	735.1 ± 137.6	808.5 ± 14.8	367.0 ± 58.5	
	24 hrs	478.9 ± 24.9	406.4 ± 27.0	291.1 ± 22.2	
Tumor	**2 hrs**	3832.7 ± 769	2883.7 ± 567.7	936.2 ± 132.2	219.0
	4 hrs	3679.4 ± 225.9	3104.6 ± 162.4	1008.8 ± 166.8	
	24 hrs	2716.2 ± 512.0	2239.8 ± 459.6	644.9 ± 60.6	
Liver	**2 hrs**	1968.9 ± 354.6	1614.4 ± 152	488.2 ± 38.9	210.9
	4 hrs	1726.6 ± 343.2	1517.9 ± 26.1	405.6 ± 71.1	
	24 hrs	1290.2 ± 82.3	650.6 ± 131.0	314.1 ± 27.1	
Kidney	**2 hrs**	6047.7 ± 619.5	6584.5 ± 640.1	5262.3 ± 562.0	160.2
	4 hrs	4757.6 ± 360.8	4896.5 ± 656.5	5459.7 ± 928.5	
	24 hrs	5010.1 ± 364.3	5269.3 ± 923.6	4576.4 ± 489.9	

Table S2. Tumor/muscle, tumor/kidney and tumor/liver ratio values.

Ratios	Time post-injection	WT	Var3	Var7
Alexa546-pHLIPs				
Tumor/Muscle	**2 hrs**	3.62 ± 0.77	4.86 ± 0.75	2.89 ± 0.76
	4 hrs	4.68 ± 0.57	5.29 ± 1.27	4.62 ± 0.67
	24 hrs	5.22 ± 1.47	9.32 ± 1.45	4.23 ± 1.00
Tumor/Kidney	**2 hrs**	3.13 ± 0.84	5.30 ± 0.83	2.40 ± 0.26
	4 hrs	5.39 ± 1.70	5.23 ± 1.18	3.36 ± 0.36
	24 hrs	2.45 ± 0.80	2.21 ± 0.52	1.03 ± 0.38
Tumor/Liver	**2 hrs**	2.31 ± 0.60	2.83 ± 0.36	4.09 ± 0.80
	4 hrs	2.88 ± 0.62	4.09 ± 0.98	5.60 ± 0.36
	24 hrs	2.67 ± 1.03	9.57 ± 3.14	3.76 ± 1.02
Alexa647-pHLIPs				
Tumor/Muscle	**2 hrs**	2.88 ± 0.21	2.95 ± 0.26	3.60 ± 0.23
	4 hrs	3.25 ± 0.12	3.61 ± 0.81	3.09 ± 0.58
	24 hrs	2.67 ± 0.44	3.62 ± 1.66	2.81 ± 0.63
Tumor/Kidney	**2 hrs**	0.68 ± 0.55	0.93 ± 0.26	0.65 ± 0.10
	4 hrs	0.75 ± 0.12	0.85 ± 0.09	0.45 ± 0.05
	24 hrs	0.66 ± 0.04	0.62 ± 0.16	0.38 ± 0.14
Tumor/Liver	**2 hrs**	1.42 ± 0.30	1.48 ± 0.09	2.52 ± 0.07
	4 hrs	1.34 ± 0.41	1.61 ± 0.27	2.51 ± 0.25
	24 hrs	1.53 ± 0.28	2.82 ± 1.04	2.64 ± 0.70
Alexa750-pHLIPs				
Tumor/Muscle	**2 hrs**	3.22 ± 0.18	3.80 ± 0.18	3.08 ± 0.18
	4 hrs	4.16 ± 0.29	4.33 ± 0.59	3.14 ± 0.11
	24 hrs	4.06 ± 0.10	2.88 ± 0.30	1.54 ± 0.03
Tumor/Kidney	**2 hrs**	0.39 ± 0.03	0.41 ± 0.03	0.32 ± 0.02
	4 hrs	0.39 ± 0.04	0.45 ± 0.02	0.18 ± 0.01
	24 hrs	0.46 ± 0.03	0.35 ± 0.04	0.14 ± 0.01
Tumor/Liver	**2 hrs**	0.80 ± 0.05	0.82 ± 0.03	1.36 ± 0.12
	4 hrs	0.80 ± 0.08	1.48 ± 0.05	1.15 ± 0.05
	24 hrs	0.82 ± 0.07	1.17 ± 0.04	0.76 ± 0.04
Cy5.5-pHLIPs				
Tumor/Muscle	**2 hrs**	3.28 ± 0.23	3.54 ± 0.57	3.02 ± 0.37
	4 hrs	4.50 ± 0.71	4.23 ± 0.25	4.39 ± 0.32
	24 hrs	5.27 ± 0.63	5.41 ± 0.53	3.91 ± 0.30
Tumor/Kidney	**2 hrs**	1.04 ± 0.09	1.26 ± 0.31	0.70 ± 0.07
	4 hrs	1.83 ± 0.19	1.42 ± 0.08	0.88 ± 0.15
	24 hrs	2.60 ± 0.20	2.11 ± 0.47	1.06 ± 0.13
Tumor/Liver	**2 hrs**	0.50 ± 0.04	0.41 ± 0.09	0.34 ± 0.05

	4 hrs	0.80 ± 0.11	0.50 ± 0.03	0.49 ± 0.06
	24 hrs	0.91 ± 0.07	1.52 ± 0.10	1.20 ± 0.14
IR680-pHLIPs				
Tumor/Muscle	**2 hrs**	1.79 ± 0.14	2.21 ± 0.08	1.57 ± 0.23
	4 hrs	1.67 ± 0.26	2.22 ± 0.12	1.50 ± 0.21
	24 hrs	1.22 ± 0.12	1.58 ± 0.28	1.16 ± 0.13
Tumor/Kidney	**2 hrs**	0.90 ± 0.16	1.67 ± 0.24	0.66 ± 0.06
	4 hrs	1.21 ± 0.17	1.76 ± 0.12	0.89 ± 0.12
	24 hrs	1.37 ± 0.12	1.82 ± 0.23	1.36 ± 0.25
Tumor/Liver	**2 hrs**	1.03 ± 0.19	1.23 ± 0.11	1.26 ± 0.10
	4 hrs	1.46 ± 0.18	1.45 ± 0.34	1.40 ± 0.20
	24 hrs	1.40 ± 0.16	1.64 ± 0.32	1.45 ± 0.12
IR800-pHLIPs				
Tumor/Muscle	**2 hrs**	2.70 ± 0.66	3.15 ± 0.37	3.46 ± 0.72
	4 hrs	3.24 ± 0.82	4.18 ± 0.18	4.45 ± 0.80
	24 hrs	2.88 ± 0.92	5.79 ± 0.67	2.97 ± 0.61
Tumor/Kidney	**2 hrs**	0.38 ± 0.09	0.39 ± 0.02	0.48 ± 0.02
	4 hrs	0.50 ± 0.10	0.50 ± 0.02	0.49 ± 0.02
	24 hrs	0.24 ± 0.06	0.35 ± 0.05	0.15 ± 0.04
Tumor/Liver	**2 hrs**	0.54 ± 0.07	0.59 ± 0.04	0.80 ± 0.11
	4 hrs	0.67 ± 0.15	0.97 ± 0.08	0.80 ± 0.08
	24 hrs	0.39 ± 0.12	1.23 ± 0.12	0.56 ± 0.07
Dy680-pHLIPs				
Tumor/Muscle	**2 hrs**	3.11 ± 0.29	4.32 ± 0.53	2.98 ± 0.33
	4 hrs	3.28 ± 1.09	4.21 ± 0.33	2.77 ± 0.10
	24 hrs	2.51 ± 0.61	3.25 ± 1.02	1.35 ± 0.03
Tumor/Kidney	**2 hrs**	1.24 ± 0.29	1.86 ± 0.20	0.83 ± 0.02
	4 hrs	1.30 ± 0.39	2.06 ± 0.06	0.87 ± 0.18
	24 hrs	1.58 ± 0.48	2.40 ± 0.90	1.05 ± 0.07
Tumor/Liver	**2 hrs**	1.45 ± 0.09	1.60 ± 0.10	2.09 ± 0.15
	4 hrs	1.77 ± 0.56	2.29 ± 0.21	1.99 ± 0.25
	24 hrs	1.53 ± 0.19	2.38 ± 0.64	1.17 ± 0.08
DyP680-pHLIPs				
Tumor/Muscle	**2 hrs**	4.62 ± 0.19	3.86 ± 1.22	2.24 ± 0.23
	4 hrs	5.15 ± 1.14	3.84 ± 0.13	2.78 ± 0.59
	24 hrs	5.65 ± 0.81	5.48 ± 0.84	2.21 ± 0.04
Tumor/Kidney	**2 hrs**	0.64 ± 0.15	0.44 ± 0.09	0.18 ± 0.02
	4 hrs	0.78 ± 0.09	0.64 ± 0.11	0.19 ± 0.01
	24 hrs	0.55 ± 0.12	0.42 ± 0.03	0.14 ± 0.02
Tumor/Liver	**2 hrs**	1.94 ± 0.14	1.78 ± 0.23	1.92 ± 0.27
	4 hrs	2.17 ± 0.31	2.05 ± 0.12	2.49 ± 0.03
	24 hrs	2.11 ± 0.40	3.44 ± 0.02	2.06 ± 0.19

Table S3. Contrast Index (CI) calculated for 2 and 4 hours time points.

Time post-injection	WT	Var3	Var7
Alexa546-pHLIPs			
2 hrs	4.06 ± 0.88	5.60 ± 0.92	3.18 ± 0.90
4 hrs	5.22 ± 0.61	6.01 ± 1.55	5.54 ± 0.81
Alexa647-pHLIPs			
2 hrs	4.03 ± 0.58	3.41 ± 0.35	2.61 ± 0.07
4 hrs	5.12 ± 0.39	4.72 ± 1.39	7.18 ± 3.70
Alexa750-pHLIPs			
2 hrs	3.59 ± 0.40	4.19 ± 0.37	3.49 ± 0.39
4 hrs	4.88 ± 0.92	4.95 ± 1.28	4.13 ± 0.39
Cy5.5-pHLIPs			
2 hrs	4.96 ± 0.56	4.55 ± 1.19	4.58 ± 1.47
4 hrs	7.16 ± 2.54	6.44 ± 0.63	9.27 ± 0.37
IR680-pHLIPs			
2 hrs	1.79 ± 0.14	2.21 ± 0.08	1.57 ± 0.23
4 hrs	1.67 ± 0.26	2.22 ± 0.12	1.50 ± 0.21
IR800-pHLIPs			
2 hrs	3.13 ± 0.87	3.61 ± 0.55	4.21 ± 1.00
4 hrs	3.80 ± 0.10	4.82 ± 0.21	6.37 ± 1.46
Dy680-pHLIPs			
2 hrs	3.67 ± 0.48	6.27 ± 1.13	4.69 ± 0.71
4 hrs	3.97 ± 1.50	5.63 ± 0.56	4.72 ± 0.07
DyP680-pHLIPs			
2 hrs	5.55 ± 0.40	4.99 ± 2.44	2.92 ± 0.36
4 hrs	6.43 ± 1.50	4.53 ± 0.15	4.25 ± 1.40

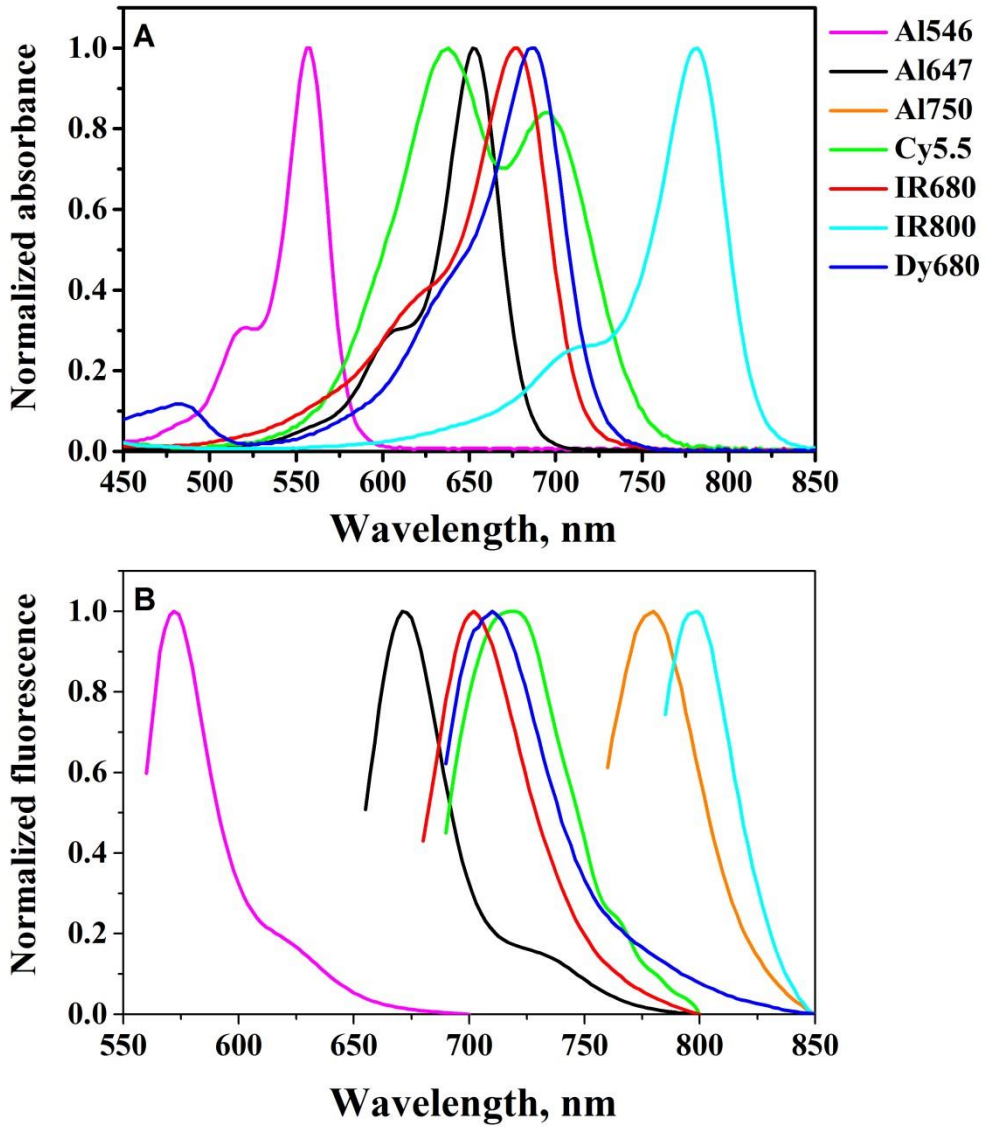

Figure S1. Absorbtion (A) and fluorescence (B) spectra of fluorescent-constructs measured in PBS.